

Provenance of Pennsylvanian-Permian sedimentary rocks associated with the Ancestral Rocky Mountains orogeny in southwestern Laurentia: Implications for continental-scale Laurentian sediment transport systems

Ryan J. Leary¹, Paul Umhoefer², M. Elliot Smith², Tyson M. Smith³, Joel E. Saylor⁴, Nancy Riggs², Greg Burr², Emma Lodes², Daniel Foley², Alexis Licht⁵, Megan A. Mueller⁵, and Chris Baird⁵

DEPARTMENT OF EARTH AND ENVIRONMENTAL SCIENCE, NEW MEXICO INSTITUTE OF MINING AND TECHNOLOGY, SOCORRO, NEW MEXICO 87801, USA

²SCHOOL OF EARTH AND SUSTAINABILITY, NORTHERN ARIZONA UNIVERSITY, FLAGSTAFF, ARIZONA 86011, USA

DEPARTMENT OF EARTH AND ATMOSPHERIC SCIENCES, UNIVERSITY OF HOUSTON, HOUSTON, TEXAS 77204, USA

ABSTRACT

The Ancestral Rocky Mountains system consists of a series of basement-cored uplifts and associated sedimentary basins that formed in southwestern Laurentia during Early Pennsylvanian–middle Permian time. This system was originally recognized by aprons of coarse, arkosic sandstone and conglomerate within the Paradox, Eagle, and Denver Basins, which surround the Front Range and Uncompahgre basement uplifts. However, substantial portions of Ancestral Rocky Mountain–adjacent basins are filled with carbonate or fine-grained quartzose material that is distinct from proximal arkosic rocks, and detrital zircon data from basins adjacent to the Ancestral Rocky Mountains have been interpreted to indicate that a substantial proportion of their clastic sediment was sourced from the Appalachian and/or Arctic orogenic belts and transported over long distances across Laurentia into Ancestral Rocky Mountain basins. In this study, we present new U-Pb detrital zircon data from 72 samples from strata within the Denver Basin, Eagle Basin, Paradox Basin, northern Arizona shelf, Pedregosa Basin, and Keeler–Lone Pine Basin spanning ~50 m.y. and compare these to published data from 241 samples from across Laurentia. Traditional visual comparison and inverse modeling methods map sediment transport pathways within the Ancestral Rocky Mountains system and indicate that proximal basins were filled with detritus eroded from nearby basement uplifts, whereas distal portions of these basins were filled with a mix of local sediment and sediment derived from marginal Laurentian sources including the Arctic Ellesmerian orogen and possibly the northern Appalachian orogen. This sediment was transported to southwestern Laurentia via a ca. 2,000-km-long longshore and aeolian system analogous to the modern Namibian coast. Deformation of the Ancestral Rocky Mountains slowed in Permian time, reducing basinal accommodation and allowing marginal clastic sources to overwhelm the system.

LITHOSPHERE; v. 12; no. 1; p. 88–121; GSA Data Repository Item 2020103 | Published online 30 January 2020

https://doi.org/10.1130/L1115.1

INTRODUCTION

Over the last several decades, increasing attention has been focused on the importance of treating sediment production, transport, and storage processes within an integrated source-to-sink framework (e.g., Allen, 2008; Tinker et al., 2008; Covault et al., 2011; Romans et al., 2016; Wang et al., 2019). Vital to this approach is the determination of both the spatial and temporal extent of the source-to-sink system, or alternately stated, it is imperative to understand the degree to which the source is separated from the sink, both by physical distance and by the time elapsed between erosion and deposition. This can be relatively straightforward for small, short-lived basins and/or those with limited catchment areas (e.g., Sømme et al., 2011; Cheng et al., 2016; Sickmann et al., 2016). However, there is increasing documentation of the importance of continent/

Ryan Leary http://orcid.org/0000-0003-4245-9736

supercontinent-scale sediment transport systems in the geologic record (Gehrels et al., 2011; Blum and Pecha, 2014; Benyon et al., 2014; Blum et al., 2017) and in modern systems (Garzanti et al., 2014). Of particular importance in mixed terrestrial/marine systems are the roles of littoral and aeolian processes (Garzanti et al., 2014, 2018), and "axial" sediment transport (perpendicular to the steepest surface path across a source-to-sink system) in controlling sediment transport patterns and sediment budgets (Garzanti et al., 2014; Romans, et al., 2016). Recent work has demonstrated that transport by longshore current can result in mixing of provenance signals at long spatial and temporal wavelengths (e.g., Liu et al., 2007; Garzanti et al., 2014; Sickmann et al., 2016), but these processes are not as well considered in deep-time provenance records.

The late Paleozoic Ancestral Rocky Mountains (ARM) system presents an exceptionally well-documented opportunity to explore these concepts at a continental scale because the ARM preserves mixed marine/terrestrial depositional systems that were active across much of southern Laurentia

DEPARTMENT OF EARTH, OCEAN AND ATMOSPHERIC SCIENCES, UNIVERSITY OF BRITISH COLUMBIA, VANCOUVER, BRITISH COLUMBIA V6T1Z4, CANADA

DEPARTMENT OF EARTH AND SPACE SCIENCES, UNIVERSITY OF WASHINGTON, SEATTLE, WASHINGTON 98195, USA

over a period of ~50 m.y. (Fig. 1; McKee and McKee, 1967; Mallory, 1972; Rascoe and Baars, 1972; McKee and Crosby, 1975). Moreover, basement ages of rocks within the ARM system from which detritus would have been locally derived are well dated (e.g., Sims et al., 2005; Karlstrom et al., 2004; Whitmeyer and Karlstrom, 2007), allowing relatively high confidence in provenance interpretations. Here, we present new U-Pb detrital zircon data from 72 samples throughout the ARM system and integrate these data with published data from an additional 241 samples to track the evolution of sediment provenance and transport pathways and their relationship to basin formation and orogenesis.

GEOLOGIC BACKGROUND

The Ancestral Rocky Mountains system consists of a series of basement-cored uplifts bounded by reverse faults that were active during the Pennsylvanian through early Permian periods. Movement along these faults resulted in the formation of asymmetric flexural basins proximal to uplifts (e.g., Barbeau, 2003); however, ARM-coeval subsidence and sediment accumulation is not confined to discrete basins but extends across much of southwestern Laurentia. The Ancestral Rocky Mountains were first recognized in central Colorado and Utah (e.g., Ver Weibe, 1930), but the system also extends across most of southwestern Laurentia including southern New Mexico, Texas, and Oklahoma (Kluth and Coney, 1981; Fig. 1). The ARM system was situated at or near equatorial latitudes during Pennsylvanian and early Permian time, during which Laurentia was rotated approximately 45 degrees clockwise from its current orientation (Scotese and McKerrow, 1990; Domeier and Torsvik, 2014; Cao et al., 2017; note that the modern reference frame and cardinal directions are used throughout this study).

The ARM system was bounded on three sides by convergent tectonic plate boundaries (Leary et al., 2017; Fig. 1). To the south and east of the ARM system, convergence between Gondwanaland and Laurentia created a series of paired fold-and-thrust belts and foreland basins including the Appalachian orogen and basin, the Ouachita belt, and the Black Warrior,

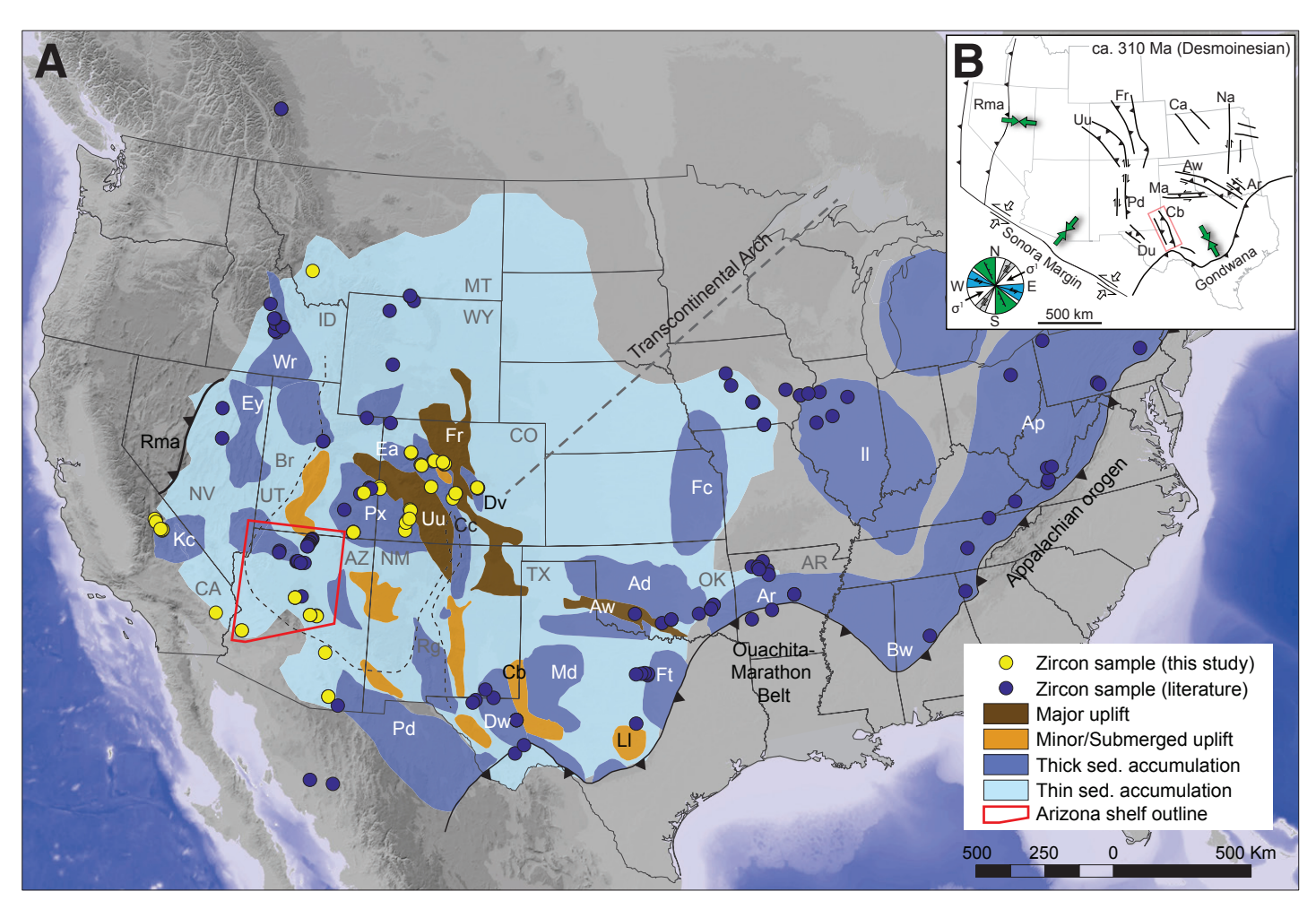


Figure 1. (A) Regional map of late Paleozoic Laurentian tectonic elements after Mckee and Mckee (1967), Mallory et al. (1972), McKee and Crosby (1975). Basins: Cc—Central Colorado Trough; Kc—Keeler—Lone Pine; Ey—Ely; Wr—Wood River; Ea—Eagle; Px—Paradox; Dv—Denver; Pd—Pedregosa; Dw—Delaware; Md—Midland; Ft—Fort Worth; Ad—Anadarko; Fc—Forest City; Ar—Arkoma; II—Illinois; Bw—Black Warrior; Ap—Appalachian. Uplifts: Uu—Uncompahgre; Fr—Front Range; Cb—Central Basin Platform; Aw—Amarillo—Wichita; Rma—Roberts Mountains allochthon; LI—Llano. CA—California; NV—Nevada; UT—Utah; ID—Idaho; MT—Montana; WY—Wyoming; CO—Colorado; AZ—Arizona; NM—New Mexico; TX—Texas; OK—Oklahoma; AR—Arkansas. Br—Area of Basin and Range extension; Rg—Rio Grande Rift. Fine dotted line indicates approximate limit of Cenozoic Basin and Range and Rio Grande Rift extension. (B) Plate tectonic setting and kinematics of the Ancestral Rocky Mountains after Leary et al. (2017). Opposed green arrows show interpreted tectonic stress. Fault orientations in lower right are from the Central Basin Platform (Shumaker, 1992). Du—Diablo uplift; Ca—Cambridge arch; Na—Nemaha uplift. See A for other abbreviations.

Arkoma, Fort Worth, Val Verde, and Marfa Basins, in which subsidence propagated to the southwest over time (Graham et al., 1975; Ross, 1986; Dickinson and Lawton, 2003). By Pennsylvanian time, final Pangean suturing was complete in the southern Appalachians, and contractile deformation and foreland basin formation migrated to the Ouachita-Marathon fold-thrust belt and adjacent Delaware and Midland Basins of west Texas (Whiting and Thomas, 1994; Thomas, 1988). To the west, convergence along westward-dipping subduction zones resulted in a series of arc collision and accretion events that affected the paleo-Nevada continental margin (Dickinson et al., 2000). These include the Devonian-Mississippian Antler event that emplaced the Roberts Mountain Allochthon and late Permian-Triassic Sonoma collision that emplaced the Golconda Allochthon, both of which contributed to flexural subsidence and foreland formation (Speed and Sleep, 1982; Burchfiel and Royden, 1991; Dickinson et al., 2000). Although tectonic activity along this margin may have been concentrated during accretion events, the entire margin was subject to ongoing convergent deformation events from at least Mississippian through Permian time (Erickson and Marsh, 1974; Trexler et al., 1991, 2004; Cashman et al., 2011). The southwestern margin of the ARM system is poorly exposed in present-day northern Mexico and southern Arizona and has been strongly overprinted by several major episodes of tectonism (e.g., McQuarrie and Wernicke, 2005; Clinkscales and Lawton, 2018). Paleotectonic reconstructions (Dickinson and Lawton, 2001), recent late Paleozoic global plate models (Domeier and Torsvik, 2014), and kinematic analysis of the ARM deformation suggest that this margin evolved from oblique convergence to subduction during late Paleozoic time (Leary et al., 2017; Lawton et al., 2017).

The tectonic driver(s) of Ancestral Rocky Mountain basement deformation remain a topic of debate, and proposed models include collision along the Ouachita-Marathon belt (Kluth and Coney, 1981), left-lateral shear along major transcontinental faults (Budnik, 1986), flat-slab subduction along the southwestern continental margin (Ye et al., 1996), reactivation of pre-existing rift structures (Marshak et al., 2000), wrenching associated with the zippering closure of the Iapetus Ocean (Dickinson and Lawton, 2003), dynamic uplift/subsidence due to stress-field interaction with underplated Proterozoic mafic rocks (Soreghan et al., 2012), and oblique convergence along the southwestern Laurentian margin (Leary et al., 2017; Lawton et al., 2017). A complete discussion of the strengths and limitations of these models is beyond the scope of this paper; however, we emphasize several salient aspects of this system that are relevant to the current study: (1) The ARM system developed within an area underlain by Proterozoic Yavapai and Mazatzal basement rocks that were accreted to the Archean Wyoming Craton between 1.7 Ga and 1.6 Ga (Karlstrom and Bowring, 1988; Bickford et al., 1989; Reed et al., 1993) and were later intruded by ca. 1.4 Ga and ca.1.1 Ga alkaline "A-type" granitic intrusions (Anderson and Bender, 1989; Bickford et al., 2015). (2) The core of the ARM system in Colorado straddles the trace of the Transcontinental Arch, an enigmatic line of mid-cratonic positive relief that seems to have reduced accommodation and acted as a barrier to sediment transport for most of the Phanerozoic (Weimer, 1978; Garfield et al., 1988; Carlson, 1999; Amato and Mack, 2012). (3) ARM uplifts and resulting flexural basins strike generally to the northwest-southeast (modern reference frame) (Fig. 1; Ye et al., 1996), with preserved kinematic data suggesting northeast-southwest-oriented shortening (Brewer et al., 1983; Granath, 1989; Shumaker, 1992; Hoy and Ridgway, 2002; Cather et al., 2006; Cox, 2009). Uplift and basin orientations in several cases follow the trends of Proterozoic rifts (Karlstrom and Humphreys, 1998; Marshak et al., 2000), and multiple tectonic models have proposed that associated faults controlled the localization of ARM deformation (Marshak and Paulsen, 1996; Marshak et al., 2000; Soreghan et al., 2012; Leary et al., 2017). (4) ARM deformation did not

substantially affect Archean crust of the Wyoming Craton (Karlstrom and Humphreys, 1998), although whether that can be attributed to crustal rheology or distance from active continental margins remains unknown. (5) The ARM system was amagmatic, which prohibits precise radioisotopic geochronology; however, marine strata within the ARM system are well dated biostratigraphically and can be precisely correlated to strata in the Donets Basin and the Ural Mountains of eastern Europe (Schmitz and Davydov, 2012). Available geochronology suggests that ARM-related subsidence (and inferred uplift) began more or less synchronously across most of the region during the Early Pennsylvanian (Leary et al., 2017).

Sedimentary facies within the ARM basins evolved from regional exposure and terrestrial facies during the Late Mississippian (e.g., Huddle and Dobrovolny, 1945; Evans and Reed, 2007) into locally thick accumulations of marine carbonate, shale, and evaporite during the Pennsylvanian (McKee and Crosby, 1975), then transitioned to terrestrial deposition during the early Permian (McKee and McKee, 1967), approximately consistent with the end of ARM deformation.

STRATIGRAPHY AND SAMPLING

Samples analyzed in this study were collected from ARM-related sedimentary rocks from the core of the ARM system-the Denver, Eagle, and Paradox Basins-as well as peripheral areas in New Mexico, Arizona, and southeast California. Regional sample locations and stratigraphy are described in Figures 1 and 2; detailed sample locations and detrital zircon data are presented in Figures 3-8 and Table 1. Below, we briefly describe the sampled strata of each area. We refer readers to GSA Data Repository File DR11 for precise locations, measured sections, and interpretations of lithofacies, age, and depositional environments. Although previously published data from Grand Canyon samples (Gehrels et al., 2011) are reviewed in the results, the stratigraphy and sampling within that study is not described here. Most locations sampled in this study do not require substantial palinspastic restoration to account for Sevier, Rio Grande Rift, and/or Basin and Range deformation (e.g., DeCelles, 2004; McQuarrie and Wernicke, 2005; McQuarrie and Oskin, 2010) (Fig. 1). Note, however, that locations affected by these episodes of deformation are not palinspastically restored in maps within this study.

Western Mogollon Rim

This section consists of Mississippian through middle Permian rocks (Figs. 2 and 4, panel 1). The Mississippian Redwall Limestone makes up the base of the section and is overlain by the predominantly siliciclastic Supai Group, Hermit Formation, and Schnebly Hill Formation (Blakey, 1980, 1990; McKee, 1982). We collected samples from very

¹GSA Data Repository Item 2020103, File DR1: Complete description of strata sampled as part of this study including facies, age determinations, depositional settings, and measured sections; File DR2: Biostratigraphic report by Greg Wahlman for Pennsylvanian strata in central Arizona on which age determinations were made within this study (report provided with permission); File DR3: All zircon data presented in this study and locations, ages, and sources for all other data included; File DR4: Input data for all cross-correlation statistics; File DR5: Sample group details and n-values for detrital zircon samples used in NMF modeling; File DR6: Results of DZStats PDF cross-correlation, K-S Test, and KDE likeness calculations; File DR7: Sample locations and cross-correlation statistics for individual samples compared to Arizona shelf data; File DR8: NMF results detailing factorized sources and source proportions models of 2 to 30 factorized probability density plot (PDF) sources; File DR9: NMF results detailing factorized sources and source proportions models of 2 to 30 factorized kernel density estimate (KDE) (50 m.y. bandwidth) sources; File DR10: Factorized source names used in the paper and their equivalent names assigned during NMF modeling, is available at http://www.geosociety.org/ datarepository/2020, or on request from editing@geosociety.org.

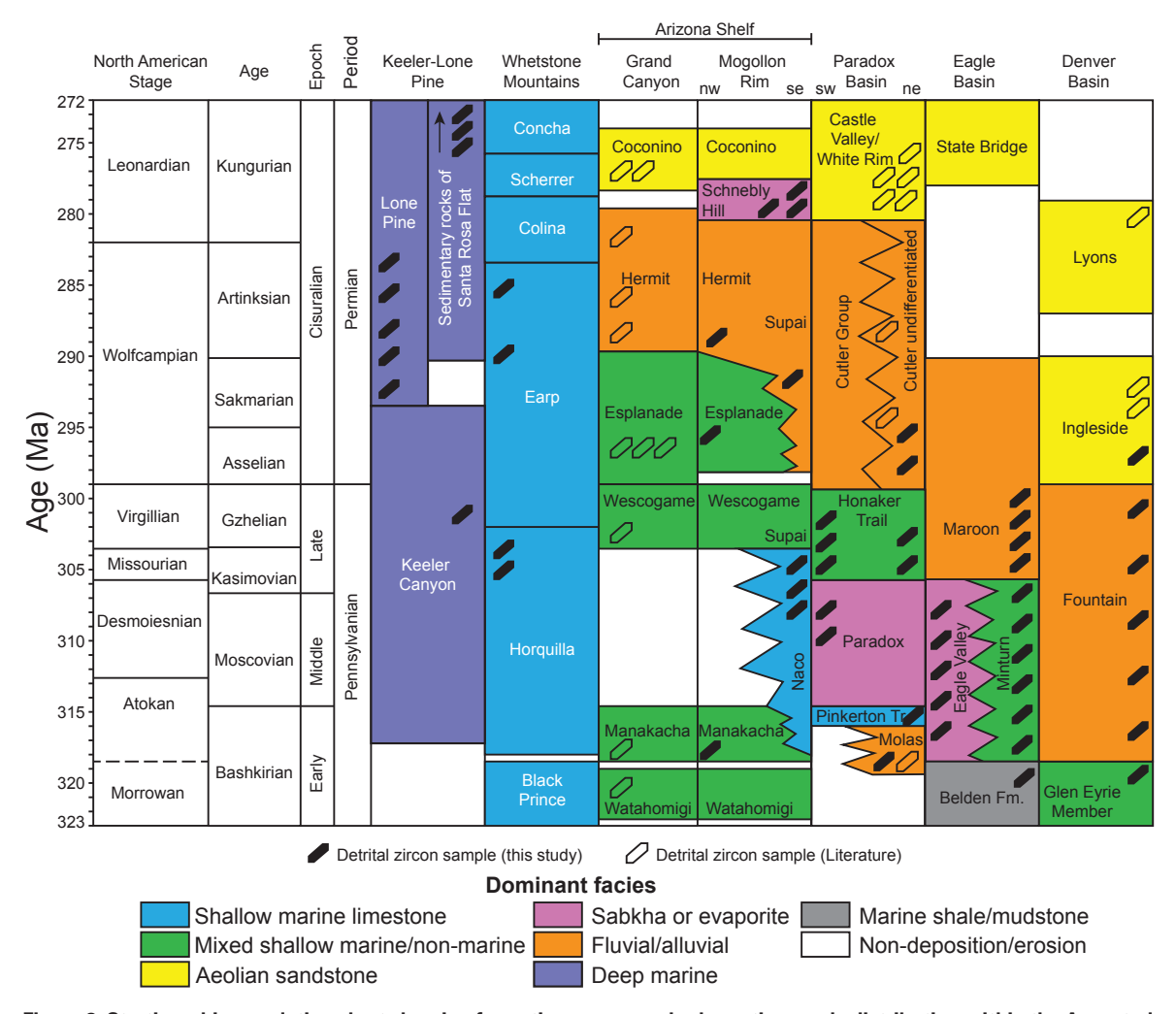


Figure 2. Stratigraphic correlation chart showing formation names and schematic sample distribution within the Ancestral Rocky Mountain province. Note that the Plomosa Mountains section is not included in this diagram. Timescale after Menning et al. (2006) and Schmitz and Davydov (2012). Stratigraphy after Armin (1987), Blakey (1990), Lawton et al. (2015), and Sweet et al. (2015).

fine-grained to fine-grained sandstone of the Manakacha, Esplanade, Hermit and Schnebly Hill Formations.

Central Mogollon Rim

In this section, the base of the Pennsylvanian–Permian section was deposited above a disconformable karst surface developed on the Mississippian Redwall Limestone (Huddle and Dobrovolny, 1945; McKee and Gutschick, 1969) (Figs. 2 and 4, panel 3). A wide range of stratigraphic schemes have been proposed for this region, which is transitional between the siliciclastic Pennsylvanian–Permian section to the northwest and the carbonate dominated Pennsylvanian section to the southeast (e.g., Huddle and Dobrovolny, 1945; McKee and Gutschick, 1969; Brew, 1970; Ross, 1973; Blakey and Knepp, 1989) (Fig. 2). Here, we adopt the stratigraphy of Blakey and Knepp (1989), in which the Pennsylvanian Naco Group (equivalent to the Horquilla Limestone of Southeast Arizona; Ross, 1973; Brew and Beus, 1976; Blakey and Knepp, 1989) is overlain by the Permian Hermit Formation, Schnebly Hill Formation, and the Coconino Sandstone. We collected three samples from fine-grained and medium-grained

sandstones and a granule conglomerate within the Middle Pennsylvanian Naco Group; a medium-grained sandstone from the lower Permian Hermit Formation; and two samples from fine and very fine-grained sandstone of the middle Permian Schnebly Hill Formation.

Plomosa Mountains (Southwest Arizona)

The Paleozoic succession in southwestern Arizona lithologically resembles the Paleozoic section preserved within the Grand Canyon and Mogollon Rim and has been inferred to be stratigraphically and lithologically equivalent (Richard et al., 1993; Blakey, 2008) (Figs. 2 and 4, panel 2). The Plomosa Mountains are currently ~200 km southwest of the mostly undeformed western Mogollon Rim section (above), but palinspastic restoration of Basin and Range extension (not shown on figures within this study) locates the original depositional position of these strata within ~100 km of the edge of the Colorado Plateau (McQuarrie and Wernicke, 2005).

We collected one sample each from medium-grained sandstone in the basal Supai Group, coarse-grained sandstone of the lower Permian Hermit Formation, and fine-grained sandstone of the Coconino Sandstone

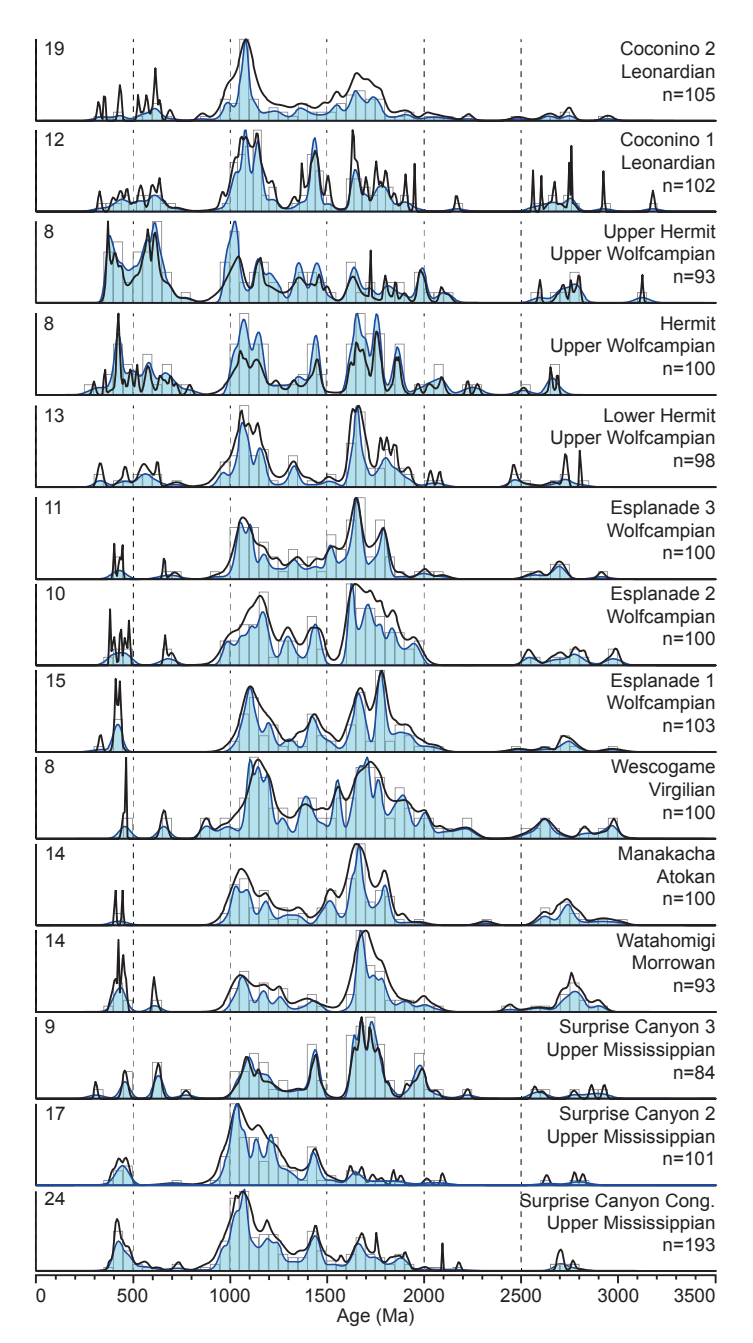


Figure 3. Detrital zircon plots of data from Grand Canyon National Park presented by Gehrels et al. (2011). Black line: Probability Density Function (PDF); blue line: Kernel Density Estimate (KDE) with bandwidth of 20 Ma; gray boxes: histogram with 50 Ma bin width; number at upper left of each plot: max value of *y*-axis for histogram.

exposed in the southern Plomosa Mountains southeast of the town of Quartzsite. These rocks are exposed in a steeply dipping, fault-bounded panel within a zone that has been subjected to multiple episodes of intense compressional and extensional deformation (Miller, 1970; Richard, 1992, 1993; Richard et al., 1993; McQuarrie and Wernicke, 2005; McQuarrie and Oskin, 2010; Spencer et al., 2015). Most late Paleozoic sedimentary rocks in this region have been intensely deformed and metamorphosed. The section sampled for this study is a rare exception and is preserved largely unmetamorphosed.

Mescal Mountains (South-Central Arizona)

The section is fault-bounded and consists of ca. 375 m of strata mapped as Pennsylvanian Horquilla Limestone deposited conformably atop Mississippian Escrabrosa Limestone (Wrucke et al., 2004) (Figs. 2 and 4, panel 4). The only siliciclastic material identified in this section was collected from 5 m of horizontally laminated, wavy-bedded, and currentripple, cross-stratified, fine-grained quartzose sandstone; one sample was collected from this interval. Data Repository File DR2 provides a detailed report on fususlinid dating of this section.

Whetstone Mountains (Southeast Arizona)

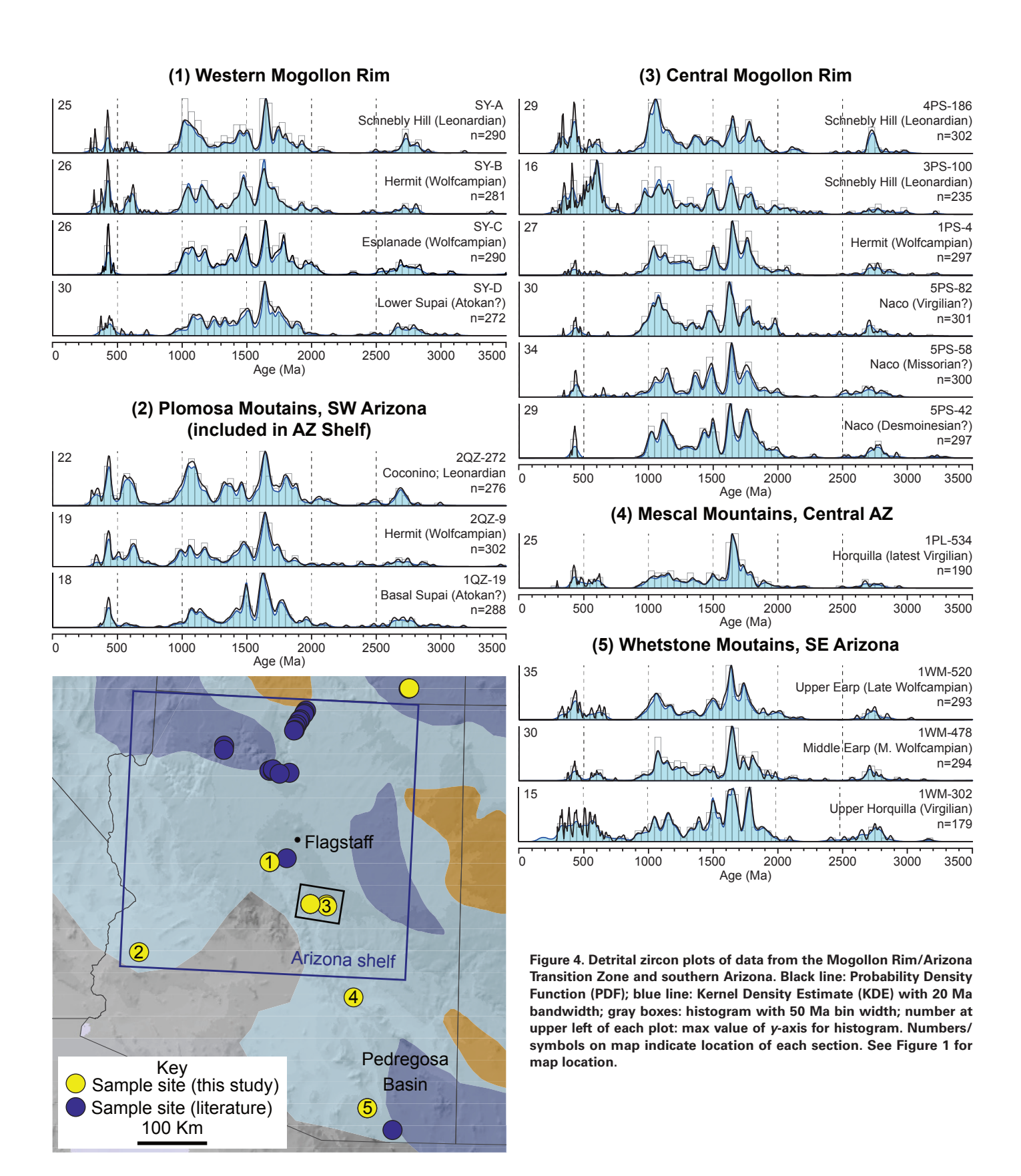
The interval sampled from this section spans Middle Pennsylvanian through middle Permian (late Wolfcampian) (Figs. 2 and 4, panel 5). We collected one sample from a green, non-calcareous siltstone within the Horquilla Limestone and two samples from the Earp Formation (Creasy, 1967). Earp Formation samples were collected from a chert granule conglomerate in the middle Earp Formation (Red Chert Conglomerate of Armin, 1987) and from a fine-grained sandstone of the upper Earp Formation.

Paradox Basin

Samples were collected from three localities along a roughly northeast-southwest transect across the central western Paradox Basin (Figs. 2 and 6, panels 1-3). These three locations span distal, medial, and proximal basin positions along this transect. In the distal basin position, we collected samples of quartzose sandstone from two localities within the Paradox Formation and three within the Honaker Trail Formation. These units consist of nested 4th and 5th order sequence stratigraphic cycles of fine-grained siliciclastic and carbonate facies (Goldhammer et al., 1991). From the medial basin section (Cane Creek), we collected one sample of quartzose sandstone from the upper Honaker Trail Formation. In the proximal basin near Gateway, Colorado, we sampled two sandstones of the Cutler Formation Undivided, deposited in buttress unconformity with crystalline rocks of the ancient Uncompangre Uplift to the northeast (Moore et al., 2008). Overall, these samples span the early Desmoinesian to Wolfcampian time. Seven samples were also collected from the eastern proximal Paradox Basin between Durango, Colorado, and just north of Ouray, Colorado (Figs. 2 and 6, panel 4). Sampled strata along this transect include the Lower Pennsylvanian Molas Formation; the middle Pennsylvanian Hermosa Group, which includes the Pinkerton Trail, Paradox, and Honaker Trail Formations; the overlying Rico Formation; and the lower Permian Cutler Formation (Campbell, 1981).

Eagle Basin and Central Colorado Trough

Pennsylvanian—Permian strata within the Eagle Basin were sampled along a generally east—west transect consisting of four detailed measured sections across the basin (Figs. 2 and 5, panels 1–4). These strata span Early Pennsylvanian through Late Pennsylvanian time. Sampled formations include the Belden (1 sample), Minturn (6 samples), the Eagle Valley (4 samples), the Eagle Valley Evaporite (1 sample), and the Maroon (4 samples). Three samples spanning Late Mississippian to Early—Middle Pennsylvanian were collected from the Central Colorado trough, the southeast extension of the Eagle Basin, northeast of Salida, Colorado, from the Leadville, Kerber, and Sharpsdale Formations (Fig. 5, panels 5–6). One sample from the Lower Pennsylvanian Belden Formation was collected near Crested Butte, Colorado (Fig. 5, panel 5).



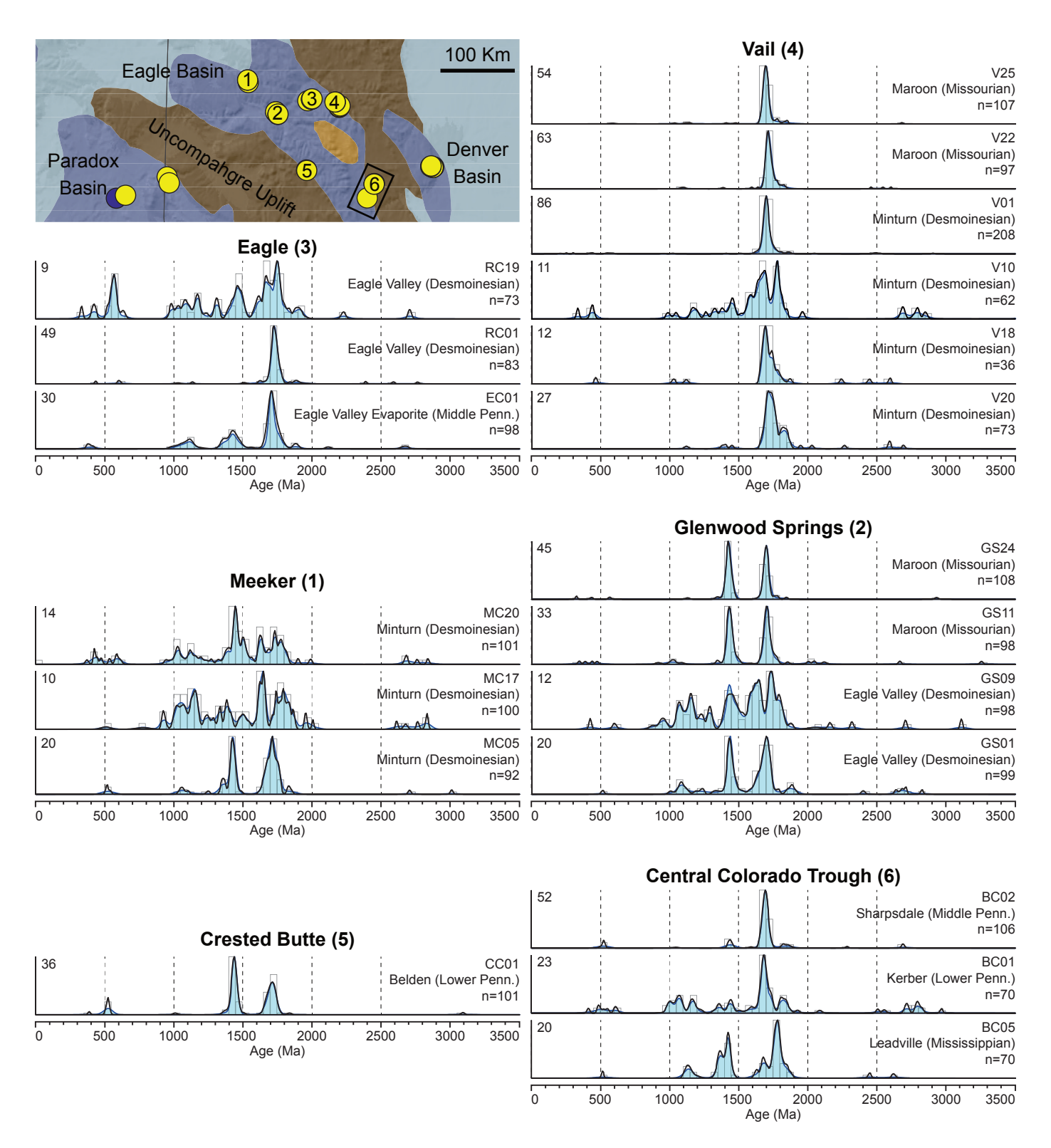
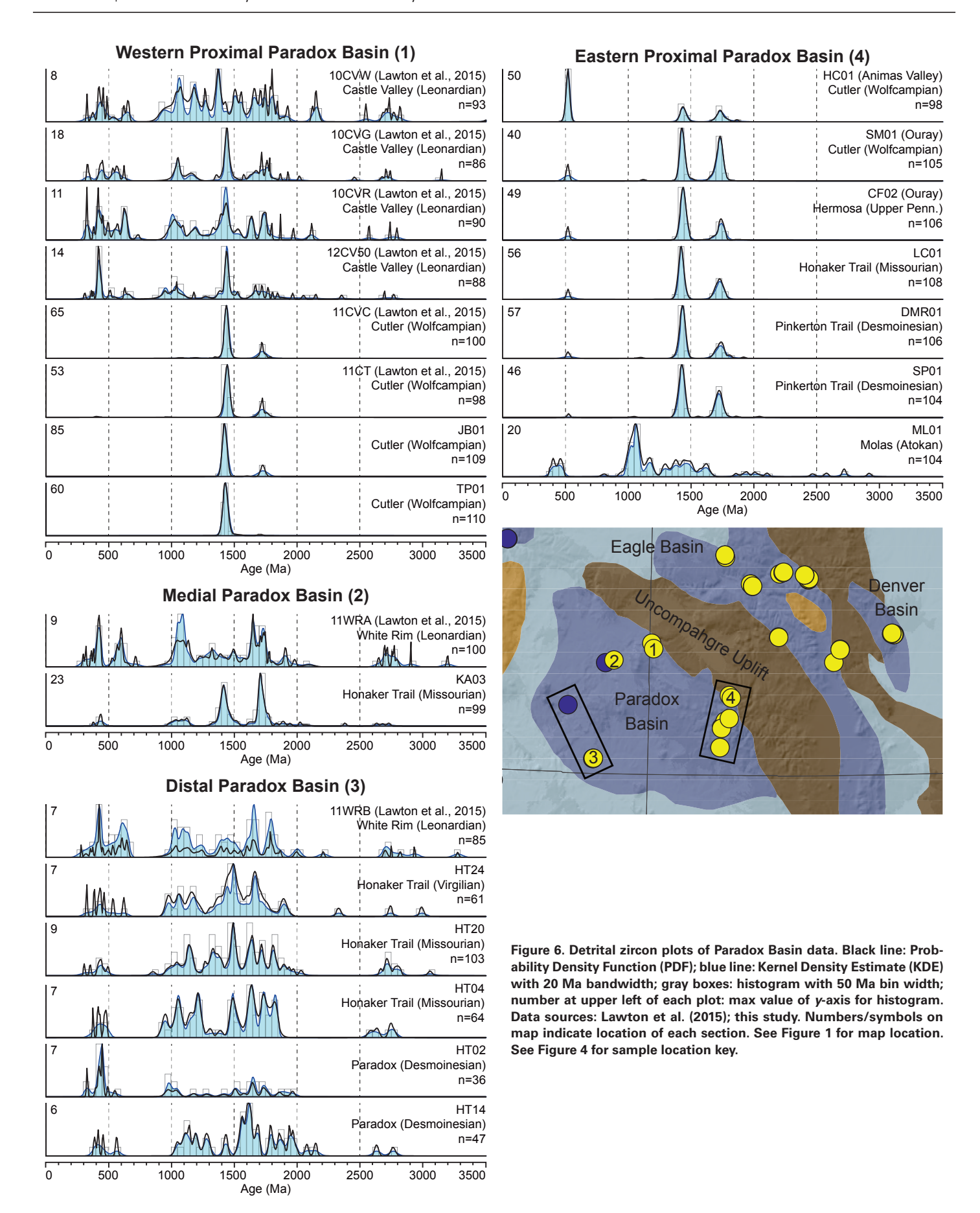


Figure 5. Detrital zircon plots of data from the Eagle Basin. Black line: Probability Density Function (PDF); blue line: Kernel Density Estimate (KDE) with 20 Ma bandwidth; gray boxes: histogram with 50 Ma bin width; number at upper left of each plot: max value of y-axis for histogram. Numbers/symbols on map indicate location of each section. See Figure 1 for map location. See Figure 4 for sample location key.



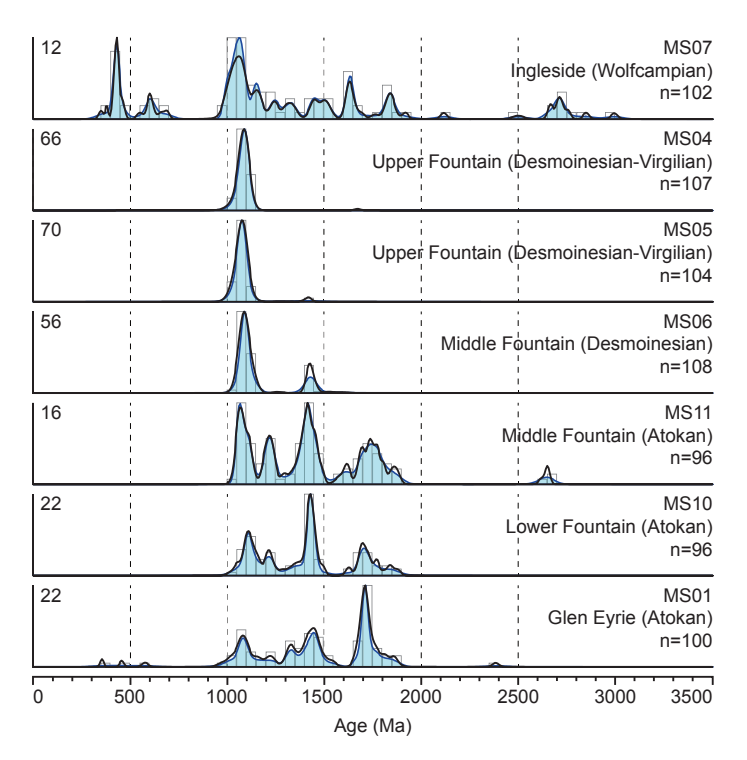


Figure 7. Detrital zircon plots of data from the Denver Basin. Black line: Probability Density Function (PDF); blue line: Kernel Density Estimate (KDE) with 20 Ma bandwidth; gray boxes: histogram with 50 Ma bin width; number at upper left of each plot: max value of y-axis for histogram. See Figures 5 or 6 for detailed sample locations.

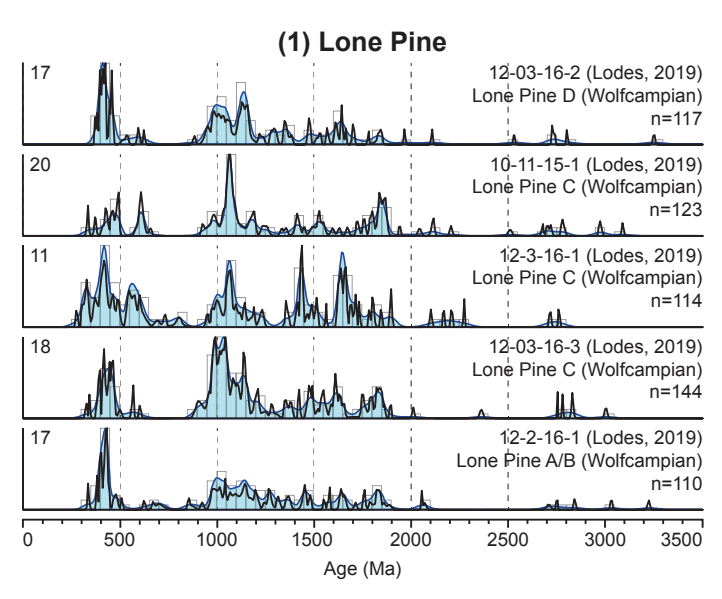
Denver Basin

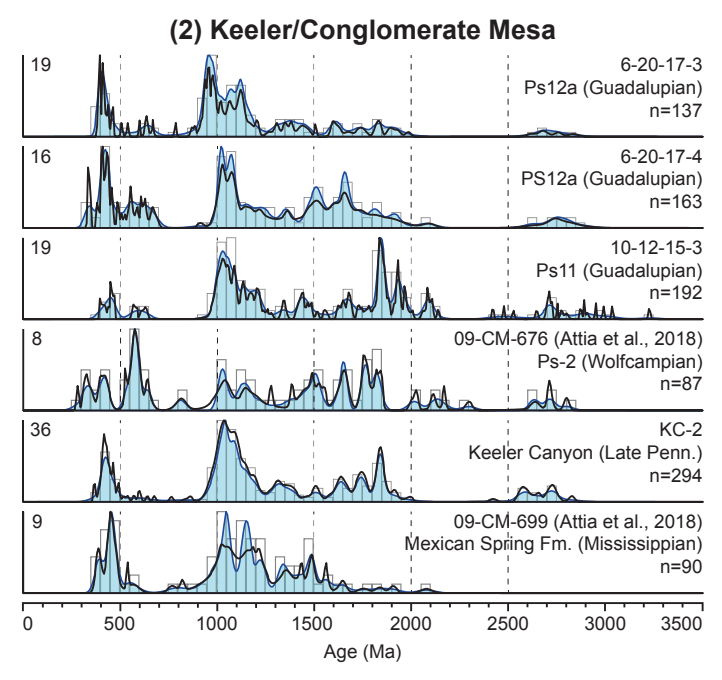
We collected six samples from the Lower Pennsylvanian Glen Eyrie Member and fluvial strata from the lower, middle, and upper Fountain Formation (Suttner et al., 1984; Sweet and Soreghan, 2010) (Figs. 2 and 7). Above this, we collected one sample from aeolian Permian rocks that were originally mapped as the Lyons Formation (Keller et al., 2005; Sweet and Soreghan, 2010) but recently reinterpreted as equivalent to the Ingleside Formation (Sweet et al., 2015). To the south, the section is in fault contact with the Pikes Peak Granite (Keller et al., 2005), a 1.09 Ga intrusive suite (Schärer and Allègre, 1982).

Keeler-Lone Pine Basin

We collected samples from Pennsylvanian and Permian rocks exposed in two areas within the southern Inyo Mountains of eastern California (Figs. 2 and 8). The northeastern area, north of Lone Pine, consists of the Pennsylvanian Keeler Canyon Formation and the overlying Permian Lone Pine Formation (Fig. 8, panel 1). Five samples were collected from the Lone Pine Formation. This formation is within the Owens Valley Group (Merriam and Hall, 1957; Stone and Stevens, 1987) and is subdivided, in ascending order, into Members A/B (1 sample), C (3 samples), D (1 sample), and the Reward Conglomerate (Stone and Stevens, 1987; Stone et al., 2000).

The other sampled area is located northeast of the town of Keeler, California (Fig. 8, panel 2). The late Paleozoic section here consists of the Keeler Canyon Formation and the informally named sedimentary rocks of Santa Rosa Flat, consisting of members 1–12 (Stone et al., 2009). Samples from calcic sandstones were collected from one location within the lower





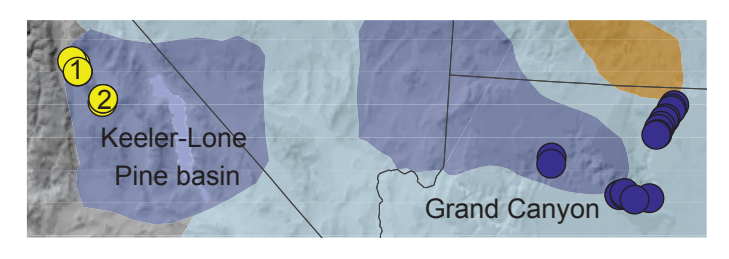


Figure 8. Detrital zircon plots of data from the Keeler–Lone Pine Basin, eastern California. Black line: Probability Density Function (PDF); blue line: Kernel Density Estimate (KDE) with 20 Ma bandwidth; gray boxes: histogram with 50 Ma bin width; number at upper left of each plot: max value of *y*-axis for histogram. See Figure 4 for location key. Numbers/symbols on map indicate location of each section. See Figure 1 for map location. Data sources: Attia et al. (2018), Lodes (2019), this study.



TABLE 1. DETRITAL ZIRCON SAMPLES, AGES, LITHOLOGIES, AND DEPOSITIONAL ENVIRONMENTS

Actions Shelf (see Fig. 4 for may locations) 202-272 Coconino Sandstone 879-100 Schneidy Hill Formation 879-100 Marabacha Formation 879-100 Maraba	Comple	Unit		Lithology and grain size	
English Engl	Sample		Age	Lithology and grain size	Interpreted depositional environment
SS-10 Schneby Hill Formation Leonardian Pine-grained sandstone Sabhka 4PS-160 Top Scheby Hill Formation Leonardian Part Programmed Sabhka 1PS-160 Top Scheby Hill Formation Leonardian Pine-grained sandstone Sabhka 4PS-160 Top Scheby Hill Formation Leonardian Pine-grained sandstone Pine-grained sand		· · · · · · · · · · · · · · · · · · ·			
SPS-100 Schneby Hill Formation Leonardian Prins-grained sandstone Fine-grained sandstone Prins-grained				· ·	· ·
4PS-18B Top Scheby Hill Formation Leonardian Fine-grained sandstone Mised shallow manie/coastal plain Fine-grained sandstone Fin		•		9	
Search Hermit Formation Lower Perminn Very fine-grained annatione Fine-grained sandstone Fine-grained sandsto		-		, ,	
SPS		'		9	
195-4 Sanal Hermit Formation SYC Lowest Esphanede Wolfcampian in Sychology Cowest Esphanede Miscontral SPS-82 Naco Formation Virgilian Missourian Sendence granule conglomente Fine-grained sandstone Sendence Granule Costal accellant under Interdistributary channel Interdistributary channel Missourian Sendence granule conglomente Fine-grained sandstone Mixed shallow marine/coastal plain Modern Missourian Medium-grained sandstone Mixed shallow marine/coastal plain Mixed Sendence Mixed Sendence Mixed Sendence Sendence Mixed Sendence Sendence Mixed Sendence Sendence Sendence Mixed Sendence Se				_	•
SPG-82 Naco Formation Missourian SPS-83 Naco Formation SPS-84 Naco Formation Missourian SPS-84 Naco Formation SPS-84 Naco Formation Missourian SPS-84 Naco Formation Demorphism Missourian SPS-84 Naco Formation Demorphism Missourian Pine-grained sandstone Missourian Corate SPS-84 Naco Formation Demorphism Missourian Pine-grained sandstone Missourian Missourian Pine-grained sandstone Missourian Missourian Pine-grained sandstone Missourian Missourian Pine-grained sandstone Carate-grained SPS-84 Naco Formation Missourian Missourian Missourian Missourian Pine-grained sandstone Demorphism Missourian Misso				, ,	
SPS-98.8 Naco Formation Missourian Fine-grained sandstone Medium-arraine/coastal plain North Manalekanha Formation Alokan Fine-grained sandstone Missourian Missourian Fine-grained sandstone Missourian Missouri	SY-C	Lowest Esplanade	•	<u> </u>	Coastal aeolian dune
SPS-42 Naco Formation Demonicesian Modern Sandstone Mixed shallow manifocoastal plain Not State of Manakacha Formation Atokan Fine-grained sandstone Mixed shallow manifocoastal plain Not State of Manakacha Formation Atokan Fine-grained sandstone Mixed shallow manifocoastal plain Demore Basin Manakacha Formation Modern Fine-grained sandstone Mixed shallow manifocoastal plain Demore Basin Mixed State of Mixed	5PS-82	Naco Formation	Virgilian	Medium-grained sandstone	Interdistributary channel
Basal Supal Group Lower Pennsylvanian Medium-grained sandstone Mixed shallow marine/coastal plain	5PS-58	Naco Formation	Missourian	Sandstone granule conglomerate	Interdistributary channel
SPCD Manakacha Formation Alokan Fine-grained sandstone Mixed shallow marine/coastal plain	5PS-42	Naco Formation	Desmoinesian	Fine-grained sandstone	Mixed shallow marine/coastal plain
Denver Basin MSO7			-	•	·
MS04 Upper Fountain Formation MS05 Upper Fountain Formation MS05 Upper Fountain Formation MS06 Upper Fountain Formation MS07 Upper Fountain Formation MS11 Modifie Pountain Formation MS11 Lower Pennsylvanian Coarse-grained acadistone Fan-delta Fan-delta MS07 Coarse-grained acadistone Fan-delta MS07 Coarse-grained acadistone Fan-delta Fan-delta MS07 Coarse-grained acadistone Fan-delta Fan-delta MS07 Coarse-grained acadistone Fan-delta MS07 Coarse-grained acadistone MS07 Coarse-grained acadistone MS07 Coarse-grained acadistone Fan-delta MS08 Coarse-grained acadistone PS09 Coarse-grained acadistone Coarse-grained acadistone PS09 Coarse-grained acadistone Coarse-grained acadistone PS09 Coarse-grained acadistone PS	SY-D	Manakacha Formation	Atokan	Fine-grained sandstone	Mixed shallow marine/coastal plain
MS96 Upper Fountial Formation Windle Pennsylvanian Coarse-grained sandstone Raided fluvial MS96 Upper Fountial Formation Middle Pennsylvanian Coarse-grained sandstone Fan-delta MS96 Upper Fountial Formation Middle Pennsylvanian Coarse-grained sandstone Fan-delta MS10 Lower Fountial Cower Pennsylvanian Coarse-grained sandstone Fan-delta MS10 Lower Fountial Lower Pennsylvanian Coarse-grained sandstone Fan-delta MS10 Lower Fountial Lower Pennsylvanian Coarse-grained sandstone Near-delta MS10 Lower Fountial MS10 Middle Pennsylvanian Coarse-grained sandstone Near-delta MS10 Missourian Fine-grained sandstone Missourian Fine-grained sandstone Missourian Fine-grained sandstone Missourian Missourian Fine-grained sandstone Missourian Missourian Fine-grained sandstone Missourian Missourian Fine-grained sandstone Fine-grain	Denver Basin				
MSDS Upper Fountain Formation Upper Femnsylvanian Coarse-grained sandstone Braided fluvial MS11 Middle Fountain Formation Middle Pennsylvanian Coarse-grained sandstone Fan-delta MS10 Clower Fountain Lower Pennsylvanian Coarse-grained sandstone Fan-delta MS01 Glen Eyrie Alokan Fine-grained sandstone Nearshore marine Central Colorado Trough/Eagle Basin GS11 Maroon Formation Missourian Medium-grained sandstone Mixed fluvial-aeolian MC20 Maroon Formation Missourian Fine-grained sandstone Mixed fluvial-aeolian V22 Maroon Formation Missourian Fine-grained sandstone Mixed fluvial-aeolian MS01 Eagle Valley Exeportee Desmoinesian Fine-grained sandstone Mixed fluvial-aeolian MC05 Minturn Formation Desmoinesian Medium-grained sandstone Restricted marine MS01 Eagle Valley Formation Desmoinesian Medium-grained sandstone Fine-delta MC05 Minturn Formation Desmoinesian Medium-grained san	MS07	Ingleside*	Wolfcampian	Fine-grained sandstone	Aeolian
MS61 Upper Fountain Formation Middle Pennsylvanian Coarse-grained sandstone Fan-delta MS11 Middle Fountain Formation MS10 Lower Fountain Lower Pennsylvanian Coarse-grained sandstone Fan-delta Septiment of MS10 Lower Pennsylvanian Coarse-grained sandstone Fan-delta Septiment MS11 MS10 MS10 MS10 MS10 MS10 MS10 MS10	MS04	Upper Fountain Formation	Upper Pennsylvanian	Coarse-grained sandstone	Braided fluvial
MS10 Lower Fountain Lower Pennylyvanian Coarse-grained sandstone Fan-delta MS01 Glen Eyrie Atokan Fine-grained sandstone Nearshore marine Contral Colorado Trough/Eagle Basin MS01 Marcon Formation Missourian Medium-grained sandstone Mixed fluvial-aeolian MS02 Marcon Formation Missourian Fine-grained sandstone Mixed fluvial-aeolian MS02 Marcon Formation Missourian Fine-grained sandstone Mixed fluvial-aeolian Fine-grained sandstone Mixed fluvial-aeolian Mixed fluvial f		• •		Coarse-grained sandstone	
MS01 Gien Eyrie Alokan Coarse-grained sandstone Fan-delta Nearshore marine Central Colorado Trough/Eagle Basin GS11 Marcon Formation Missourian Fine-grained sandstone Mixed fluvial-aeolian MC20 Marcon Formation Missourian Fine-grained sandstone Mixed fluvial-aeolian MC20 Marcon Formation Missourian Fine-grained sandstone Mixed fluvial-aeolian MC20 Marcon Formation Missourian Fine-grained sandstone Mixed fluvial-aeolian MC25 Marcon Formation Missourian Fine-grained sandstone Mixed fluvial-aeolian MC26 Marcon Formation Missourian Fine-grained sandstone Mixed fluvial-aeolian MC26 Marcon Formation Missourian Fine-grained sandstone Mixed fluvial-aeolian MC27 Marcon Formation Missourian Fine-grained sandstone Mixed fluvial-aeolian MC27 Marcon Formation Desmoinesian Medium-grained sandstone Restricted marine MC36 Minturn Formation Desmoinesian Medium-grained sandstone Fan-delta GS01 Eagle Valley Formation Desmoinesian Medium-grained sandstone Restricted marine MC17 Minturn Formation Desmoinesian Medium-grained sandstone Restricted marine PC20 Minturn Formation Desmoinesian Pebble conglomerate Fan-delta Mc17 Minturn Formation Desmoinesian Medium-grained sandstone Fan-delta Mc17 Minturn Formation Desmoinesian Medium-grained sandstone Fan-delta RC01 Eagle Valley Formation Desmoinesian Medium-grained sandstone Restricted marine PC19 Eagle Valley Formation Desmoinesian Medium-grained sandstone Restricted marine MC19 Minturn Formation Desmoinesian Medium-grained sandstone Restricted marine PC19 Eagle Valley Formation Desmoinesian Medium-grained sandstone Restricted marine Mc19 Minturn Formation Desmoinesian Medium-grained sandstone Restricted marine Mc20 Sharpsdale Formation Desmoinesian Medium-grained sandstone Restricted marine Mc20 Moltram Molt		• •	-	•	
MSO1 Glen Eyrie Alokan Fine-grained sandstone Nearshore marine				_	
Central Colorado Trough/Eagle Basin GS11 Maroon Formation Missourian Medium-grained sandstone Mixed fluvial-aeolian Mc20 Maroon Formation Missourian Fine-grained sandstone Mixed fluvial-aeolian V22 Maroon Formation Missourian Fine-grained sandstone Mixed fluvial-aeolian Medium-grained sandstone Restricted marine Mixed fluvial-aeolian Mixed fluvial-aeolian Medium-grained sandstone Particled marine Pable conjoineriate Flan-delta Medium-grained sandstone Mixed fluvial-aeolian Mixed fluvial-aeolian Medium-grained sandstone Particled marine Pable conjoinerialed sandstone Medium-grained sandstone Particled marine Medium-grained sandstone Particled marine Medium-grained sandstone Mixed fluvial-aeolian Mixed fluvial-aeolian Medium-grained sandstone Particled marine Medium-grained sandstone Mixed fluvial-aeolian Mixed fluvial-aeolian Medium-grained sandstone Medium-grained sandstone Shallow marine Medium-grained sandstone Mixed fluvial-aeolian			-	•	
Missourian Medium-grained sandstone Mixed fluvial-aeolian Mixed	MS01	Glen Eyrie	Atokan	Fine-grained sandstone	Nearshore marine
Mc20 Marcon Formation Missourian Fine-grained sandstone Mixed fluvial-aeolian V22 Marcon Formation Missourian Fine-grained sandstone Mixed fluvial-aeolian S24 Marcon Formation Missourian Fine-grained sandstone Mixed fluvial-aeolian S24 Marcon Formation Missourian Fine-grained sandstone Mixed fluvial-aeolian S05 Mintum Formation Desmoinesian Medium-rigariand sandstone Restricted marine GS09 Eagle Valley Formation Desmoinesian Medium-rigariand sandstone Fastricted marine MC17 Mintum Formation Desmoinesian Coarse-grained sandstone Fastricted marine V18 Mintum Formation Desmoinesian Pebble conglomerate Fan-delta RC01 Eagle Valley Formation Desmoinesian Medium-grained sandstone Fastricted marine RC19 Eagle Valley Formation Desmoinesian Medium-grained sandstone Restricted marine RC19 Eagle Valley Formation Desmoinesian Medium-grained sandstone Fan-delta RC20 <	Central Color	ado Trough/Eagle Basin			
V22 Maroon Formation Missourian Medium-grained sandstone Mixed fluvial-aeolian GS24 Maroon Formation Missourian Fine-grained sandstone Mixed fluvial-aeolian EC01 Eagle Valley Evaporite Desmoinesian Medium-fine-grained sandstone Restricted marine MC05 Mintum Formation Desmoinesian Medium-fine-grained sandstone Fan-delta GS09 Eagle Valley Formation Desmoinesian Medium-grained sandstone Restricted marine MC17 Mintum Formation Desmoinesian Fine-grained sandstone Fastricted marine MC17 Mintum Formation Desmoinesian Febbe conglomerate Fan-delta MC01 Eagle Valley Formation Desmoinesian Medium-grained sandstone Restricted marine RC01 Eagle Valley Formation Desmoinesian Medium-grained sandstone Restricted marine RC19 Eagle Valley Formation Desmoinesian Medium-grained sandstone Fastricted marine RC19 Eagle Valley Formation Desmoinesian Medium-grained sandstone Fastricted marine <t< td=""><td>GS11</td><td>Maroon Formation</td><td>Missourian</td><td>Medium-grained sandstone</td><td>Mixed fluvial-aeolian</td></t<>	GS11	Maroon Formation	Missourian	Medium-grained sandstone	Mixed fluvial-aeolian
Nazon Formation Missourian Fine-grained sandstone Mixed fluvial-aeolian EC01 Eagle Valley Evaporite Desmoinesian Medium-fine-grained sandstone Fan-delta Bagle Valley Formation Desmoinesian Medium-fine-grained sandstone Fan-delta Bagle Valley Formation Desmoinesian Medium-grained sandstone Restricted marine RS09 Eagle Valley Formation Desmoinesian Medium-grained sandstone Restricted marine MC17 Minturn Formation Desmoinesian Medium-grained sandstone Restricted marine MC17 Minturn Formation Desmoinesian Fine-grained sandstone Fan-delta Minturn Formation Desmoinesian Fine-grained sandstone Fan-delta Part Minturn Formation Desmoinesian Medium-grained sandstone Fan-delta Part Part Part Part Part Part Part Pa	MC20	Maroon Formation	Missourian	Fine-grained sandstone	Mixed fluvial-aeolian
GS24 Maroon Formation ECO1 Eagle Valley Evaporite Desmoinesian Medium-fine-grained sandstone Restricted marine Fine-GS01 Eagle Valley Evaporite Desmoinesian Medium-grained sandstone Fan-delta Restricted marine GS09 Eagle Valley Formation Desmoinesian Medium-grained sandstone Restricted marine GS09 Eagle Valley Formation Desmoinesian Coarse-grained sandstone Restricted marine GS09 Eagle Valley Formation Desmoinesian Fine-grained sandstone Fan-delta Minturn Formation Desmoinesian Pebble conglomerate Fan-delta Pan-delta Minturn Formation Desmoinesian Medium-grained sandstone Fan-delta Pan-delta Pan-del	V22	Maroon Formation	Missourian	Medium-grained sandstone	Mixed fluvial-aeolian
ECO1 Eagle Valley Evaporite Desmoinesian Medium-fine-grained sandstone Restricted marine MC05 Mintum Formation Desmoinesian Medium-grained sandstone Restricted marine GS01 Eagle Valley Formation Desmoinesian Medium-grained sandstone Restricted marine MC17 Mintum Formation Desmoinesian Fine-grained sandstone Fan-delta V18 Mintum Formation Desmoinesian Medium-grained sandstone Fan-delta V20 Mintum Formation Desmoinesian Medium-grained sandstone Fan-delta RC01 Eagle Valley Formation Desmoinesian Medium-grained sandstone Restricted marine RC19 Eagle Valley Formation Desmoinesian Medium-grained sandstone Restricted marine RC19 Eagle Valley Formation Desmoinesian Medium-grained sandstone Fan-delta RC19 Sharpsdale Formation Desmoinesian Medium-grained sandstone Fan-delta RC20 Sharpsdale Formation Lower Pennsylvanian Medium-grained sandstone Shallow marine RC01				9	
MCO5 Minturn Formation Desmoinesian Fine-grained sandstone Restricted marine				· ·	
GS01 Eagle Valley Formation Desmoinesian Medium-grained sandstone Restricted marine MC17 Minturn Formation Desmoinesian Fine-grained sandstone Fan-delta V18 Minturn Formation Desmoinesian Fine-grained sandstone Fan-delta V20 Minturn Formation Desmoinesian Medium-grained sandstone Fan-delta V20 Minturn Formation Desmoinesian Medium-grained sandstone Fan-delta RC01 Eagle Valley Formation Desmoinesian Medium-grained sandstone Restricted marine RC19 Eagle Valley Formation Desmoinesian Fine-grained sandstone Restricted marine Page V10 Minturn Formation Desmoinesian Fine-grained sandstone Restricted marine V10 Minturn Formation Desmoinesian Medium-grained sandstone Fan-delta V11 Minturn Formation Desmoinesian Medium-grained sandstone Fan-delta V11 Minturn Formation Desmoinesian Medium-grained sandstone Fan-delta V11 Minturn Formation Desmoinesian Medium-fine-grained sandstone Shallow marine DC01 Rerie Formation Morrowan Medium-fine-grained sandstone Shallow marine DC01 Belden Formation Morrowan Medium-fine-grained sandstone Shallow marine Dc01 Belden Formation Morrowan Medium-fine-grained sandstone Delta-front Desco Leadville Limestone Mississippian Limestone Carbonate shelf V11 Desco V11 Desc					
GS09 Eagle Valley Formation Desmoinesian Coarse-grained sandstone Restricted marine MC17 Mintum Formation Desmoinesian Fine-grained sandstone Fan-delta V20 Mintum Formation Desmoinesian Medium-grained sandstone Fan-delta RC01 Eagle Valley Formation Desmoinesian Medium-grained sandstone Restricted marine RC19 Eagle Valley Formation Desmoinesian Medium-grained sandstone Restricted marine V10 Mintum Formation Desmoinesian Medium-grained sandstone Restricted marine V10 Mintum Formation Desmoinesian Medium-grained sandstone Fan-delta BC02 Sharpsdale Formation Morrowan Medium-fine-grained sandstone Shallow marine BC01 Kerber Formation Morrowan Medium-fine-grained sandstone Shallow marine BC05 Leadville Limestone Mississippian Carse-grained sandstone Alluvial fan BC05 Leadville Limestone Wolfcampian Coarse-grained sandstone Alluvial fan MD01 Cutler Undivide				9	
NC17 Mintum Formation Desmoinesian Fine-grained sandstone Fan-delta Will Mintum Formation Desmoinesian Pebble conglomerate Fan-delta Pan-delta Pan				_	
V18 Mintum Formation Desmoinesian Pebble conglomerate Fan-delta V20 Mintum Formation Desmoinesian Medium-grained sandstone Restricted marine RC19 Eagle Valley Formation Desmoinesian Medium-grained sandstone Restricted marine RC19 Eagle Valley Formation Desmoinesian Medium-grained sandstone Restricted marine V10 Mintum Formation Desmoinesian Medium-grained sandstone Fan-delta V01 Mintum Formation Desmoinesian Medium-fine-grained sandstone Fan-delta BC02 Sharpsdale Formation Morrowan Medium-fine-grained sandstone Shallow marine BC01 Kerber Formation Lower Pennsylvanian Medium-fine-grained sandstone Shallow marine BC05 Leadville Limestone Morrowan Medium-fine-grained sandstone Delta-front BC05 Leadville Limestone Wolfcampian Coarse-grained sandstone Alluvial fan HC01 Cutler Undivided Wolfcampian Coarse-grained sandstone Alluvial fan MB01 Cutler Undivide		9		9	
V20 Minturn Formation Desmoinesian Medium-grained sandstone Fan-delta RC01 Eagle Valley Formation Desmoinesian Medium-grained sandstone Restricted marine RC19 Eagle Valley Formation Desmoinesian Fine-grained sandstone Fan-delta V10 Minturn Formation Desmoinesian Medium-grained sandstone Fan-delta BC02 Sharpsdale Formation Morrowan Medium-fine-grained sandstone Shallow marine BC01 Kerber Formation Lower Pennsylvanian Medium-fine-grained sandstone Shallow marine BC05 Leadville Limestone Mississippian Limestone Carbonate shelf Pravadox Basin HC01 Cutler Undivided Wolfcampian Coarse-grained sandstone Alluvial fan SM01 Cutler Undivided Wolfcampian Coarse-grained sandstone Alluvial fan HC01 Cutler Undivided Wolfcampian Coarse-grained sandstone Alluvial fan HC01 Cutler Undivided Wolfcampian Coarse-grained sandstone Calvonate shelf				9	
RC01 Eagle Valley Formation Desmoinesian Medium-grained sandstone Restricted marine RC19 Eagle Valley Formation Desmoinesian Fine-grained sandstone Restricted marine V10 Minturn Formation Desmoinesian Medium-grained sandstone Fan-delta V11 Minturn Formation Desmoinesian Medium-grained sandstone Fan-delta V12 Medium-grained sandstone Shallow marine RC10 Merber Formation Lower Pennsylvanian Medium-fine-grained sandstone Shallow marine RC10 Refree Formation Morrowan Medium-fine-grained sandstone Shallow marine Delta-front RC10 Redefine Formation Morrowan Medium-fine-grained sandstone Delta-front Delta-front RC10 RC20 R					
V10 Minturn Formation Minturn Formation Desmoinesian Desmoinesian Medium-grained sandstone Medium-fine-grained sandstone Fan-delta Fan-delta BCO2 Sharpsdale Formation Kerber Formation Lower Pennsylvanian Morrowan Medium-fine-grained sandstone Shallow marine BCO1 Kerber Formation Belden Formation Lower Pennsylvanian Morrowan Medium-fine-grained sandstone Shallow marine BCO5 Leadville Limestone Delta-front Delta-front BCO5 Leadville Limestone Carbonate shelf Praradox Basin HCO1 Cutler Undivided Wolfcampian Coarse-grained sandstone Alluvial fan SM01 Cutler Undivided Wolfcampian Coarse-grained sandstone Alluvial fan HT01 Cutler Undivided Wolfcampian Coarse-grained sandstone Alluvial fan HT02 Cutler Undivided Wolfcampian Coarse-grained sandstone Alluvial fan HT24 Honaker Trail Formation Virgilian Fine-grained sandstone Carbonate shelf LC01 Honaker Trail Formation Missourian Medium-grained sandstone Carbonate s	RC01	Eagle Valley Formation	Desmoinesian	<u> </u>	Restricted marine
V01 Minturn Formation Desmoinesian Medium-grained sandstone Fan—delta BC02 Sharpsdale Formation Morrowan Medium-fine-grained sandstone Shallow marine BC01 Kerber Formation Lower Pennsylvanian Medium-fine-grained sandstone Shallow marine CC01 Belden Formation Morrowan Medium-fine-grained sandstone Delta-front BC05 Leadville Limestone Mississippian Limestone Carbonate shelf Paradox Basin HC01 Cutler Undivided Wolfcampian Coarse-grained sandstone Alluvial fan SM01 Cutler Undivided Wolfcampian Coarse-grained sandstone Alluvial fan JB01 Cutler Undivided Wolfcampian Coarse-grained sandstone Alluvial fan HT24 Honaker Trail Formation Virgilian Fine-grained sandstone Carbonate shelf LC01 Honaker Trail Formation Virgilian Fine-grained sandstone Carbonate shelf HT20 Honaker Trail Formation Missourian Medium-fine-grained sandstone Carbonate shelf <	RC19	Eagle Valley Formation	Desmoinesian	Fine-grained sandstone	Restricted marine
BC02 Sharpsdale Formation Morrowan Medium-fine-grained sandstone Shallow marine BC01 Kerber Formation Lower Pennsylvanian Medium-fine-grained sandstone Shallow marine CC01 Belden Formation Morrowan Medium-fine-grained sandstone Delta-front BC05 Leadville Limestone Mississippian Limestone Carbonate shelf Paradox Basin HC01 Cutler Undivided Wolfcampian Coarse-grained sandstone Alluvial fan SM01 Cutler Undivided Wolfcampian Coarse-grained sandstone Alluvial fan JB01 Cutler Undivided Wolfcampian Coarse-grained sandstone Alluvial fan HT24 Honaker Trail Formation Virgilian Fine-grained sandstone Carbonate shelf LC01 Honaker Trail Missourian Wery fine-grained sandstone Carbonate shelf HT20 Honaker Trail Formation Missourian Medium-fine-grained sandstone Carbonate shelf KA03 Honaker Trail Formation Missourian Medium-fine-grained sandstone Carbonate shelf	V10	Minturn Formation	Desmoinesian	Medium-grained sandstone	Fan-delta
BC01 Kerber Formation Belden Formation Lower Pennsylvanian Morrowan Medium-fine—grained sandstone Medium-fine—grained sandstone Shallow marine Delta—front Belden Formation BC05 Leadville Limestone Mississippian Limestone Carbonate shelf Paradox Basin HC01 Cutler Undivided Wolfcampian Coarse-grained sandstone Alluvial fan SM01 Cutler Undivided Wolfcampian Coarse-grained sandstone Alluvial fan JB01 Cutler Undivided Wolfcampian Coarse-grained sandstone Alluvial fan JB01 Cutler Undivided Wolfcampian Coarse-grained sandstone Alluvial fan JB01 Cutler Undivided Wolfcampian Coarse-grained sandstone Alluvial fan HT24 Honaker Trail Formation Virgilian Fine-grained sandstone Carbonate shelf LC01 Honaker Trail Formation Missourian Medium-grained sandstone Carbonate shelf HT20 Honaker Trail Formation Missourian Medium-grained sandstone Carbonate shelf KA03 Honaker Trail Formation Missouria			Desmoinesian		
CC01 Belden Formation Leadville Limestone Morrowan Mississippian Medium-fine-grained sandstone Limestone Delta-front Carbonate shelf Paradox Basin HC01 Cutler Undivided Wolfcampian Coarse-grained sandstone Alluvial fan SM01 Cutler Undivided Wolfcampian Coarse-grained sandstone Alluvial fan JBO1 Cutler Undivided Wolfcampian Coarse-grained sandstone Carbonate shelf LC01 Honaker Trail Missourian medium-fine-grained sandstone Carbonate shelf LC01 Honaker Trail Formation Missourian Medium-grained sandstone Carbonate shelf KA03 Honaker Trail Formation Missourian Medium-grained sandstone				S .	
BC05 Leadville Limestone Mississippian Limestone Carbonate shelf Paradox Basin HC01 Cutler Undivided Wolfcampian Coarse-grained sandstone Alluvial fan SM01 Cutler Undivided Wolfcampian Coarse-grained sandstone Alluvial fan JBO1 Cutler Undivided Wolfcampian Coarse-grained sandstone Carbonate shelf LC01 Honaker Trail Formation Missourian Fine-grained sandstone Carbonate shelf HT04 Lower Honaker Trail Missourian Medium-grained sandstone Carbonate shelf HT20 Honaker Trail Formation Missourian Medium-grained sandstone Carbonate shelf KA03 Honaker Trail Formation Missourian Medium-fine-grained sandstone Shallow marine			-	<u> </u>	
Paradox Basin HC01 Cutler Undivided Wolfcampian Coarse-grained sandstone Alluvial fan SM01 Cutler Undivided Wolfcampian Coarse-grained sandstone Alluvial fan JB01 Cutler Undivided Wolfcampian Coarse-grained sandstone Carbonate shelf LC01 Honaker Trail Formation Missourian Very fine-grained sandstone Carbonate shelf KA03 Honaker Trail Formation Missourian Medium-grained sandstone Carbonate shelf KA03 Hornosa Group Middle-Upper Pennsylvanian medium-fine-grained sandstone Carbonate shelf				<u> </u>	
HC01 Cutler Undivided Wolfcampian Coarse-grained sandstone Alluvial fan SM01 Cutler Undivided Wolfcampian Coarse-grained sandstone Alluvial fan TP01 Cutler Undivided Wolfcampian Coarse-grained sandstone Alluvial fan JB01 Cutler Undivided Wolfcampian Coarse-grained sandstone Alluvial fan JB01 Cutler Undivided Wolfcampian Coarse-grained sandstone Alluvial fan HT24 Honaker Trail Formation Virgilian Fine-grained sandstone Carbonate shelf LC01 Honaker Trail Missourian medium-fine-grained sandstone Carbonate shelf HT04 Lower Honaker Trail Missourian Wery fine-grained sandstone Carbonate shelf HT20 Honaker Trail Formation Missourian Medium-grained sandstone Carbonate shelf CF02 Hermosa Group Middle—Upper Pennsylvanian Medium-grained sandstone Carbonate shelf CF02 Hermosa Group Middle—Upper Pennsylvanian medium-fine-grained sandstone Shallow marine HT02 Paradox Formation Desmoinesian Very fine-grained sandstone Carbonate shelf HT14 Paradox Formation Desmoinesian Fine-grained sandstone Carbonate shelf SP01 Pinkerton Trail—Hermosa Desmoinesian medium-fine-grained sandstone Shallow marine DMR01 Pinkerton Trail—Hermosa Desmoinesian medium-fine-grained sandstone Shallow marine ML01 Molas Formation Atokan Very fine-grained sandstone Fluvial/aeolian Central/Southeastern Arizona Basins Prv Rain Valley Formation Guadalupian Medium-fine—grained sandstone Carbonate shelf MM-478 Middle Earp Formation Wolfcampian Graule conglomerate Braided fluvial MWM-520 Upper Earp Formation Wolfcampian Fine-grained sandstone Marginal marine HWM-302 Horquilla Formation Virgilian Non-calcareous siltstone Carbonate shelf	BC05	Leadville Limestone	Mississippian	Limestone	Carbonate shelf
SM01Cutler UndividedWolfcampianCoarse-grained sandstoneAlluvial fanTP01Cutler UndividedWolfcampianCoarse-grained sandstoneAlluvial fanJBO1Cutler UndividedWolfcampianCoarse-grained sandstoneAlluvial fanHT24Honaker Trail FormationVirgilianFine-grained sandstoneCarbonate shelfLC01Honaker TrailMissourianWery fine-grained sandstoneCarbonate shelfHT04Lower Honaker TrailMissourianWery fine-grained sandstoneCarbonate shelfHT20Honaker Trail FormationMissourianMedium-grained sandstoneCarbonate shelfKA03Honaker Trail FormationMissourianMedium-grained sandstoneCarbonate shelfCF02Hermosa GroupMiddle—Upper Pennsylvanianmedium-fine-grained sandstoneShallow marineHT02Paradox FormationDesmoinesianVery fine-grained sandstoneCarbonate shelfHT14Paradox FormationDesmoinesianFine-grained sandstoneCarbonate shelfSP01Pinkerton Trail-HermosaDesmoinesianmedium-fine-grained sandstoneShallow marineDMR01Pinkerton Trail-HermosaDesmoinesianmedium-fine-grained sandstoneShallow marineML01Molas FormationAtokanVery fine-grained sandstoneCarbonate shelfCentral/Southeastern Arizona BasinsPrvRain Valley FormationGuadalupianMedium-fine-grained sandstoneCarbonate shelf1WM-478Middle Earp Formation<	Paradox Basi	<u>1</u>			
TP01 Cutler Undivided Wolfcampian Coarse-grained sandstone Alluvial fan JBO1 Cutler Undivided Wolfcampian Coarse-grained sandstone Alluvial fan Coarse-grained sandstone Alluvial fan Coarse-grained sandstone Alluvial fan TF124 Honaker Trail Formation Virgilian Fine-grained sandstone Carbonate shelf LC01 Honaker Trail Missourian medium-fine-grained sandstone Carbonate shelf HT04 Lower Honaker Trail Missourian Very fine-grained sandstone Carbonate shelf HT20 Honaker Trail Formation Missourian Medium-grained sandstone Carbonate shelf KA03 Honaker Trail Formation Missourian Medium-grained sandstone Carbonate shelf KA03 Honaker Trail Formation Missourian Medium-grained sandstone Carbonate shelf CF02 Hermosa Group Middle—Upper Pennsylvanian medium-fine—grained sandstone Shallow marine HT04 Paradox Formation Desmoinesian Very fine-grained sandstone Carbonate shelf SP01 Pinkerton Trail—Hermosa Desmoinesian Fine-grained sandstone Carbonate shelf SP01 Pinkerton Trail—Hermosa Desmoinesian medium-fine—grained sandstone Shallow marine ML01 Molas Formation Atokan Very fine-grained sandstone Shallow marine ML01 Molas Formation Guadalupian Medium-fine—grained sandstone Carbonate shelf Kaibab Formation Guadalupian Medium-fine—grained sandstone Carbonate shelf Kaibab Formation Guadalupian Medium-fine—grained sandstone Carbonate shelf MM-478 Middle Earp Formation Wolfcampian Granule conglomerate Braided fluvial 1WM-520 Upper Earp Formation Wolfcampian Fine-grained sandstone Marginal marine 1WM-302 Horquilla Formation Virgilian Non-calcareous siltstone Carbonate shelf	HC01	Cutler Undivided	Wolfcampian	Coarse-grained sandstone	Alluvial fan
JBO1Cutler UndividedWolfcampianCoarse-grained sandstoneAlluvial fanHT24Honaker Trail FormationVirgilianFine-grained sandstoneCarbonate shelfLC01Honaker TrailMissourianmedium-fine-grained sandstoneCarbonate shelfHT04Lower Honaker TrailMissourianVery fine-grained sandstoneCarbonate shelfHT20Honaker Trail FormationMissourianMedium-grained sandstoneCarbonate shelfKA03Honaker Trail FormationMissourianMedium-grained sandstoneCarbonate shelfCF02Hermosa GroupMiddle-Upper Pennsylvanianmedium-fine-grained sandstoneShallow marineHT02Paradox FormationDesmoinesianVery fine-grained sandstoneCarbonate shelfHT14Paradox FormationDesmoinesianFine-grained sandstoneCarbonate shelfSP01Pinkerton Trail-HermosaDesmoinesianmedium-fine-grained sandstoneShallow marineDMR01Pinkerton Trail-HermosaDesmoinesianmedium-fine-grained sandstoneShallow marineML01Molas FormationAtokanVery fine-grained sandstoneFluvial/aeolianCentral/Southeastern Arizona BasinsFormationMedium-fine-grained sandstoneCarbonate shelfPrvRain Valley FormationGuadalupianMedium-fine-grained sandstoneCarbonate shelf1WM-478Middle Earp FormationWolfcampianGranule conglomerateBraided fluvial1WM-520Upper Earp FormationWolfcampianFine-grained sandstone			·	•	
HT24 Honaker Trail Formation Virgilian Fine-grained sandstone Carbonate shelf LC01 Honaker Trail Missourian medium-fine-grained sandstone Carbonate shelf HT04 Lower Honaker Trail Missourian Very fine-grained sandstone Carbonate shelf HT20 Honaker Trail Formation Missourian Medium-grained sandstone Carbonate shelf HT20 Honaker Trail Formation Missourian Medium-grained sandstone Carbonate shelf KA03 Honaker Trail Formation Missourian Medium-grained sandstone Carbonate shelf CF02 Hermosa Group Middle—Upper Pennsylvanian medium-fine—grained sandstone Shallow marine HT02 Paradox Formation Desmoinesian Very fine-grained sandstone Carbonate shelf HT14 Paradox Formation Desmoinesian Fine-grained sandstone Carbonate shelf SP01 Pinkerton Trail—Hermosa Desmoinesian medium-fine—grained sandstone Shallow marine DMR01 Pinkerton Trail—Hermosa Desmoinesian medium-fine—grained sandstone Shallow marine ML01 Molas Formation Atokan Very fine-grained sandstone Fluvial/aeolian Central/Southeastern Arizona Basins Prv Rain Valley Formation Guadalupian Medium-fine—grained sandstone Carbonate shelf pk0125151 Kaibab Formation Guadalupian Medium-fine—grained sandstone Carbonate shelf 1WM-478 Middle Earp Formation Wolfcampian Granule conglomerate Braided fluvial 1WM-520 Upper Earp Formation Volfcampian Fine-grained sandstone Marginal marine 1WM-302 Horquilla Formation Virgilian Non-calcareous siltstone Carbonate shelf			·	9	
LC01Honaker TrailMissourianmedium-fine-grained sandstoneCarbonate shelfHT04Lower Honaker TrailMissourianVery fine-grained sandstoneCarbonate shelfHT20Honaker Trail FormationMissourianMedium-grained sandstoneCarbonate shelfKA03Honaker Trail FormationMissourianMedium-grained sandstoneCarbonate shelfCF02Hermosa GroupMiddle-Upper Pennsylvanianmedium-fine-grained sandstoneShallow marineHT02Paradox FormationDesmoinesianVery fine-grained sandstoneCarbonate shelfHT14Paradox FormationDesmoinesianFine-grained sandstoneCarbonate shelfSP01Pinkerton Trail-HermosaDesmoinesianmedium-fine-grained sandstoneShallow marineDMR01Pinkerton Trail-HermosaDesmoinesianmedium-fine-grained sandstoneShallow marineML01Molas FormationAtokanVery fine-grained sandstoneShallow marineML01Molas FormationAtokanVery fine-grained sandstoneCarbonate shelfCentral/Southeastern Arizona BasinsPrvRain Valley FormationGuadalupianMedium-fine-grained sandstoneCarbonate shelf1WM-478Middle Earp FormationWolfcampianGranule conglomerateBraided fluvial1WM-520Upper Earp FormationWolfcampianFine-grained sandstoneCarbonate shelf			•	•	
HT04 Lower Honaker Trail Missourian Very fine-grained sandstone Carbonate shelf HT20 Honaker Trail Formation Missourian Medium-grained sandstone Carbonate shelf KA03 Honaker Trail Formation Missourian Medium-grained sandstone Carbonate shelf CF02 Hermosa Group Middle—Upper Pennsylvanian medium-fine—grained sandstone Shallow marine HT02 Paradox Formation Desmoinesian Very fine-grained sandstone Carbonate shelf HT14 Paradox Formation Desmoinesian Fine-grained sandstone Carbonate shelf HT14 Pinkerton Trail—Hermosa Desmoinesian medium-fine—grained sandstone Shallow marine DMR01 Pinkerton Trail—Hermosa Desmoinesian medium-fine—grained sandstone Shallow marine ML01 Molas Formation Atokan Very fine-grained sandstone Fluvial/aeolian Central/Southeastern Arizona Basins Prv Rain Valley Formation Guadalupian Medium-fine—grained sandstone Carbonate shelf pk0125151 Kaibab Formation Guadalupian Medium-fine—grained sandstone Carbonate shelf 1WM-478 Middle Earp Formation Wolfcampian Granule conglomerate Braided fluvial 1WM-520 Upper Earp Formation Wolfcampian Fine-grained sandstone Marginal marine 1WM-302 Horquilla Formation Virgilian Non-calcareous siltstone Carbonate shelf			<u> </u>	8	
HT20 Honaker Trail Formation Missourian Medium-grained sandstone Carbonate shelf KA03 Honaker Trail Formation Missourian Medium-grained sandstone Carbonate shelf CF02 Hermosa Group Middle—Upper Pennsylvanian medium-fine—grained sandstone Shallow marine HT02 Paradox Formation Desmoinesian Very fine-grained sandstone Carbonate shelf HT14 Paradox Formation Desmoinesian Fine-grained sandstone Carbonate shelf SP01 Pinkerton Trail—Hermosa Desmoinesian medium-fine—grained sandstone Shallow marine DMR01 Pinkerton Trail—Hermosa Desmoinesian medium-fine—grained sandstone Shallow marine ML01 Molas Formation Atokan Very fine-grained sandstone Fluvial/aeolian Central/Southeastern Arizona Basins Prv Rain Valley Formation Guadalupian Medium-fine—grained sandstone Carbonate shelf pk0125151 Kaibab Formation Guadalupian Medium-fine—grained sandstone Carbonate shelf 1WM-478 Middle Earp Formation Wolfcampian Granule conglomerate Braided fluvial 1WM-520 Upper Earp Formation Voirgilian Non-calcareous siltstone Carbonate shelf				_	
KA03Honaker Trail FormationMissourianMedium-grained sandstoneCarbonate shelfCF02Hermosa GroupMiddle-Upper Pennsylvanianmedium-fine-grained sandstoneShallow marineHT02Paradox FormationDesmoinesianVery fine-grained sandstoneCarbonate shelfHT14Paradox FormationDesmoinesianFine-grained sandstoneCarbonate shelfSP01Pinkerton Trail-HermosaDesmoinesianmedium-fine-grained sandstoneShallow marineDMR01Pinkerton Trail-HermosaDesmoinesianmedium-fine-grained sandstoneShallow marineML01Molas FormationAtokanVery fine-grained sandstoneFluvial/aeolianCentral/Southeastern Arizona BasinsPrvRain Valley FormationGuadalupianMedium-fine-grained sandstoneCarbonate shelfpk0125151Kaibab FormationGuadalupianMedium-fine-grained sandstoneCarbonate shelf1WM-478Middle Earp FormationWolfcampianGranule conglomerateBraided fluvial1WM-520Upper Earp FormationWolfcampianFine-grained sandstoneMarginal marine1WM-302Horquilla FormationVirgilianNon-calcareous siltstoneCarbonate shelf					
CF02 Hermosa Group Middle—Upper Pennsylvanian medium-fine—grained sandstone Carbonate shelf HT02 Paradox Formation Desmoinesian Very fine-grained sandstone Carbonate shelf HT14 Paradox Formation Desmoinesian Fine-grained sandstone Carbonate shelf SP01 Pinkerton Trail—Hermosa Desmoinesian medium-fine—grained sandstone Shallow marine DMR01 Pinkerton Trail—Hermosa Desmoinesian medium-fine—grained sandstone Shallow marine ML01 Molas Formation Atokan Very fine-grained sandstone Fluvial/aeolian Central/Southeastern Arizona Basins Prv Rain Valley Formation Guadalupian Medium-fine—grained sandstone Carbonate shelf pk0125151 Kaibab Formation Guadalupian Medium-fine—grained sandstone Carbonate shelf 1WM-478 Middle Earp Formation Wolfcampian Granule conglomerate Braided fluvial 1WM-520 Upper Earp Formation Volrgilian Non-calcareous siltstone Carbonate shelf				<u> </u>	
HT02 Paradox Formation Desmoinesian Very fine-grained sandstone Carbonate shelf HT14 Paradox Formation Desmoinesian Fine-grained sandstone Carbonate shelf SP01 Pinkerton Trail—Hermosa Desmoinesian medium-fine—grained sandstone Shallow marine DMR01 Pinkerton Trail—Hermosa Desmoinesian medium-fine—grained sandstone Shallow marine ML01 Molas Formation Atokan Very fine-grained sandstone Fluvial/aeolian Central/Southeastern Arizona Basins Prv Rain Valley Formation Guadalupian Medium-fine—grained sandstone Carbonate shelf pk0125151 Kaibab Formation Guadalupian Medium-fine—grained sandstone Carbonate shelf 1WM-478 Middle Earp Formation Wolfcampian Granule conglomerate Braided fluvial 1WM-520 Upper Earp Formation Volrgilian Non-calcareous siltstone Carbonate shelf				<u> </u>	
HT14 Paradox Formation Desmoinesian Fine-grained sandstone Carbonate shelf SP01 Pinkerton Trail—Hermosa Desmoinesian medium-fine—grained sandstone Shallow marine DMR01 Pinkerton Trail—Hermosa Desmoinesian medium-fine—grained sandstone Shallow marine ML01 Molas Formation Atokan Very fine-grained sandstone Fluvial/aeolian Central/Southeastern Arizona Basins Prv Rain Valley Formation Guadalupian Medium-fine—grained sandstone Carbonate shelf pk0125151 Kaibab Formation Guadalupian Medium-fine—grained sandstone Carbonate shelf 1WM-478 Middle Earp Formation Wolfcampian Granule conglomerate Braided fluvial 1WM-520 Upper Earp Formation Wolfcampian Fine-grained sandstone Marginal marine 1WM-302 Horquilla Formation Virgilian Non-calcareous siltstone Carbonate shelf		•		•	
SP01 Pinkerton Trail—Hermosa Desmoinesian medium-fine—grained sandstone Shallow marine DMR01 Pinkerton Trail—Hermosa Desmoinesian medium-fine—grained sandstone Shallow marine ML01 Molas Formation Atokan Very fine-grained sandstone Fluvial/aeolian Central/Southeastern Arizona Basins Prv Rain Valley Formation Guadalupian Medium-fine—grained sandstone Carbonate shelf pk0125151 Kaibab Formation Guadalupian Medium-fine—grained sandstone Carbonate shelf 1WM-478 Middle Earp Formation Wolfcampian Granule conglomerate Braided fluvial 1WM-520 Upper Earp Formation Wolfcampian Fine-grained sandstone Marginal marine 1WM-302 Horquilla Formation Virgilian Non-calcareous siltstone Carbonate shelf					
ML01 Molas Formation Atokan Very fine-grained sandstone Fluvial/aeolian Central/Southeastern Arizona Basins Prv Rain Valley Formation Guadalupian Medium-fine—grained sandstone Carbonate shelf pk0125151 Kaibab Formation Guadalupian Medium-fine—grained sandstone Carbonate shelf 1WM-478 Middle Earp Formation Wolfcampian Granule conglomerate Braided fluvial 1WM-520 Upper Earp Formation Wolfcampian Fine-grained sandstone Marginal marine 1WM-302 Horquilla Formation Virgilian Non-calcareous siltstone Carbonate shelf	SP01	Pinkerton Trail-Hermosa	Desmoinesian	9	Shallow marine
Central/Southeastern Arizona BasinsPrvRain Valley Formation pk0125151Guadalupian Kaibab FormationMedium-fine—grained sandstone Medium-fine—grained sandstoneCarbonate shelf1WM-478Middle Earp Formation 1WM-520Wolfcampian Upper Earp Formation Upper Earp Formation WolfcampianGranule conglomerate Fine-grained sandstoneBraided fluvial Marginal marine1WM-302Horquilla FormationVirgilianNon-calcareous siltstoneCarbonate shelf				medium-fine-grained sandstone	
Prv Rain Valley Formation Guadalupian Medium-fine—grained sandstone Carbonate shelf pk0125151 Kaibab Formation Guadalupian Medium-fine—grained sandstone Carbonate shelf 1WM-478 Middle Earp Formation Wolfcampian Granule conglomerate Braided fluvial 1WM-520 Upper Earp Formation Wolfcampian Fine-grained sandstone Marginal marine 1WM-302 Horquilla Formation Virgilian Non-calcareous siltstone Carbonate shelf	ML01	Molas Formation	Atokan	Very fine-grained sandstone	Fluvial/aeolian
pk0125151Kaibab FormationGuadalupianMedium-fine-grained sandstoneCarbonate shelf1WM-478Middle Earp FormationWolfcampianGranule conglomerateBraided fluvial1WM-520Upper Earp FormationWolfcampianFine-grained sandstoneMarginal marine1WM-302Horquilla FormationVirgilianNon-calcareous siltstoneCarbonate shelf	Central/South	eastern Arizona Basins			
pk0125151Kaibab FormationGuadalupianMedium-fine-grained sandstoneCarbonate shelf1WM-478Middle Earp FormationWolfcampianGranule conglomerateBraided fluvial1WM-520Upper Earp FormationWolfcampianFine-grained sandstoneMarginal marine1WM-302Horquilla FormationVirgilianNon-calcareous siltstoneCarbonate shelf	Prv	Rain Valley Formation	Guadalupian	Medium-fine-grained sandstone	Carbonate shelf
1WM-478Middle Earp FormationWolfcampianGranule conglomerateBraided fluvial1WM-520Upper Earp FormationWolfcampianFine-grained sandstoneMarginal marine1WM-302Horquilla FormationVirgilianNon-calcareous siltstoneCarbonate shelf		-		<u> </u>	
1WM-302 Horquilla Formation Virgilian Non-calcareous siltstone Carbonate shelf	•	Middle Earp Formation		_	Braided fluvial
	1WM-520		Wolfcampian	Fine-grained sandstone	Marginal marine
1PL-534 Horquilla Formation Virgilian Fine-grained sandstone Carbonate shelf			_		
	1PL-534	Horquilla Formation	Virgilian	Fine-grained sandstone	Carbonate shelf

(continued)

TABLE 1. DETRITAL ZIRCON SAMPLES, AGES, LITHOLOGIES, AND DEPOSITIONAL ENVIRONMENTS (continued)

Sample	Unit	Age	Lithology and grain size	Interpreted depositional environment
Keeler Basin				
10-12-15-3	Ps11 [†]	Guadalupian	Fine-grained sandstone	Shallow marine
6-20-17-3	Ps12a [†]	Guadalupian	Coarse-grained sandstone	Submarine fan
6-20-17-4	Ps12a [†]	Guadalupian	Coarse-grained sandstone	Submarine fan
12-03-16-1	Plc [‡]	Wolfcampian/Leonardian	Fine-grained sandstone	Outer shelf
12-03-16-3	Plc [‡]	Wolfcampian/Leonardian	Fine-grained sandstone	Outer shelf
12-02-16-1	Pla/b [‡]	Late Wolfcampian	Siltstone	Outer submarine fan/basin plain
10-11-15-1	Plc [‡]	Wolfcampian/Leonardian	Fine-grained sandstone	Outer shelf
12-03-16-2	Pld‡	Wolfcampian/Leonardian	Coarse-grained sandstone	Outer shelf
KC-2	Keeler Canyon Formation, lower Salt Tram member	Virgilian	Coarse-grained sandstone	Shallow marine
Southwest Mo	ontana			
PHOS	Phosphoria Formation	Guadalupian	Medium-fine-grained sandstone	Nearshore marine
quad1	Quadrant Formation	Upper Pennsylvanian	Medium-fine-grained sandstone	Aeolian

Note: See Data Repository File DR1 (text footnote 1) for detailed descriptions, interpretations of sample locations, and complete discussion of stratigraphy, age, and depositional environment.

Salt Tram member of the Keeler Canyon Formation, one location in the sedimentary rocks of Santa Rosa Flat unit 11 (Ps11), and two locations in the sedimentary rocks of Santa Rosa Flat unit 12a (Ps12a) (Stone et al., 2009).

Additional Locations

In addition to the locations detailed above, several isolated samples were collected from the periphery of the ARM system. Strata sampled in this manner include the sandstones within the Quadrant Formation (Pennsylvanian) and the lower member of the Phosphoria Formation (Lower Permian) in southwestern Montana, the middle Permian Rain Valley Formation in southern Arizona, and the middle Permian Kaibab Formation in southeastern California (one sample each).

ANALYTICAL METHODS

All zircon samples were mechanically crushed and separated through density and magnetic methods. All processing followed standard procedures for concentrating zircon from a detrital sample (e.g., Gehrels and Pecha, 2014).

All zircon samples collected from the Lone Pine Formation and sedimentary rocks of Santa Rosa Flat (Keeler and Lone Pine Basins) were analyzed at the University of California–Santa Barbara (UCSB) Laser Ablation Split Stream (LASS) facility using a Nu Plasma high resolution multi-collector–inductively coupled plasma mass spectrometer (HR MC–ICPMS), a Nu AttoM single collector ICPMS, and an Analyte 193 excimer ArF laser-ablation system equipped with a HeLex sample cell using a 24 μ m beam. Analyses were normalized against the 91500 zircon standard as a reference material (1062 Ma; Wiedenbeck et al., 1995). Data were reduced using Iolite 2.31 software in Igor Pro 6.3. Error assessment follows Kylander-Clark et al. (2013). These data are a subset of data presented in Lodes (2019).

Samples Quad1 and Phos, collected from the Quadrant and Phosphoria Formations in southwest Montana, were analyzed at the University of Washington using an iCAP RQ Quadrupole ICP-MS coupled to an Analyte G2 excimer laser with a spot diameter of 25 µm. Data reduction was conducted with Iolite, using their Geochron Data Reduction Scheme to calculate U-Pb ages uncorrected for common lead (Paton et al., 2010) and with the Andersen Routine of the VizualAge Data Reduction Scheme

(Chew et al., 2014) for U-Pb ages corrected for common lead; detailed methods are available in Licht et al. (2018). Both approaches yielded similar zircon ages, and ages from samples Quad1 are Phos uncorrected for common lead.

All other zircon data presented in this study were collected at the Arizona Laserchron Center at the University of Arizona using a Photon Machines Analyte G2 excimer laser equipped with a HelEx ablation cell using a spot diameter of 20 µm and an Element2 HR–ICPMS (e.g., Gehrels and Pecha, 2014). See Data Repository for description of analytical methods and procedures. Typical random uncertainties in laser-ablation U-Pb analyses of zircon are 1%–2% with systematic uncertainties typically ca. 1%. All detrital zircon data presented in this study are presented in File DR3. Grain size was not individually measured, but in most samples, grain sizes of analyzed grains ranged from silt- to sand-sized.

DETRITAL ZIRCON SPECTRA

All zircon data presented in this study are plotted as probability density functions, kernel density estimates, and traditional histograms. Probability density function curves were generated using DensityPlotter (Vermeesch, 2012) and/or DZStats (Saylor and Sundell, 2016). Kernel Density Estimation plots were generated using the same programs; a bandwidth of 20 m.y. was used for all kernel density estimate (KDE) curves. Histogram bin width is 50 m.y. in all plots.

STATISTICAL ANALYSIS

Similarity Metrics

This study presents new data from analyses of 72 detrital zircon samples collected over an area of ~600,000 km². These data are compared to data from an additional 241 published samples collected over nearly the entire conterminous United States. Due to the volume of data considered and its broad geographical extent, traditional probability density function (PDF) or KDE curves for the entire data set cannot be effectively visualized and compared simultaneously, although traditional comparison is useful within individual basins (e.g., Figs. 3–8).

A variety of statistical tools has been developed to compare large detrital zircon data sets (Sircombe and Hazelton, 2004; Vermeesch, 2013;

^{*}Sweet et al., 2015.

[†]Stone et al., 2009.

[‡]Stone et al., 2000; Lodes, 2019.

Satkoski et al., 2013; Vermeesch and Garzanti, 2015; Vermeesch et al., 2016; Saylor and Sundell, 2016; Sundell and Saylor, 2017; Vermeesch, 2018; Saylor et al., 2019). For regional comparisons in this study, we employ two methods. The first is a straight statistical comparison using the tools of Saylor and Sundell (2016). The second is a "bottom up" inverse modeling approach first applied to detrital geochronology by Sharman and Johnstone (2017).

Saylor and Sundell (2016) reviewed and tested a variety of statistical comparison methodologies for reliability, minimization of artifacts, and accuracy. For samples with $n \geq 300$, cross-correlation of probability density functions showed the best performance, and we use this method in the current study.

One limitation of probability density plot cross-correlation is that similarity values calculated using this method can be sensitive to sample size below n = 300 (Saylor and Sundell, 2016). Samples analyzed as part of this study are mostly n≅100 or n≅300, although carbonate samples collected from the distal Paradox Basin had poor zircon yield, and many of the published analyses to which new data are compared also have n<100. Despite this limitation, cross-correlation of probability density plots provides the most reliable method for assessing similarity of the samples considered here. Likeness values calculated from kernel density estimation (KDE) are less sensitive to sample size but have limited capacity to distinguish differences in age spectra (Saylor and Sundell, 2016). Comparisons based on the K-S test are favored by some authors due to higher statistical robustness (e.g., Vermeesch, 2012, 2018; Vermeesch et al., 2016); however, these tests are very sensitive to sample size (Saylor and Sundell, 2016). KDE likeness statistics and Kolmogorov-Smirnov (K-S) test D-values are presented in the data repository but are not used in our interpretation.

Similarity matrices in which each analyzed sample is statistically compared to each other sample provide a detailed and granular way to determine the absolute similarity of two samples (e.g., Cowgill et al., 2016). However, large data sets such as the one presented here limit the practical functionality of this approach. To address this, we adopt an approach in which regional statistical comparison relies on comparing each individual sample to a composite data set for discrete intervals of geologic time. Here, we use aggregated samples from what we term the "Arizona shelf" (Fig. 1) divided into the four time intervals as this composite data set: Morrowan-Atokan (323-312.6 Ma); Desmoinesian-Virgilian (312.6-299 Ma); Wolfcampian (299-282 Ma); and Leonardian-lower Guadalupian (282–ca. 260 Ma). Absolute ages are assigned based on biostratigraphic correlations to well-radioisotopically dated sections (Menning et al. 2006; Schmitz and Davydov, 2012), and the ages of most strata considered in this study can be constrained to the stage level based on fusulinid and conodont taxa. The "Arizona shelf" in this study refers to a broad area of largely undeformed Pennsylvanian-Permian strata exposed across northern and central Arizona (e.g., Mckee, 1982; Blakey, 1990). Detrital zircon data from four localities in this area are employed here: the Grand Canyon (Gehrels et al., 2011), Sycamore Canyon, west of Sedona, Arizona (this study), the Mogollon Rim northeast of Payson, Arizona (this study), and a section of Pennsylvanian-Permian rocks exposed in the Plomosa Mountains of western Arizona that palinspastically restores to the Sedona-Mogollon Rim region (this study; McQuarrie and Wernicke, 2005). These sections span an age range of Late Mississippian to early Guadalupian (ca. 325-260 Ma). The Arizona shelf was selected as the statistical comparison index for this study because this area has large data sets (both sample numbers and analyzed grains) from each time interval, shows minor upsection changes in age spectra (see Results), and is adjacent to the Ancestral Rocky Mountain system. Age data for each sample and amalgamated Arizona shelf data are presented in File DR4.

Inverse Modeling of Zircon Sources

Inverse or "bottom-up" modeling via non-negative matrix factorization (NMF) was recently applied to characterize potential sources in detrital geochronology (Sharman and Johnstone, 2017; Saylor et al., 2019). NMF is based on evaluating the following equation

$$V = WH + E, \tag{1}$$

while minimizing the final residual, E (Lee and Seung, 1999; Van Benthem and Keenan, 2004; Li and Ngom, 2013). In this equation, V is a matrix made up of m elements from n samples; in the case of detrital geochronology it represents the measured age distribution from depositional (i.e., sink) samples. W is a m × k matrix representing the factorized sources and comprises m elements for each of the k factorized components. H is then a k × n matrix of weighting functions that defines the mixing of W into V. Assessment of the quality of the factorization was based on quantitative comparison of the factorized samples (WH) to known samples (V) using cross-correlation, likeness, Kuiper V value, and KS D value (Kuiper, 1960; Stephens, 1970; Amidon et al., 2005; Press et al., 2007; Satkoski et al., 2013, Saylor et al., 2012, 2013).

We use DZnmf (Saylor et al., 2019) to factorize both probability density functions (PDFs) and kernel density estimates (KDEs, 20 m.y. bandwidth) for the 108 samples and sample groups. We compiled this data set from 208 detrital zircon samples from published data and data presented herein (File DR5 provides sample group details). We combined small samples (i.e., those with low grain counts) with geologically and geographically appropriate neighbors into sample groups to better characterize sink distributions.

Inverse source modeling requires no a priori source information but rather deconvolves constituent source distributions from the sink sample set distributions. This characteristic is particularly advantageous in circumstances where source age distributions are poorly characterized in comparison to sink distributions (Sharman and Johnstone, 2017). The data set used here is an optimal candidate for NMF source characterization because of the large number of sink samples, high dissimilarity among sink sample distributions, and relatively large grain counts (n > 150) of most samples and sample groups (Saylor et al., 2019). Factorization allows calculation of reconstructed sink samples (WH) based on the factorized age distributions (W), which are common to all samples and the weighting functions (H), which are unique to each sample.

The optimal number of factorized sources is determined in DZnmf by identification of a "breakpoint" defined by a decrease in the rate of decrease of the final residual (E in Equation 1) versus the number of sources modeled (i.e., the factorization rank, Saylor et al., 2019). In order to robustly identify the breakpoint, we calculated factorized sources and final residuals for factorization ranks 2–30 for both PDFs and KDEs.

RESULTS

Arizona Shelf

Samples from Grand Canyon National Park have been previously presented and interpreted by Gehrels et al. (2011); however, because this group of samples represents the most stratigraphically complete section, we begin by reviewing these data (Fig. 3). Detrital zircon spectra from the Upper Mississippian Surprise Canyon Formation through the Leonardian Coconino Sandstone are composed of largely similar age spectra. All samples from this section have broad age spectra with individual grains ranging from 3.0 Ga to 2.5 Ga (Archean) to late Paleozoic (ca. 300 Ma).

Two samples from the Upper Mississippian Surprise Canyon Formation are dominated by 1.10 Ga peaks with numerous small Archean–Paleozoic peaks (Fig. 3). Above this, spectra from the uppermost Surprise Canyon Formation sample as well as those up to the upper Hermit Formation are dominated by 1.80–1.60 Ga grains with subequal peaks at ca. 1.80 Ga and 1.65 Ga; these samples also contain prominent 1.20–1.10 Ga peaks. A sample from the upper Hermit Formation alters this pattern and includes abundant Paleozoic and late Neoproterozoic grains as well as a prominent population at 1.10 Ga, with only minor older populations. Samples from the Leonardian Coconino Sandstone change once again with prominent peaks at 1.1 Ga and minor peaks at 1.43 Ga and 1.65 Ga.

Samples collected for this study from correlative rocks along the western Mogollon Rim northeast of Sedona, Arizona, (Fig. 4, panel 1) span Early Pennsylvanian (Atokan) to middle Permian (Leonardian) time. These samples show a high degree of similarity with PDF cross-correlation values all greater than 0.65. All samples contain Neoarchean grains between 2.5 Ga and 2.9 Ga (Fig. 4). All samples from this location also contain abundant Paleoproterozoic grains with peaks at 1.79 Ga, 1.75 Ga, and 1.65 (most prominent). Mesoproterozoic age peaks include 1.56 Ga (sample SY-A), 1.50 Ga (samples SY-D, SY-C, SY-A), and 1.48 Ga (sample SY-B). All samples contain abundant grains between 0.95 Ga and 1.30 Ga, although the shape and center of this peak varies somewhat (Fig. 4). A sample from the Hermit Formation (sample SY-D; sensu Blakey, 1990) is the only sample in this section with a substantial number of 650–550 Ma grains. All samples in this section contain 430–295 Ma grains.

Pennsylvanian through lower Permian samples from the central Mogollon Rim (Fig. 4, panel 3; 5PS-42, 5PS-58, 5PS-82; 1PS-4) yielded similar age spectra to those from the western Mogollon Rim section (above). Middle Permian (Leonardian) samples from the Schnebly Hill Formation (3PS-100 and 4PS-186) are substantially different from samples from the lower portion of this section in that they contain prominent Neoproterozoic peaks with a 1.05 Ga peak, which is the largest peak in sample 4PS-186. The most striking difference between Schnebly Hill Formation samples and those below is the abundance, particularly in 3PS-100, of Neoproterozoic grains that make up age peaks at ca. 600 Ma. Both samples also contain prominent Paleozoic age peaks and 1–2 grains near the depositional age.

The final section included in the "Arizona shelf" grouping (see Statistical Methods) was measured and sampled in the Plomosa Mountains near Quartzsite, Arizona (Fig. 4, panel 2). These samples are similar to those from the Sycamore Canyon and Mogollon Rim sections, including age peaks and upsection trends (Fig. 4), and as such are not described in detail.

Central and Southeast Arizona

A single sample from the predominantly carbonate section in the Mescal Mountains 130 km east–southeast of Phoenix, Arizona, (Fig. 4, panel 4) contains a broad distribution of Archean to Paleozoic grains with the most prominent ages centered on 1.65 Ga. A single grain overlaps the depositional age (latest Virgilian) at 296 ± 4 Ma.

Late Pennsylvanian (Virgilian) to middle Permian (late Wolfcampian) samples from the Whetstone Mountains in southeast Arizona yielded similar age peaks in each sample (Fig. 4, panel 5) and include minor populations of Archean grains between 2.9 Ga and 2.6 Ga, peaks at ca. 1.80–1.72 Ga with a large peak at 1.78 Ga in sample 1WM-302, major peaks at 1.65 Ga in all samples, peaks at 1.50 Ga in all samples, and a minor peak at 1.40 Ga at the base of the section. All samples have peaks between 1.2 Ga and 1.0 Ga. All samples contain grains between 700 Ma and 400 Ma, with a common peak at 430 Ma.

Eagle Basin, Colorado

Detrital zircon spectra from the Vail, Colorado, section are typified by unimodal age distributions (Fig. 5, panel 4). The lowest sample in the Vail section (V20) has scattered individual grains between 2.7 Ga and 1.10 Ga, a minor peak at ca. 1.82 Ga, and a major peak at 1.72–1.70 Ga. Above this, the abundance of non-ca. 1.7 Ga grains decreases, and the age peak at 1.7 Ga narrows substantially (Fig. 5). The only exception to this is sample V10, collected from the middle of the Minturn Formation (Fig. 5). This sample contains minor Archean peaks, major peaks at 1.78 Ga and 1.69 Ga, multiple minor peaks between 1.45 Ga and 1.00 Ga, and two minor peaks between 500 Ma and 300 Ma.

In the Red Canyon section (Fig. 4, panel 3), a sample from the Eagle Valley Evaporite (EC01) contains a major peak at 1.7 Ga, secondary peaks at 1.43 Ga and 1.11 Ga, and minor peaks at 2.67 Ga, 1.88 Ga, and 380 Ma (Fig. 5). Above this, the sample from the lower Eagle Valley Formation (RC01) contains a single, narrow dominant peak centered on 1.71 Ga with scattered individual grains between 2.8 Ga and 400 Ma. Sample RC19 from the upper–middle Eagle Valley Formation contains a broad range of ages that includes major peaks at 1.75 Ga, 1.57 Ga, 1.45 Ga, and ca. 570 Ma as well as minor peaks at 1.30 Ga, 1.08 Ga, 980 Ma, and 420 Ma. This sample is moderately similar (PDF cross-correlation of 0.48) to sample V10 from the Vail section, which was collected from nearly identical stratigraphic positions.

Most samples from the Glenwood Springs section (Fig. 5, panel 2) are dominated by two subequal peaks at 1.70 Ga and 1.42 Ga. In samples with these peaks, scattered Archean grains as well as small peaks at 1.89 Ga, 1.08 Ga, and scattered individual Neoproterozoic and early Paleozoic grains are present but decrease in abundance upsection. One exception to this pattern is sample GS09, which was collected from the upper Eagle Valley Formation. This sample contains a much broader range of ages than samples above and below, and major peaks are centered on 1.73 Ga, 1.65 Ga, 1.43 Ga, and 1.15 Ga, with smaller peaks at 1.29 Ga and 1.07 Ga; scattered individual Archean–early Paleozoic grains are also present. Stratigraphically, this sample is roughly correlative with samples V10 and RC19 described above.

The stratigraphically lowest sample from a section near Meeker, Colorado, (Fig. 5, panel 1; MC05) is dominated by two subequal age peaks at 1.71 Ga and 1.42 Ga; scattered Archean–early Paleozoic grains make up small peaks at 1.06 Ma and 510 Ma (Fig. 5). Above this, sample MC17 contains a broad distribution of grains with many individual peaks (Fig. 5). The most prominent of these are peaks at 1.80 Ga, 1.73 Ga, 1.65 Ga, and 1.16 Ga. Sample MC20 contains a similar overall distribution of age peaks except for the appearance of a major 1.45 Ga peak as well as a minor peak at 420 Ma.

Central Colorado Trough

A sample from the Upper Mississippian Leadville Limestone (Fig. 5, panel 6) contains major populations at ca. 1.79 Ga and 1.43 Ga with minor peaks at 1.68 Ga, 1.38 Ga, and 1.13 Ga. Above this, samples from the Morrowan Kerber and Atokan Sharpsdale Formations (De Voto et al., 1986) are dominated by a single peak at ca. 1.70 Ga. The Kerber Formation also contains scattered minor Archean to late Paleozoic peaks, and these decrease in prominence up section in the Sharpsdale Formation.

Paradox Basin

Samples from the Middle to Upper Pennsylvanian Paradox and Honaker Trail Formations within the distal Paradox Basin (Fig. 6, panel 3)

mostly returned poor zircon yield, and the number of grains analyzed from each range between 36–103. These samples are qualitatively similar and contain sparse 2.5–3.0 Ga grains, abundant 1.80–1.40 Ga grains (except for sample HT02), abundant 1.30–0.90 Ga grains, and several small populations of 500–300 Ma grains. Sample HT02 deviates from this overall pattern because its largest population is composed of 500–400 Ma grains. Upper Honaker Trail samples have notable multiple small peaks at ca. 1.80 Ga, 1.72 Ga, 1.65 Ga, 1.50 Ga, 1.32 Ga, 1.20 Ga, 1.15 Ga, 1.05 Ga, and 0.98 Ga.

Sample KA03, collected from the Honaker Trail Formation in the western medial basin (Fig. 6, panel 2), contains major age peaks centered on 1.70 Ga and 1.42 Ga with minor peaks at 1.00–1.12 Ga and 450 Ma.

Proximal basin samples from the Cutler Formation (undifferentiated) near Gateway, Colorado, (Fig. 6, panel 1) yielded age spectra dominated by 1.40–1.45 Ga grains with a minor secondary population centered on 1.73 Ga, although this secondary population is nearly absent in sample TP01.

In the eastern Paradox Basin (Fig. 6, panel 4), sample ML01 from the Morrowan–Atokan Molas Formation contains a broad range of ages including scattered 1.8–3.0 Ga grains, several small peaks between 1.62 Ga and 1.30 Ga, a major peak at 1.05 Ga, and two minor peaks between 500 Ma and 400 Ma. Stratigraphically above this, age spectra change drastically to spectra dominated by a major peak at 1.43 Ga, a secondary but still major peak at 1.73 Ga, and a small peak at 520 Ma. A few samples (SM01, SP01, DMR01) contain 1–2 single grain ages between 1.20 Ga and 1.00 Ga. Sample HC01, collected from the Cutler Formation (undifferentiated) north of Durango, Colorado, departs markedly from other samples in this area. Although the same age peaks are present, this sample is dominated by a peak at 520 Ma, and the 1.73 Ga and 1.43 Ga peaks are much less prominent.

Denver Basin

Samples from Denver Basin strata analyzed in this study can be broadly organized into three similar groups arranged stratigraphically (Fig. 7).

- (1) Samples from Atokan strata within the Glen Eyrie and Fountain Formations (samples MS01, MS10, MS11) are similar and have broad age spectra with most grain ages concentrated between 1.90 Ga and 1.00 Ga (Fig. 7). Within this range, major age peaks are centered on 1.75–1.70 Ga, 1.45–1.42 Ga, and 1.10–1.08 Ga, with a minor peak centered on 1.21 Ga. Sample MS01 from the Glenn Eyrie Formation contains three individual grains between 600 Ma and 350 Ma.
- (2) Stratigraphically above this, the second group of samples (MS06, MS05, MS04) is statistically similar with PDF cross-correlation coefficients > 0.81. These samples contain one major peak centered on 1.09 Ga and a minor peak at 1.43 Ga that vanishes entirely up-section such that sample MS04 contains only the 1.09 Ga peak (Fig. 7).
- (3) At the top of the section, a sample from the Wolfcampian Ingleside Formation (Sweet et al., 2015) contains a broad distribution of ages including minor peaks centered at ca. 2.7 Ga, 1.82 Ga, 1.62 Ga, and 600 Ma and major peaks centered at ca. 1.05 Ga and 430 Ma.

Keeler-Lone Pine Basin

One sample from the Salt Tram Member of the Keeler Canyon Formation (Stevens et al., 2001) contains minor 2.8–2.5 Ga grains, multiple 1.9–1.3 Ga peaks, a major peak at 1.1–1.0 Ga, and a prominent 450–400 Ma peak (Fig. 8, panel 2).

Age spectra from samples collected in Wolfcampian strata of the Lone Pine Formation are qualitatively self-similar (Fig. 8, panel 1). Most of these samples contain scattered Archean grains, and minor age peaks occur between ca. 1.85 Ga, 1.65 Ga, 1.43 Ga, and 600–550 Ma. Major peaks are centered on ca. 1.1–1.05 Ga and 400 Ma. There is no systematic up-section change in these data.

Guadalupian samples also contain broad distributions of ages (Fig. 8, panel 2). These samples contain small Archean peaks and major peaks at 1.85 Ga, 1.05 Ga, and 400 Ma. Additional peaks present in single samples include a major 950 Ma peak in sample 6–20–17–3 and minor peaks at 1.65 Ga and 1.5 Ga in sample 6–20–17–4. Grains with 500–400 Ma ages are more abundant in the upper two samples in this group.

PDF Cross-Correlation

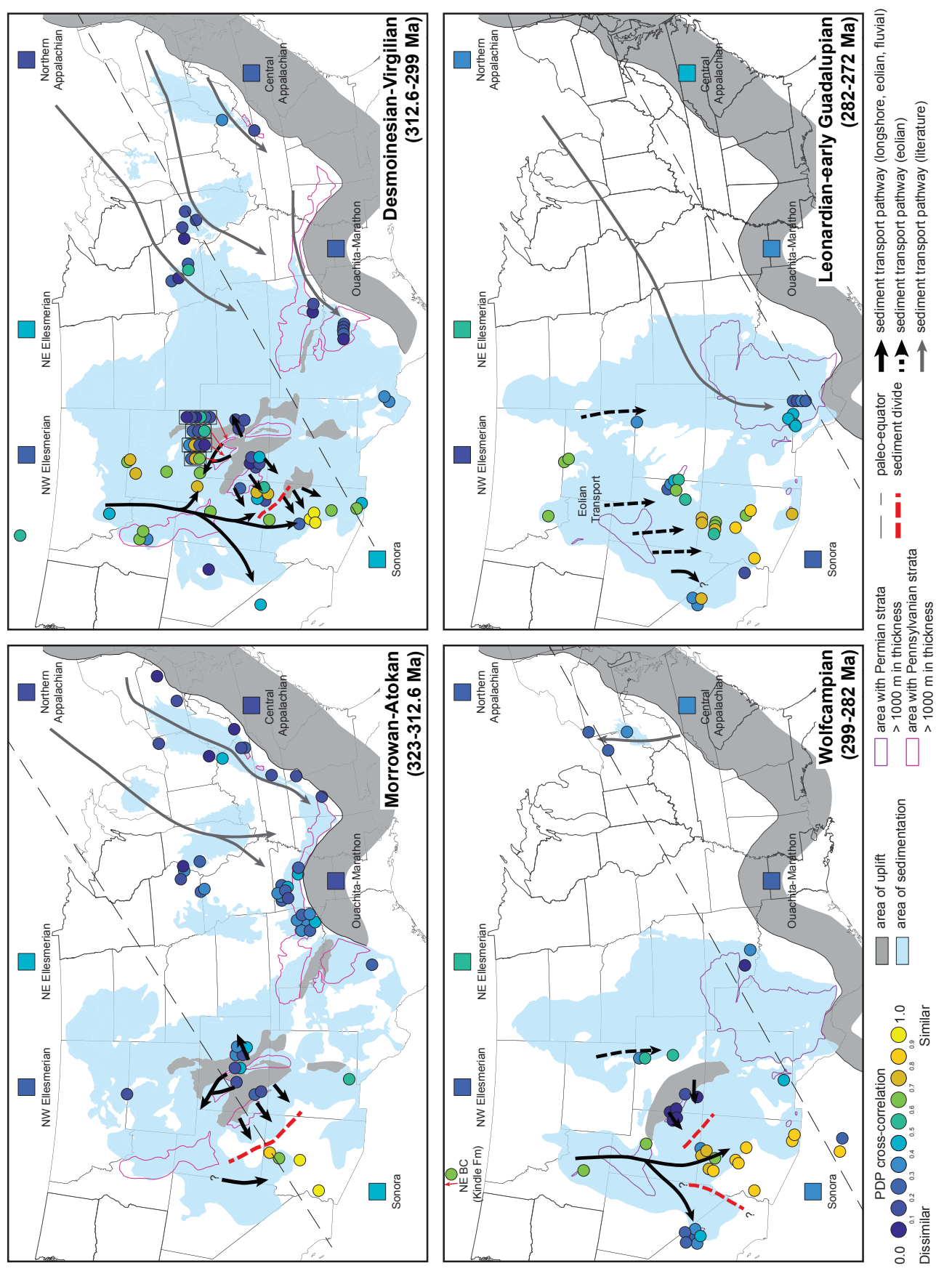
Results of similarity calculations between each sample and amalgamated samples of the Arizona shelf are presented visually in Figure 9. The aggregated Arizona shelf data set is also compared to aggregated data sets from six potential source terranes, which are discussed in detail in the subsequent discussion section. It is important to note that the cross-correlation values shown in Figure 9 reflect only the similarity of each individual sample or source terrane to the aggregated Arizona shelf data set in a specific timestep; there is no measure of similarity of individual samples to other individual samples in Figure 9. Cross-correlation values can range from zero (completely different) to one (identical). Complete results are presented in Files DR6 and DR7.

Samples from Morrowan–Atokan (323–321.6 Ma) strata show substantial statistical separation between the Arizona shelf and other Laurentian strata (Fig. 9) with all Laurentian, non-Arizona shelf samples returning values of <0.5. All samples within the ARM region have cross-correlation values <0.5, and most samples have values near 0.2. Comparison of the Arizona shelf during this time step to potential source regions yielded values of 0.1–0.5, with the northeast Ellesmerian orogen having the highest value (0.45).

Calculations from Desmoinesian–Virgilian (312.6–299 Ma) samples show low cross-correlation values (<0.4) between proximal ARM basin strata within the Paradox, Eagle, and Denver Basins. Strata in distal portions of the Paradox and Eagle Basins are more similar to the Arizona shelf, and these samples and those from the Bighorn and Wood River Basins have cross-correlation values >0.6. Samples from the Appalachian Basin, American midcontinent, and Ouachita-Marathon Basins have low cross-correlation values (<0.3 except for two samples). Aggregated potential source regions yielded cross-correlation values of 0.1–0.5 with the northeast Ellesmerian orogen having the highest value (0.48).

Samples from Wolfcampian (299–282 Ma) strata have the highest homogeneity within the Arizona shelf (cross-correlation values mostly >0.7), and samples collected from southern Arizona have similarly high cross-correlation values. Two samples from northern Utah and central Idaho have cross-correlation values >0.6. Like underlying Pennsylvanian strata, proximal Paradox samples have cross-correlation values <0.2 with most near zero. In contrast with the underlying Pennsylvanian strata, Denver Basin samples have values from 0.3 to 0.6. Samples from the Lone Pine Basin in eastern California have cross-correlation values of 0.2–0.4. Potential source region cross-correlation values are 0.2–0.6, and like underlying strata, the highest value (0.56) was calculated for northeast Ellesmerian orogen data.

Leonardian—early Guadalupian (ca. 282–260 Ma) strata show higher cross-correlation values than older strata (Fig. 9), and most samples from within the ARM region have cross-correlation values mostly >0.6. Proximal Paradox Basin samples are more similar to the Arizona shelf than are samples from older strata with cross-correlation values of 0.2–0.7. Samples from Permian Basin strata of this age have cross-correlation



from McKee and McKee (1967) and McKee and Crosby (1975). Black arrows are interpreted sediment transport pathways; red lines are interpreted sediment transport divides/barriers. Thin red arrows indicate the locations of Eagle Basin samples surrounded by black boxes. Paleo-equator position from paleogeographic maps by Blakey (2013), Scotese and McKer-Figure 9. Probability density function (PDF) cross-correlation of individual samples compared to aggregated Arizona shelf data in four time steps. Light blue areas of sedimentation row (1990), and Domeier and Torsvik (2014). Appalachian and eastern United States sediment transport pathways after Kissock et al. (2018), Buratowski (2014), Alsalem et al. (2018) Thomas et al. (2016, 2017), and Xie et al. (2018)

values of 0.1–0.5. Potential source terranes have values of 0.1–0.6, with the northeast Ellesmerian orogen having the highest value of 0.55.

Inverse Modeling

Samples used in DZnmf are distributed across North America and divided into five age divisions: Mississippian, Early Pennsylvanian, Middle-Late Pennsylvanian, early Permian, and middle Permian. Factorization of PDFs and KDEs produced similar results but differed in their identification of the optimum number of sources. Factorization of PDFs and KDEs yielded either 8 or 10 as the optimal number of sources, respectively. However, the 8-source factorization for both PDF and KDE models, which are nearly identical (Fig. 10), is more reasonable when considering modeling artifacts and geologic context (see discussion of NMF caveats below); we therefore focus discussion on results produced by the PDF model. The mean of quantitative similarity metrics for the PDF optimal source number model indicate that 95% of the reconstructed samples yield close matches to their empirical counterparts (likeness > 0.7 (94%), cross-correlation > 0.7 (98%), V values < 0.15 (96%), D value < 0.08 (92%); see Files DR8–DR10). The median cross-correlation coefficient is 0.87 with a maximum of 1.00 and a minimum of 0.61. We projected the factorized weighting functions (H in Equation 1) onto eastnortheast-west-southwest and northwest-southeast North America-scale cross sections for each of the five age divisions (Figs. 10 and 11).

The eight factorized sources produced by DZnmf exhibit geologically reasonable age distributions (Fig. 10) and are described below. Source A contains two dominant age modes in the early Paleozoic and late Neoproterozoic and a lesser age population from 0.9 Ga to 1.1 Ga. Source B contains an asymmetrically shaped age distribution from 0.9 Ga to 1.4 Ga with a mode at 1.1 Ga and minor early Paleozoic populations. Source C contains a 1.8 Ga mode with a broad age distribution and a lesser Archean age population of 2.5–2.7 Ga. Source D contains a dominant age mode at 1.65 Ga flanked by lower amplitude modes at 1.5 Ga and 1.75 Ga, a broad suite of ages from 1.1 Ga to 1.4 Ga, and minor early Paleozoic and Archean age modes. Source E contains a dominant 2.7 Ga age mode flanked by minor Archean age populations and several minor and discrete Proterozoic age populations centered around 1.1 Ga, 1.3 Ga, 1.5 Ga, 1.65 Ga, and 1.85 Ga. Source F exhibits a unimodal age distribution at 1.7 Ga. Source G contains a dominant 1.4 Ga mode and a lesser 1.7 Ga mode. Source H contains a unimodal age distribution at ca. 530 Ma.

DISCUSSION

Potential Zircon Sources

Archean Cratons

Archean crust in Laurentia is confined to several discrete regions within the northern United States, central Rocky Mountains, and Canadian Shield (Fig. 12). These include the Superior, Slave, and Wyoming Cratons and the Hearne and Rae provinces, which are interpreted to be fragments of Archean cratons surrounded by Proterozoic mobile belts (Whitmeyer and Karlstrom, 2007; Condie et al., 2009). Zircon derived from these cratons yields broadly similar ages with a few key exceptions. Dating of zircons from the Superior Craton indicates episodic zircon production in this region from 3.5 Ga to 2.6 Ga (Bickford et al., 2006; Schmitz et al., 2006). This resembles zircon populations recovered from the Canadian Superior province (Percival et al., 1994). Zircon from the Superior Craton form an age peak at ca. 2.7 Ga as do grains from the Hearne Craton (Condie et al., 2009). In contrast, zircon ages from the Wyoming Craton are more widely distributed with the most prominent peak centered at

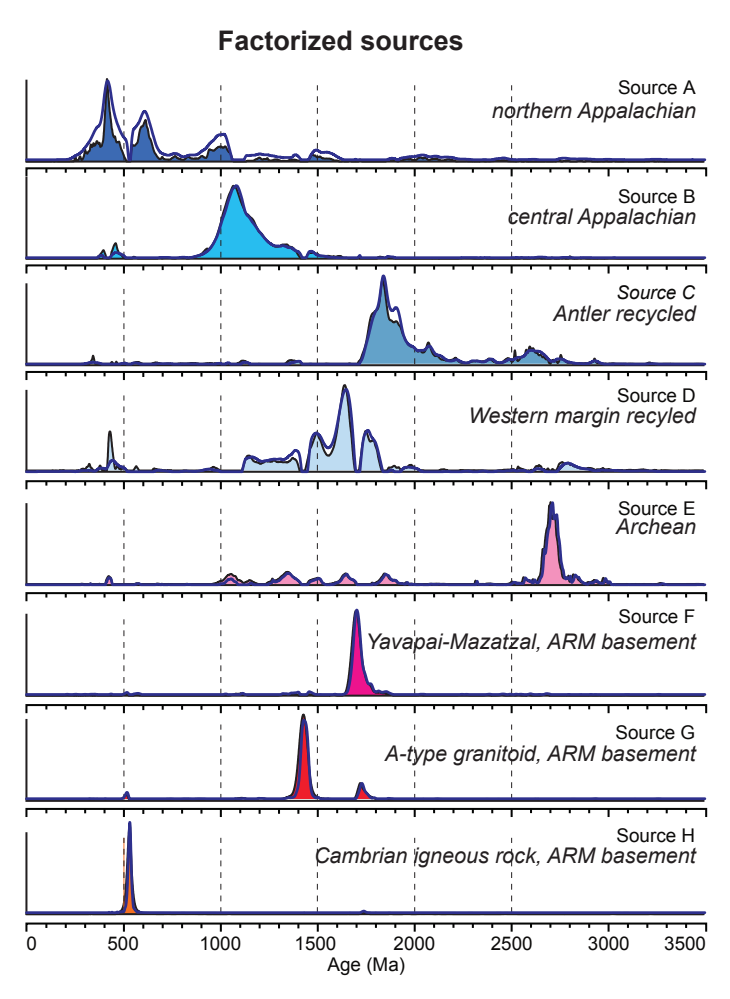


Figure 10. Probability density plots (PDFs, filled) and kernel density estimates with 20 m.y. bandwidth (KDEs, unfilled) for the eight sources produced by non-negative matrix factorization (NMF) modeling. Italicized text below factorized source name indicates interpreted geologic source. Color of PDF fill corresponds to colors used in cross-section panels in Figure 11. File DR8 (see text footnote 1) provides further details.

ca. 2.65 Ga and a greater abundance of > 3.0 Ga grains than in Archean terranes farther north.

Paleoproterozoic before 1.8 Ga

Grains between 2.5 Ga and 1.8 Ga could have originated from a variety of Laurentian sources. During the 2.4–2.0 Ga time period, a series of rifting events occurred and was followed by a series of collisions between 2.0 Ga and 1.80 Ga that assembled the Slave–Rae–Hearne and Superior Cratons (Sims et al., 1993; Whitmeyer and Karlstrom, 2007). The remnants of these collisions are preserved as juvenile arcs and accreted material separating Archean blocks (Fig. 12; Whitmeyer and Karlstrom, 2007). Roughly concurrent convergent orogenesis at 1.85–1.78 Ga and 1.88–1.83 Ga occurred in the Trans-Hudson and Penokean events, respectively, in northern Canada and the north central United States (Van Schmus, 1976; Schulz and Cannon, 2007; Whitmeyer and Karlstrom, 2007).

Paleoproterozoic Yavapai-Mazatzal Orogen

Proterozoic basement rocks of southwest Laurentia were accreted to the Wyoming and Superior Cratons, are well dated, and likely contributed sediment to many of the strata analyzed in this study. The Yavapai

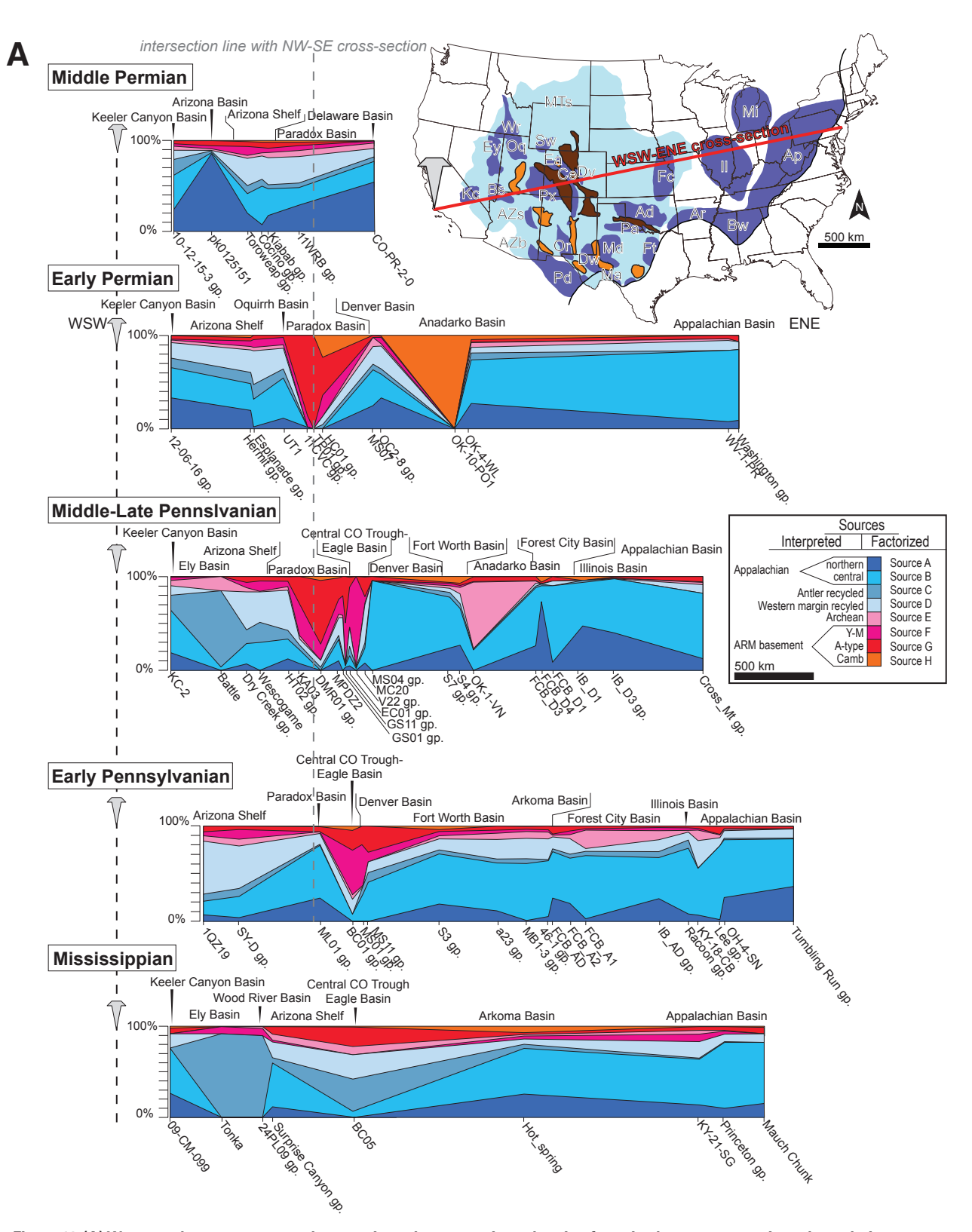


Figure 11. (A) West-southwest to east-northeast-oriented cross sections showing factorized source proportions through time; cross sections are arranged from oldest at the bottom to youngest at the top. Samples or sample groups and depocenters are projected onto the cross section illustrated in the inset map and are indicated by labels at the bottom and top of the cross sections, respectively. The cross sections are pinned at the western edge, as indicated by the gray pin in the cross section and inset map. Vertical gray dashed line along left side of cross sections indicates an alignment of reference position marked on the inset map as the gray spike. Vertical black lines inside of cross sections mark the intersection with the northwest-southeast cross section. Details of sample groups and non-negative matrix factorization (NMF) results are in Files DR5 and DR8-DR10 (see text footnote 1). See Figure 1 for sample locations. All cross-section lines are displayed at the same scale. (Continued on following page.)

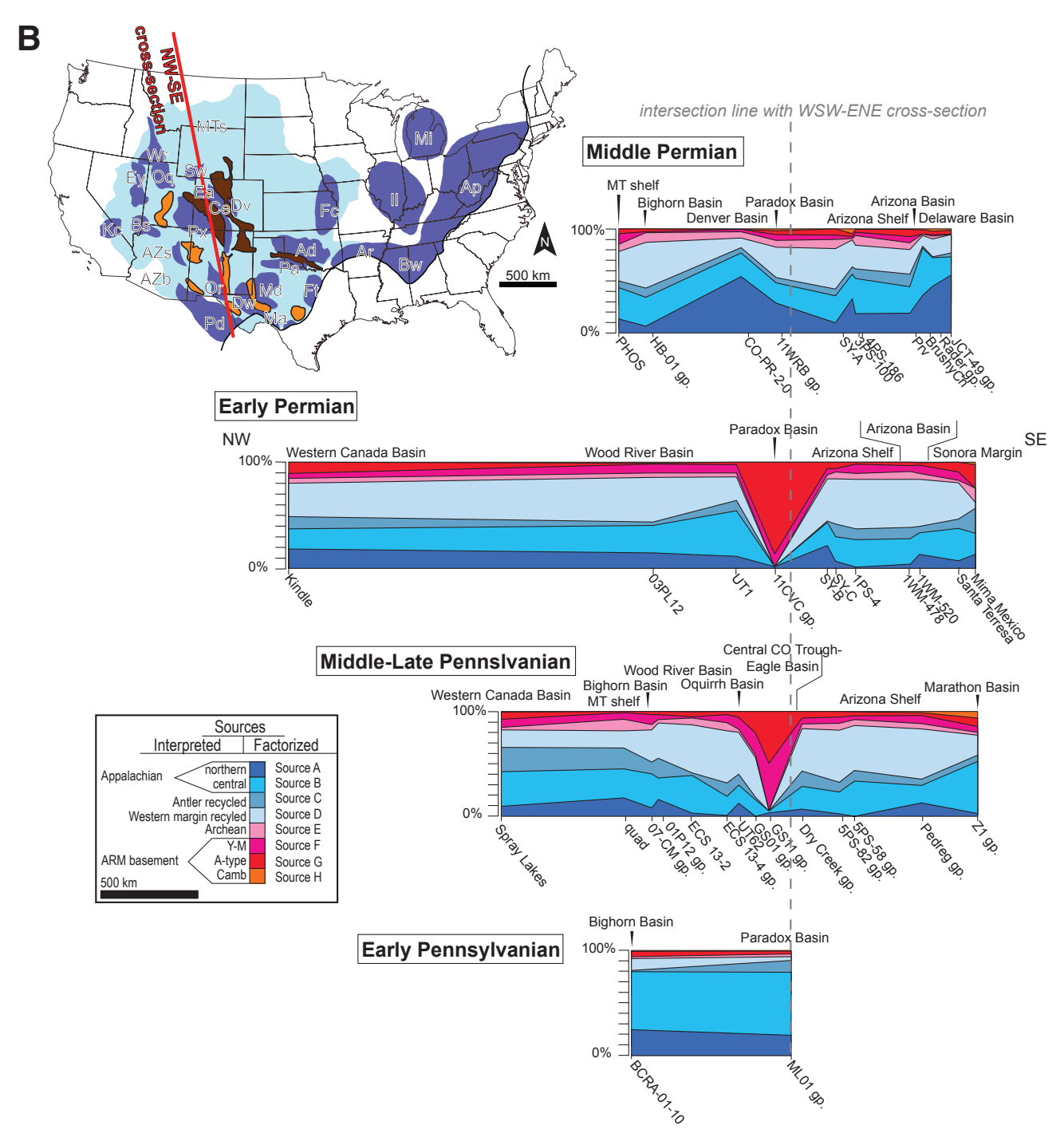


Figure 11 (continued). (B) Northwest- to southeast-oriented cross sections showing factorized source proportions through time; cross sections are arranged from oldest at the bottom to youngest at the top. Inset map does not display full northern extent of cross-section line into the western Canada Basin. The is no Mississippian northwest-southeast cross section because all data points are displayed in this cross section. Samples or sample groups and depocenters are projected onto the cross section illustrated in the inset map and are indicated by labels at the bottom and top of the cross sections, respectively. The vertical gray dashed line indicates intersection with the west-southwest-east-northeast cross section. Details of sample groups and non-negative matrix factorization (NMF) results are in Files DR5 and DR8-DR10 (see text footnote 1). See Figure 1 for sample locations. CO—Colorado; gp.—group; MT—Montana. Basins: Ap—Appalachian; Ar—Arkoma; AZb—Arizona; AZs—Arizona shelf; Bs—Bird Springs; Bw—Black Warrior; Ce—Central Colorado Trough; Ea—Eagle; Ey—Ely; Dv—Denver; Dw—Delaware; Fc—Forest City; Ad—Anadarko; Ft—Fort Worth; II—Illinois; Kc—Keeler Canyon; Ma—Marathon; Md—Midland; Mi—Michigan; MTs—Montana shelf; Oq—Oquirrh; Or—Orogrande; Pa—Palo Duro; Pd—Pedregosa; Px—Paradox; Sw—Sweetwater Trough; Wr—Wood River.

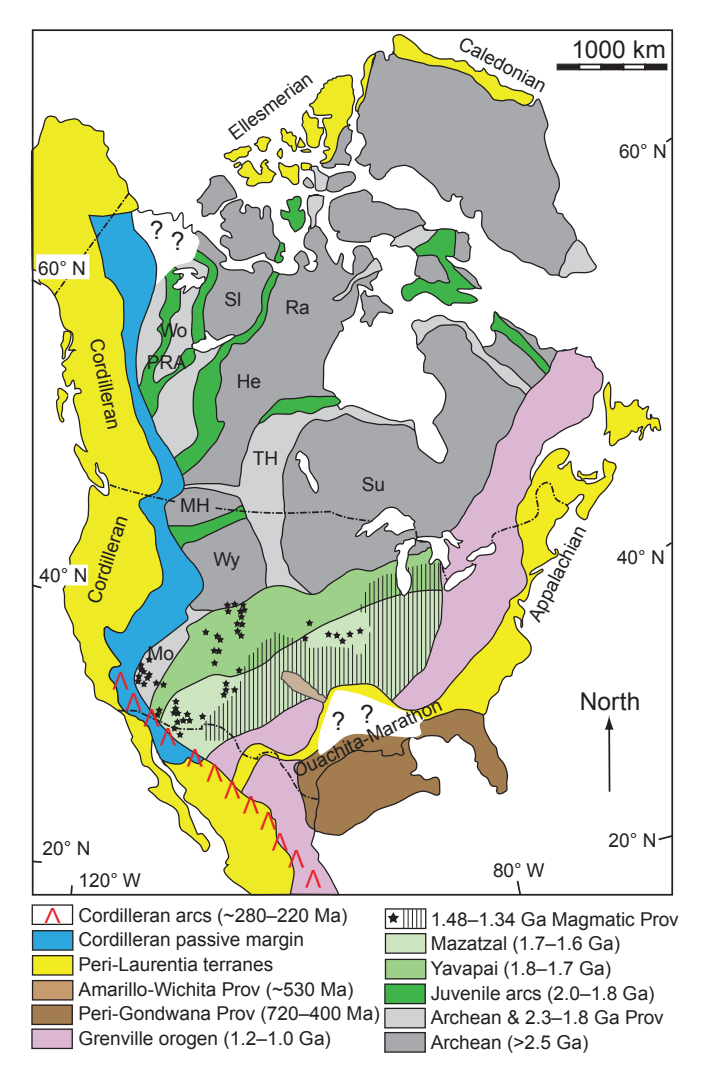


Figure 12. Map of North American basement age provinces adapted from Hoffman (1989), Whitmeyer and Karlstrom (2007), Gehrels et al. (2011), and Gehrels and Pecha (2014). PRA—Peace River Arch region; Mo—Mojave province; Wy—Wyoming province; MH—Medicine Hat province; Su—Superior province; TH—Trans-Hudson province; Ra—Rae province; He—Hearne province; SI—Slave province; Wo—Wopmay province.

province was initially defined only for basement rocks of northern Arizona (Karlstrom and Bowring, 1988; Karlstrom et al., 1993), but it is now understood to extend from Arizona to the southern Great Lakes region (Fig. 12; Hoffman, 1989; Whitmeyer and Karlstrom, 2007; Gehrels and Pecha, 2014). Yavapai province basement generally yields zircon crystallization ages between 1.8 Ga and 1.7 Ga (Gehrels et al., 2011; Karlstrom et al., 1987; Condie and Knoper, 1986; Bickford et al., 1989, 2008). The ca. 1.7–1.6 Ga Mazatzal province extends from southern Arizona into the central and southern mid-continent (Whitmeyer and Karlstrom, 2007; Gehrels et al., 2011; Gehrels and Pecha, 2014). Though Mazatzal province ages are generally younger than Yavapai ages, the boundary between the two provinces is somewhat diffuse, reflecting orogenic processes that overprinted the region several times as terranes were accreted to Laurentia's cratonic core (Karlstrom et al., 1987; Karlstrom and Bowring, 1988; Duebendorfer et al., 2015). In central and southern Arizona, Mazatzal province basement ages range between 1.76 Ga and 1.62 Ga (Karlstrom

and Bowring, 1988; Karlstrom et al., 1993). Granites in central Colorado were emplaced at 1.7–1.66 Ga (Bickford et al., 1989), and northern New Mexico (mostly Yavapai) basement comprises rocks dated at 1.8–1.63 Ga (Maxon, 1976; Karlstrom et al., 2004). Southern New Mexico (Mazatzal) basement has been dated at 1.73–1.61 Ga (Stacey and Hedlund, 1983; Bowring et al., 1983; Roths, 1991).

Mesoproterozoic Alkaline "A-type" Granites and Granite-Rhyolite Province

Mesoproterozoic intrusions of the 1.5-1.3 Ga granite-rhyolite province in the U.S. midcontinent and coeval alkaline plutons in western Laurentia (Bickford et al., 2015) may also be important sources for zircons in ARM basins. These intrusive bodies gained the name "anorogenic" due to their general lack of metamorphic fabrics and timing relative to more deformed Yavapai-Mazatzal rocks; however, closer study has revealed that these rocks formed while orogenic processes were still ongoing (Bickford et al., 2015). Due to their alkaline composition, they are still referred to as "A-type" granites (Bickford et al., 2015). Mesoproterozoic plutonism initiated in eastern Laurentia around 1.5 Ga, and most ages in this area are 1.5-1.45 Ga with an additional peak in age distribution at ca. 1.37 Ga (Bickford et al., 2015). Mesoproterozoic magmatism appears to have younged to the southwest, and granite-rhyolite province rocks in the U.S. midcontinent have been dated at ca. 1.5-1.35 Ga with major peaks at 1.47 Ga and 1.36 Ga (Bickford et al., 2015). From the Rocky Mountains west (the area most proximal to ARM uplifts), Mesoproterozoic pluton ages are 1.48–1.34, with most ages at 1.45–1.41 Ga (Bickford et al., 2015).

Mesoproterozoic Grenville Orogen

The Grenville province consists of a band of ca. 1.3–0.9 Ga crystal-line rocks stretching discontinuously from Newfoundland to Texas and into Mexico (Fig. 12; Rivers, 1997; Bickford et al., 2000; Heumann et al., 2006; Whitmeyer and Karlstrom, 2007). This province formed by accretion of arc and continental blocks to (modern) eastern Laurentia at ca. 1350–1220 Ma during the Elzevirian orogeny (Moore and Thompson, 1980), 1200–1140 Ma during the Shawinigan orogeny (Rivers, 1997; Corrigan and Breemen, 1997), and culminated with the interpreted collision of the Amazonia Craton during the 1090–1020 Ma Ottawan orogeny (Rivers, 1997; Hynes and Rivers, 2010). Deformation continued in the northern part of the orogen until ca. 980 Ma (Hynes and Rivers, 2010). In Texas and southeastern New Mexico, Grenville-age rocks with zircon U-Pb ages between 1.38 Ga and 1.07 Ga are exposed in the Llano Uplift, the Van Horn region, and the Franklin Mountains (Walker, 1992; Bickford et al., 2000).

Late Mesoproterozoic

Within the ARM system, the late Mesoproterozoic Pikes Peak batholith, now exposed west of Colorado Springs, may have shed sediment into adjacent basins. This voluminous batholith is considered a type example of A-type plutonism but has been precisely dated at ca. 1.09 Ga, several hundred million years after the most voluminous phase of A-type plutonism in the western United States (Schärer and Allègre, 1982; Smith et al., 1999; Guitreau et al., 2016). Recent analyses of zircons from ring dikes intruding roof pendants within this batholith yielded ages between 1115 ± 12 Ma and 1078 ± 11 Ma (Guitreau et al., 2016). A granitic pluton in the Little Hatchet Mountains of southern New Mexico has also been dated at 1.07 Ga (Amato and Mack, 2012), and plutons of the Aibo granite in northern Sonora have been dated at 1.11 Ga (Farmer et al., 2005). Diabase intrusions of similar age are widespread throughout the southwestern United States (Heaman and Grotzinger, 1992; Stewart et al., 2001), although here we assume that diabase would be substantially less

zircon fertile than granitic intrusions (e.g., Moecher and Samson, 2006). Bimodal volcanic rocks erupted at ca. 1.1 Ga in the midcontinent rift system and now exposed northern Minnesota could also have been potential sources for detritus zircon of this age (Green and Fitz, 1993).

Neoproterozoic-Cambrian lapetan Rift Related Rocks

Bimodal rift-related igneous suites exposed in the Amarillo–Wichita uplift have been dated at 539–530 Ma (Thomas et al., 2012; Hanson et al., 2013). A detrital sample collected from the Post Oak Conglomerate adjacent to the Amarillo–Wichita uplift and interpreted to have been sourced exclusively from basement rocks therein yielded a unimodal age peak at 535 Ma with 95% of grains dated between 560 Ma and 515 Ma (Thomas et al., 2016).

Neoproterozoic-early Paleozoic Cordilleran margin

Neoproterozoic and early Paleozoic alkalic plutonic suites in north-central Idaho have been dated at 665–650 Ma (Lund et al., 2010) and 500–485 Ma (Evans and Zartman, 1988; Lund et al., 2010), and similar age igneous rocks are present along most of the western miogeocline boundary (Lund et al., 2010). Recent investigation of mafic rocks in the southern Yukon Territory yielded zircon ages of 488–473 Ma (Campbell et al., 2019).

Cambrian Alkalic Rocks of Colorado and New Mexico

Zircons separated from a hornblende–biotite syenite in the Wet Mountains of south–central Colorado yielded a crystallization age of ca. 523.98 ± 0.19 Ma (Schoene and Bowring, 2006). Zircons from syenites in the Powderhorn area of southwest Colorado yielded ages of 525 Ma and 583 Ma (Jaffe et al., 1959, p. 127). Rocks within this suite have yielded K-Ar and Rb-Sr ages of 579–565 Ma (Olson et al., 1977). Zircons from alkalic rocks in the Florida Mountains of southwestern New Mexico have been dated between 523 Ma and 503 Ma (Loring et al., 1987; Evans and Clemons, 1988).

Paleozoic Appalachian Orogen

Several episodes of orogenesis within the Appalachian system produced zircon-rich plutons and metamorphic rocks (Becker et al., 2005, 2006; Bream et al., 2004; Park et al., 2010). Early stages of the Taconic orogeny produced volcanic rocks at 550–500 Ma (Drake et al., 1989), and kyanite-grade metamorphism and magmatism occurred at 470–440 Ma (Hatcher et al., 1989; Drake et al., 1989). The Devonian to Early Mississippian Acadian orogeny resulted in abundant 423–315 Ma plutonism (Osberg et al., 1989; Bradley et al., 2000). Finally, 330–265 Ma plutonism within the Appalachian belt is associated with the Alleghenian orogeny, which marks the final stage of collision with Africa and Laurentia (Hatcher et al., 1989). There is little evidence of similar igneous activity in the Ouachita–Marathon belt to the southwest.

Sources Predicted by Inverse Methods

Caveats with NMF results

The results of NMF must be interpreted within the geologic framework in which samples are found. Interpretation of samples outside of this context is likely to result in incorrect conclusions. Below we present two potential pitfalls inherent in NMF, including (1) factorization artifacts, and (2) incorrect attribution of sources. A common artifact of the NMF modeling of this data set is the presence of nadirs (low points) in more complex distributions that align with unimodes in simple factorized source distributions. We interpret this behavior as a function of the algorithmic nature of NMF where, once a unimodal source is identified and factorized

out, inclusion of that mode in complex distributions is not necessary, and hence the more complex distributions are left with anomalous nadirs. The ca. 1.4 Ga nadir in Source B (Fig. 10) is an inconsequential example of this phenomenon, but the 1.4 Ga and 1.7 Ga nadirs in Source D may contribute to the difficulty in identifying its real source match. As an example of the second pitfall, we conclude that NMF sediment source characterization incorrectly attributes the broad Appalachian-like source (B) to Denver Basin samples (MS04, MS05, MS06, and perhaps MS11; Fig. 7). Denver Basin samples exhibit zircon age unimodes at ca. 1.1 Ga, but we interpret these ages to be locally sourced from the Pike's Peak batholith in the Ancestral Front Range based on the leptokurtic (narrow) nature of the peak. In PDF and KDE NMF model runs with more sources (> 8), a leptokurtic ca. 1.1. Ga unimodal age distribution is identified, but this results in a nadir in a source distribution that otherwise closely matches Appalachian sources (B; Fig. 10 and see Files DR8–DR10). These issues may be common features of inverse modeled source scenarios that contain both simple and complex distributions and should be considered when interpreting factorized sources.

Possible Geological Source Matches for Factorized Sources

We suggest real source matches for NMF-generated sources with varying degrees of confidence. Source A's age distribution is similar to the northern Appalachian detrital zircon source invoked for Pennsylvanian sandstone in the Illinois and Forest City Basins (Kissock et al., 2018). In this interpretation, exhumation of Pan-African metasedimentary terranes (presently in the subsurface) within the northern Appalachian Mountains, containing Neoproterozoic zircons (Zartman et al., 1988; Heatherington et al., 1999; Wortman et al., 2000; Hibbard et al., 2002; Pollock et al., 2007; Fyffe et al., 2009), mixed with early Paleozoic (490-270 Ma) and Grenville (1.3-0.9 Ga) detrital zircons while en route to the midcontinent (Kissock et al., 2018) and possibly North American western margin. Source B's age distribution is similar to the commonly invoked Appalachian detrital zircon age signature observed in the central Appalachian Basin (Fig. 13) from Mississippian through early Permian (Eriksson et al., 2004; Thomas et al., 2004; Becker et al., 2005, 2006; Gehrels et al., 2011; Kissock et al., 2018; Thomas et al., 2017). Source C's age distribution closely resembles early Paleozoic rocks along North America's western margin exhumed during the Antler orogeny (Beranek et al., 2016). Source D is the most difficult factorized source to find a realistic match for and is discussed in greater detail below. Source E's dominant Archean modal age is similar to the cratonic Archean basement terranes of North America (e.g., Superior and Hearne Cratons; Condie et al., 2009) but also closely resembles Cambrian sandstone detrital zircon distributions in the midcontinent (Konstantinou et al., 2014). Source F's 1.7 Ga unimodal age distribution is a close match to North American basement rocks in the Yavapai–Mazatzal terrane (Whitmeyer and Karlstrom, 2007; Gehrels et al., 2011; Laskowski et al., 2013). Source G also closely resembles a North American basement terrane commonly referred to as A-Type (a.k.a. "Picuris"; Daniel et al., 2013) granitoids with a minor contribution from the associated Yavapai-Mazatzal basement terrane (Anderson and Morrison, 1992; Bickford and Anderson, 1993). The age distribution of Source H is consistent with Cambrian age igneous rocks of North America, which are primarily associated with the Oklahoma Aulacogen (Thomas et al., 2016) but also present as minor alkali intrusions throughout the western interior (Olson et al., 1977; Loring et al., 1987; McMillan and McLemore, 2004; Schoene and Bowring, 2006).

Geographic Trends and Basin-Level Description

Most of the factorized sources produced by *DZnmf* exhibit geologically reasonable spatial distributions consistent with the source interpretations

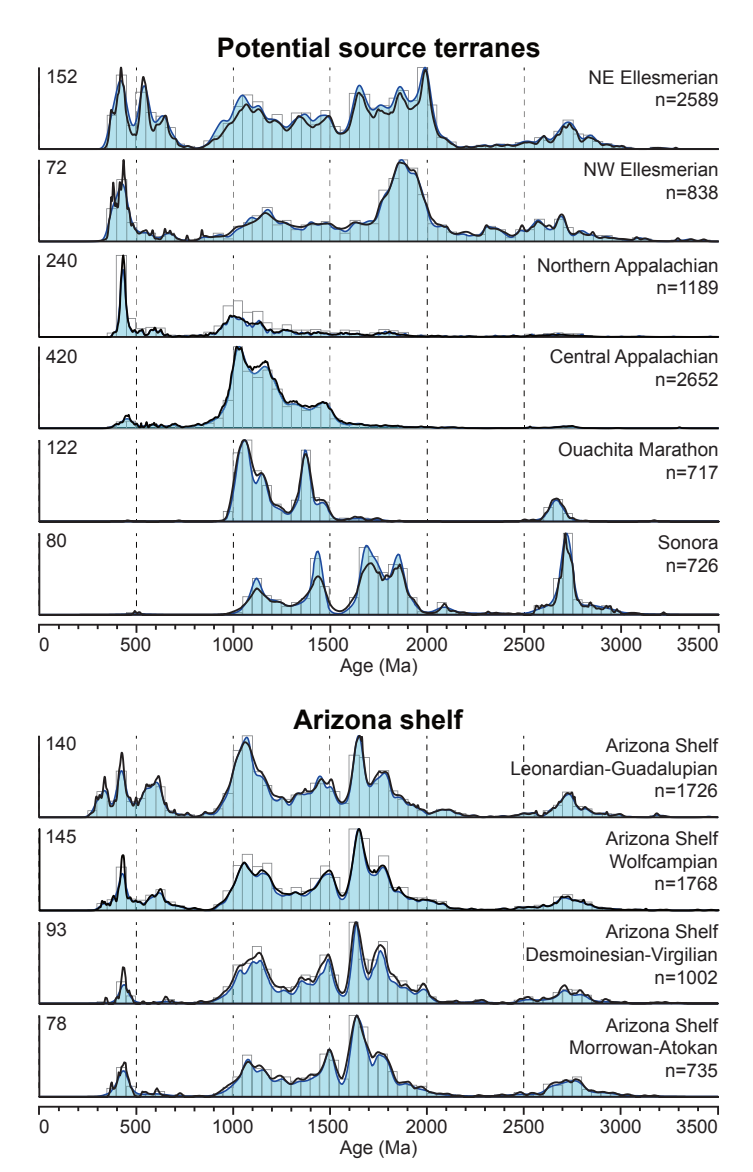


Figure 13. Detrital zircon plots of data from the potential source terranes and aggregated Arizona shelf data. See Figures 1 and 4 for location of Arizona shelf samples. Black line: Probability Density Function (PDF); blue line: Kernel Density Estimate (KDE) with optimized bandwidth (Saylor and Sundell, 2016); gray boxes: histogram with 50 Ma bin width; number at upper left of each plot: max value of y-axis for histogram.

discussed above. The Appalachian-like synthetic sources (A, B) are more prevalent to the east but are present in western depocenters from Mississippian through middle Permian. This is consistent with the development of a North American transcontinental sediment dispersal system by Late Mississippian time (Gehrels et al., 2011; Chapman and Laskowski, 2019). Both Ely Basin samples (Tonka, Battle) exhibit factorized Source C dominance, suggesting a recycled Paleozoic contribution from the Mississippian through Middle–Late Pennsylvanian (Beranek et al., 2016). However, factorized Source C dominance in the Mississippian Wood River Basin yields to Appalachian-like sources (A, B) and Source D dominance in the Middle–Late Pennsylvanian and early Permian. These observations support models of continued deformation along the Antler Orogenic front during the Pennsylvanian (Trexler et al., 2004; Theodore et al., 2004; Sturmer et al., 2018) but also suggest partitioning of a once-connected

foreland basin in the Pennsylvanian that was potentially associated with onset of Ancestral Rocky Mountain (ARM) deformation.

Source D is the most difficult factorized source to find a realistic source match for. However, its predominance in the western portion of North America and increase in prevalence in the Early Pennsylvanian (Figs. 10 and 11) suggest a western-derived source that experienced exhumation coeval with early stages of ARM deformation. Its abundance in Arizona shelf samples could suggest nearby ARM exhumation within the Zuni–Defiance uplift. Conversely, the widespread, north-to-south distribution of Source D suggests a broad western margin source that was perhaps associated with continued deformation along an expanded Antler orogenic front to the north and south of the Ely Basin.

Punctuated and highly localized dominance of ARM basins by North American basement sources within them (Sources E, F, G, and H) highlights both the heterogeneous nature of locally sourced basins and the timing and pattern of ARM deformation. The Central Colorado trough and Denver Basin were the first ARM basins to receive the majority of their sediment from local basement uplifts in the Early Pennsylvanian. At this time the Denver Basin received its greatest proportion of Y-M basement-like factorized sources (Sources F and G). This proportion may be even greater if, in consideration of the issue surrounding incorrect attribution of the leptokurtic 1.1 Ga age mode to the Appalachian-like Source B described above, we consider Source B to be a locally derived basement source. This interpretation is bolstered by the increase in Source B in the Denver Basin during the Middle-Late Pennsylvanian expansion of ARM deformation (i.e., upper and middle Fountain Formation, sensu Sweet and Soreghan (2010); Fig. 7). The Paradox Basin samples are not dominated by basement-like factorized sources until the Middle-Late Pennsylvanian. During this time the Paradox Basin samples are dominated by a ca. 1.4 Ga zircon population (Source G), whereas the Central Colorado trough-Eagle Basin samples have a dominant ca. 1.7 Ga age mode (Source F). By the early Permian, areas of the Paradox Basin received exclusively locally derived basement detritus. Similarly, basement-derived (ca. 530 Ma; Source H) detrital zircons exclusively sourced areas in the Anadarko Basin from its bounding uplift (i.e., the Amarillo-Wichita Uplift). This pattern of basement-derived sediment dominance indicates spatial variability in ARM basin-uplift development and localized sediment sourcing from particular basement blocks but does not support a clear directional trend in deformation as suggested by other authors (Dickinson and Lawton, 2003).

Sediment sources in the middle Permian are more spatially homogenous and exhibit less inter-basin variability than in the early Pennsylvanian to early Permian (Figs. 10 and 11). Middle Permian factorized source attribution indicates increased sourcing by Source A and a marked decrease of basement-like sources. We interpret this regional change in sediment sourcing to reflect cessation of ARM deformation and basinal accommodation, the progressive infill of formerly marine ARM basins by far sourced aeolianites and fluvial strata, and reintegration of regional drainage networks.

Distal Source Terranes

Paleogeographic reconstructions of the late Paleozoic suggest that zircon could have been sourced from substantially outside the conterminous United States (Gehrels et al., 2011). To shed light on the potential sources for non-locally derived sediment, we compare Arizona shelf data to zircon data collected from the northeast Ellesmerian orogen, northwest Ellesmerian clastic wedge, northern and central Appalachian orogen, Ouachita–Marathon fold thrust belt (Gondwanaland sources), and Sonoran miogeoclinal rocks (Fig. 13).

Data from the northeast Ellesmerian orogen consist of 27 Neoproterozoic to Devonian sandstone from Franklinian Basin strata (Anfinson et al., 2012). These strata were deposited in the foreland basin of the Devonian–early Carboniferous Ellesmerian collision, which shed large volumes of sediment to the south (Schack Pedersen, 1986; Embry, 1988; Patchett et al., 1999; Gottlieb et al., 2014). These samples contain a broad Archean peak centered at ca. 2.7 Ga, abundant 2.0–1.6 Ga grains with peaks at 1.99 Ga, 1.86 Ga, and 1.65 Ga, a broad range of Mesoproterozoic and early Neoproterozoic grains with peaks at 1.49 Ga, 1.35 Ga, and 1.08 Ga, and 800–400 Ma grains with a minor peak at 650 Ma and major peaks at 540 Ma and 420 Ma.

To the west, 13 samples from the Late Devonian to Early Mississippian Ellesmerian clastic wedge, referred to as "northwest Ellesmerian orogen" throughout this study (Beranek et al., 2010), include a broad range of Archean through Neoproterozoic grain ages with a large peak centered at ca. 1.9 Ga. These samples also contain a prominent peak at ca. 430 Ma. Sediment eroded from the northeast Ellesmerian orogen has been interpreted to have transported through this area (Garzione et al., 1997; Beranek et al., 2010; Gehrels and Pecha, 2014), but it is also possible that some northeast Ellesmerian orogen sediment bypassed this portion of the basin through a sediment conduit farther east (Anfinson et al., 2012).

Detrital zircon data from the northern Appalachians (Fig. 13) are compiled from samples collected from Newfoundland and the Maine Appalachian orogen (Cawood and Nemchin, 2001; Bradley and O'Sullivan, 2017). In contrast with central Appalachian strata, the most abundant grains are ca. 500–400 Ma and define a major peak at 430 Ma. Northern Appalachian samples also contain abundant 1.2 Ga to 950 Ma grains with minor abundances of Archean to early Mesoproterozoic grains.

Central Appalachian orogen data consist of 22 samples from Precambrian sedimentary and metasedimentary rocks within the Blue Ridge and Inner Piedmont zones of the central Appalachians (Bream et al., 2004; Eriksson et al., 2004) and 14 samples from Cambrian to Devonian sedimentary rocks within the Appalachian foreland basin (Eriksson et al., 2004; Park et al., 2010). Collectively, Appalachian foreland basin samples contain abundant ca. 1.25 Ga to 950 Ma grains with peaks at 1.18 Ga and 1.02 Ga, moderate abundances of 1.55 Ga to 1.25 Ga grains, and minor abundances of 500–400 Ma grains (Fig. 13).

Ouachita–Marathon data consist of five samples from Ordovician and Silurian strata exposed in the Ouachita Mountains of Oklahoma and Arkansas (McGuire, 2017). Together, these samples contain populations at 2.6–2.5 Ga, 1.4–1.35 Ga, and 1.1–1.0 Ga (Fig. 13).

Data from four samples from Cambrian through Devonian Cordilleran passive margin rocks now exposed in Sonora, Mexico, (Gehrels and Pecha, 2014) consist of a major Archean peak centered at ca. 2.7 Ga, major peaks at 1.85 Ga, ca. 1.7 Ga, and 1.43 Ga, and a subordinate peak at 1.11 Ga (Fig. 13).

Provenance Interpretation

The interpretations of sediment provenance presented here begin with data from individual basins, starting in the Denver Basin and progressing counterclockwise. We then integrate these interpretations into a broader interpretation of late Paleozoic sediment routing.

Denver Basin

Age peaks from a sample of the Glen Eyrie Member (Fig. 7; MS01) are interpreted to represent multiple sediment sources including 1.7–1.9 Ga Yavapai crust and 1.4–1.5 Ga A-type granite sources. Zircons with these ages have also been identified in the Cambrian Sawatch Formation, which was deposited disconformably above the Pikes Peak Granite (Siddoway and

Gehrels, 2014), and we link grains with these ages in the Glen Eyrie Formation to erosional recycling of Paleozoic strata. Grains making up a minor peak at 1.08 Ga are interpreted to have been eroded from the upper portions of the 1.08–1.09 Ga Pikes Peak batholith just to the west of the basin. Scattered individual Paleozoic grains are interpreted to represent either minor inputs of distal Appalachian-derived grains or recycling of similar age grains from the Devonian Williams Canyon Formation within the Paleozoic section overlying the Pikes Peak granite (Siddoway and Gehrels, 2014). Upsection, the lower Fountain Formation (MS10) contains similar age peaks, but the 1.7 Ga peak is less prominent, and this sample does not contain any Paleozoic grains. Sample MS11 from the middle Fountain Formation sits directly above an intraformational unconformity (Sweet and Soreghan, 2010); an increase in prominence of the ca. 1.08 Ga peak is interpreted as increased contribution of Pikes Peak batholith sediment to the basin. This peak is increasingly dominant upsection in samples from the middle Fountain Formation (MS06, MS05, MS04). We interpret these data to indicate that material eroded from the Pikes Peak batholith was the dominant source of sediment for this portion of the Denver Basin during Desmoinesian-Virgilian time. The transition from bimodal (1.09 Ga and 1.43 Ga) to unimodal (1.09 Ga) spectra in the upper Fountain Formation coincides with a major shift in paleocurrent indicators that indicate northnortheast sediment transport in the lower and middle Fountain Formation to east-southeast sediment transport during upper Fountain Formation deposition (Sweet and Soreghan, 2010). In the upper portion of this section, the Wolfcampian Ingleside Formation yielded a broad distribution of zircon ages distinct from strata below (Fig. 7). These are interpreted to represent distal Laurentian sources such as the Canadian Shield, Grenville, and early Acadian orogeny or age equivalent, respectively. The most plausible sources for grains of these ages are the northeast and northwest Ellesmerian and northern Appalachian orogen, or some combination thereof. The Pikes Peak batholith was likely still a major contributor of sediment to the Ingleside Formation, but equal abundances of grains within the 1.00–1.05 Ga and 1.05-1.10 Ga age windows suggests the emergence of a new source from which 1.00-1.05 Ga grains were derived.

Overall, these data suggest an unroofing sequence beginning with erosion of lower Paleozoic strata (Siddoway and Gehrels, 2014) and culminating in the sole dominance of Pikes Peak granite detritus in the upper Fountain Formation. A similar unroofing trend has been interpreted by the presence or absence of quartz arenite clasts within the Fountain Formation (Sweet and Soreghan, 2010). These data suggest the onset of Ancestral Front Range exhumation by Atokan time. These data also show a rapid shift in provenance from proximally to distally derived sediment during the Wolfcampian (early Permian). This shift suggests that the basin's sediment budget was overwhelmed by aeolian material at this time (Sweet and Soreghan, 2010; Sweet et al., 2015; Sweet, 2017), a shift that suggests exhumation may have slowed or ceased within the Ancestral Front Range. These data also point to the Denver Basin being sedimentologically isolated from other Ancestral Rocky Mountain basins until Wolfcampian time.

Central Colorado Trough

West of the Ancestral Front Range uplift, samples from the Central Colorado trough are interpreted to show initiation of ARM exhumation during Morrowan time (Fig. 5, panel 6). Detrital zircon spectra show a substantial change from Mississippian (Leadville Limestone) to Morrowan (Kerber Formation), and the dominance of ca. 1.7 Ga grains in the latter is interpreted to indicate exhumation of Yavapai basement rocks, although the presence of Archean to Paleozoic grains suggests a broad mix of distal Laurentian sources as well. Above this, 1.7 Ga grains dominate the spectra from the Atokan Sharpsdale Formation. These spectra

are interpreted to reflect intensification of ARM exhumation adjacent to the Central Colorado trough during the Atokan stage.

Eagle Basin

Eagle Basin samples were collected along a transect from the proximal eastern basin (Vail, Colorado) to the distal northwestern basin (Meeker, Colorado) (Fig. 5). Unimodal 1.7 Ga age distributions from the Vail section are interpreted to represent sediment derived solely from Yavapai crust exposed by the paleo-Front Range uplift directly east of the basin; 1.7 Ga rocks are currently exposed just east of this location in the hanging wall of the Gore fault (Sims et al., 2001). The 1.7 Ga peak in sample V10 is interpreted to represent the same sediment source dominant in the other samples from this section; however, Archean, Neoproterozoic, and Paleozoic grains in this sample are interpreted to represent distally sourced grains transported into the proximal Eagle Basin through aeolian processes (e.g., Schenk, 1987) and/or during sea level highstands.

To the west, grain ages from the Eagle Valley Evaporite (Fig. 5, panel 3) are interpreted to represent sediment input from the same Yavapai basement source (1.7 Ga) as well as A-type granitic sources (1.4 Ga). This sample (EC01) contains additional peaks at 1.1 Ga and 400 Ma that are interpreted as distally sourced grains from either the northern Appalachian or northwestern Ellesmerian orogen or a combination thereof. Above this, the basal Eagle Valley Formation is interpreted to represent derivation from a single 1.7 Ga local source with scattered single grains representing distal sources. The upper sample in this section contains a broad distribution of grain ages and is interpreted to represent sediment with mixed provenance including locally derived sediment (ca. 1.7 Ga and 1.45 Ga) as well as northern Appalachian/Arctic derived grains. A prominent group of ages at ca. 550 Ma is interpreted to represent grains sourced from the northeast Ellesmerian orogen or the northern Appalachians (Fyffe et al., 2009) (Fig. 5).

The Glenwood Springs section (Fig. 5, panel 2) is adjacent to the ancestral Uncompahgre uplift and was located in the west–central Eagle Basin during Pennsylvanian to Permian time (Johnson, 1987). This proximity is reflected by a major change in detrital zircon spectra between this section and the Eagle and Vail sections to the east. In contrast with the eastern basin, samples in this section show two dominant age peaks at 1.7 Ga and 1.43 Ga, which are interpreted to represent sources in Yavapai and A-type granitic sources exposed by exhumation of the ancestral Uncompahgre uplift. Crystalline rocks of this age are exposed along the northern flank of the Paradox Basin (see below) and are interpreted in the subsurface south of the Eagle Basin (Sims et al., 2001). One sample from this section (GS09) contains a much broader distribution of ages, including a major peak at 1.65 Ga that is interpreted to represent Mazatzal derived sediment, and multiple small Proterozoic peaks are interpreted to represent Appalachian and/or Ellesmerian sourced sediment.

The basal sample from Meeker (MC05; Fig. 5, panel 1), the west-ernmost section in the Eagle Basin, contains two dominant age peaks at 1.7 Ga and 1.4 Ga that are interpreted to represent Yavapai and A-type granite sources within the ancestral Uncompahgre uplift to the south. Above sample MC05, two samples from the upper Minturn Formation have zircon spectra with broad age distributions. Major peaks at 1.65 Ga and 1.43 Ga are interpreted to represent input from Mazatzal and A-type granite sources, respectively; subordinate age peaks between 1.8 Ga and 1.73 Ga are interpreted to represent a mix of individual Yavapai sources. A prominent peak in sample MC17 at 1.15 Ga is interpreted as Grenville or Ellesmerian derived material, and small numbers of grains making peaks at 420 Ma and 580 Ma in MC20 are interpreted as Appalachian/northeast Ellesmerian, respectively. Overall, data from this section suggest that during Desmoinesian time, this portion of the basin changed from

sedimentation dominated by ancestral Uncompahgre, Front Range, and Sawatch uplift-derived material to sedimentation dominated by distally sourced material from either the Appalachian orogen (Gehrels et al., 2011) or the northeast Ellesmerian orogen (Anfinson et al., 2012; Link et al., 2014). An alternative scenario could be that spectra from these samples represent recycling of grains from lower Paleozoic strata unroofed by ARM uplift. However, we prefer the former scenario because of the similarity in spectra among samples MC17 and MC20 and age-equivalent strata to the northwest (Fig. 9; Lawton et al., 2010; Link et al., 2014). In our preferred model, the local/distal sediment mixing interface shifted from west or northwest of this section during early Desmoinesian time to east or southeast of this section by late Desmoinesian time.

Paradox Basin

Two detrital zircon transects across the Paradox Basin shed light on the sediment shed southward from the ancestral Uncompangre uplift. In the western proximal basin near Gateway, Colorado, (Fig. 6, panel 1) samples TP01 and JB01 show nearly unimodal zircon ages centered at 1.43 Ga that are interpreted to record sediment eroded from small catchments eroding A-type granites as well as minimal Yavapai rocks to produce minor populations at 1.73 Ga. Ca. 1.4 Ga granitic rocks and Paleoproterozoic metamorphic rocks are currently exposed to the northeast of this location (Sims et al., 2001), and the Cutler Formation in this location was likely sourced from similar rocks. These samples are interpreted as Wolfcampian in age (see File DR1 for detailed discussion of age interpretation), and uni- and bimodal age distributions in these samples suggest that the ancestral Uncompangre uplift still dominated the sediment budget of the proximal Paradox Basin at this time. Although this does not necessarily require active uplift (e.g., Paola et al., 1992; Heller and Paola, 1992), it does suggest at least recent, if not active, rock uplift and exhumation of the Uncompangre uplift during Wolfcampian time.

Ages from one sample from Upper Pennsylvanian (Missourian) strata (sample KA03) within the western medial Paradox Basin (Fig. 6, panel 2) are interpreted to represent a mix of proximal and distally sourced sediment (Fig. 6, location 2). Major peaks at 1.7 Ga and 1.4 Ga are interpreted to represent grains sourced from exhumation of Yavapai and A-type granite sources within the Uncompahgre uplift to the northeast (Sims et al., 2001). A minor, broad peak between 1.2 Ga and 1.0 Ga is interpreted to represent distal, Grenville orogen-derived grains as are grains making up a minor peak at 430 Ma. Scattered Archean grains are interpreted to have been eroded from the Canadian Shield or the Wyoming Craton.

Desmoinesian–Virgilian samples from the distal portion of the western Paradox Basin (Fig. 6, panel 3) contrast with samples from medial and proximal basin positions. Spectra from these samples contain broad distributions of Archean to Paleozoic ages. In these samples, Archean grains are interpreted as sourced from the Canadian Shield and/or Wyoming Craton, 1.8–1.7 Ga grains are interpreted as sourced from Yavapai rocks, and 1.7–1.6 Ga grains are interpreted to represent Mazatzal sources along the southern margin of the basin or northern portion of the Zuni/ Defiance uplift (Wengerd and Matheny, 1958). The 1.3–0.95 Ga grains are interpreted as sourced from Grenville rocks, and 500–300 Ma grains are interpreted as either northern Appalachian or Ellesmerian in origin. Overall, these strata suggest diverse sources of sediment within this portion of the basin, and these spectra contrast strikingly with those interpreted as having a single, proximal source within the proximal basin.

Analyses of Leonardian strata across the Paradox Basin (Lawton et al., 2015; Fig. 5) show a major change in zircon spectra at the Wolfcampian–Leonardian boundary. Above this boundary, rocks of the Castle Valley and White Rim Formations contain broadly distributed ages in stark contrast to the bimodal spectra from the Cutler Group below (Fig. 5, panel 1). This reflects the shift

from fluvial and alluvial depositional systems sourced from the Uncompahgre uplift to an aeolian system that overwhelmed the sedimentary environments and carried sand into the basin via longshore current and aeolian processes (Lawton et al., 2015). A prominent ca. 1.43 Ga peak is retained through the lower Castle Valley Formation (samples 12CV50, 10CVR, 10CVG) in the proximal basin (Fig. 5, panel 1), suggesting that proximal Uncompahgre sediment was a major contributor to the material that filled this portion of the basin during Leonardian time. However, 1.43 Ga grains are nearly absent from the upper Castle Valley Formation (sample 10CVW), which suggests the shutoff of Uncompahgre exhumation by this time (Fig. 5, panel 1; Lawton et al., 2015).

A transect across the eastern proximal basin (Fig. 6, panel 4) sheds light on the along-strike variability (compared to the western proximal Paradox Basin) of sediment sources contributing to the proximal basin. A sample from the Atokan Molas Formation yielded a major peak between 1.1 Ga and 1.0 Ga, a minor abundance of grains at 500-400 Ma, and a broad range of Archean-Neoproterozoic grains (Fig. 6, panel 4). This spectrum is interpreted to represent input from the Appalachian orogen via recycling of eroding Mississippian strata (e.g., Gehrels et al., 2011). Above this, all samples contain two peaks at 1.73-1.71 Ga and ca. 1.43 Ga (Fig. 6). From Desmoinesian through Wolfcampian samples, there is also an increase in prominence of a peak at 500 Ma, and grains of this age make up greater than half of the grains dated within the youngest Cutler Formation sample. These grains are interpreted to be sourced from diabase and syenitic rocks of this age in southwestern Colorado (Olson et al., 1977). Together, these data suggest an unroofing trend in which Atokan strata were sourced from erosion of the lower Paleozoic section, and Desmoinesian-Wolfcampian strata were sourced from progressive erosion of basement rocks. Increasing depth of basement exhumation and/or drainage network evolution altered the abundance of detrital ages upsection. These data in addition to previous sedimentologic observations (Wengerd and Matheny, 1958) suggest that the eastern portion of the basin was filled by sediment sourced from the San Luis highlands to the east and represent a distinct sediment source from the western basin. The absence of 550-600 Ma grains in the rest of the basin suggest that proximal sediment shed into the eastern basin did not reach the western basin.

Arizona Shelf and Southeastern Arizona

Samples from the Arizona shelf and southeastern Arizona basins have high degrees of similarity. In statistical comparison of 17 total samples, only two samples yield PDF cross-correlation values <0.5 (see File DR6). Major peaks common to most of these samples include a 1.8–1.7 Ga peak that is interpreted to represent material eroded from Yavapai-aged rocks exposed in Ancestral Rocky Mountain uplifts to the north and east (Figs. 4–6); a 1.7–1.6 Ga peak that is interpreted to represent erosion from Mazatzal rocks in northeastern Arizona and New Mexico (Karlstrom and Humphreys, 1998; Whitmeyer and Karlstrom, 2007); and a peak slightly younger than 1.5 Ga that is interpreted to represent erosion from A-type granites (Whitmeyer and Karlstrom, 2007). Alternatively, it is possible that these ages represent recycling of ca. 1.5 Ga grains from Proterozoic quartzites exposed along the Defiance uplift in northeastern Arizona (Doe et al., 2012, 2013). Broad peaks typically centered at 1.1-1.0 Ga and commonly containing a subordinate peak between 1.2 Ga and 1.1 Ga are interpreted as "Grenville" grains. However, Grenville crystalline rocks are widespread as are Mesoproterozoic to Neoproterozoic strata containing Grenville zircon (e.g., Rainbird et al., 2017), and all potential source areas considered above except for Sonoran miogeoclinal strata could have contributed grains to produce these peaks (Fig. 13). Grains of this age also could have been recycled from Mississippian strata in central and western Laurentia (Chapman and Laskowski, 2019). Also abundant in most Arizona samples are 500–300 Ma grains with well-defined peaks at ca.

430 Ma. These grains are typically interpreted as "Appalachian" orogen grains but could also have been sourced from the northwest or northeast Ellesmerian orogen (Beranek et al., 2010; Anfinson et al., 2012). Also present in many of these samples, especially from the Wolfcampian and Leonardian samples, are minor peaks/populations between 650 Ma and 500 Ma. In classical North American zircon provenance studies, grains of this age range are typically interpreted to be sourced from the pan-African/Brasiliano Craton (Gehrels et al., 2011; Gehrels and Pecha, 2014; Alsalem et al., 2018; Chapman and Laskowski, 2019). However, these peaks are also well-represented within northeast Ellesmerian orogen sources (Fig. 13; Anfinson et al., 2012). In either case, ca. 2.7 Ga grains, 1.2-1.0 Ga grains, and 650-300 Ma grains within Arizona samples were likely eroded and transported many hundreds to thousands of kilometers from their sources and represent distally sourced sediment. Recycling of these grains from strata immediately underlying the Arizona shelf is precluded by the near absence of these grain ages within the lower Paleozoic section in this region (Gehrels et al., 2011). Arizona shelf and southern Arizona spectra collectively represent mixing of distal sources with "locally" derived Yavapai, Mazatzal, and Granite-Rhyolite grains.

Unlike samples near major ARM uplifts, Arizona samples show little upsection change (Fig. 13). The only exception to this is that 650-500 Ma grains become substantially more abundant in the western Mogollon Rim (Fig. 4, panel 1) and the Plomosa Mountains section (Fig. 4, panel 2); this section structurally restores in close proximity to the Mogollon Rim (McQuarrie and Wernicke, 2005) beginning in Wolfcampian time. A similar increase in abundance occurs beginning in Leonardian time within the Eastern Mogollon Rim (Fig. 4, panel 3). Interestingly, grains of this age are present within the Pedregosa Basin by at least Virgilian time (Fig. 4, panel 5). The increasing abundance of these grains up section and their early appearance farther south could suggest a southern, African, or South American source for these grains. However, we consider it more likely that these grains were sourced from the northeast Ellesmerian orogen or northern Appalachians (Fyffe et al., 2009). A substantial portion of the Schnebly Hill Formation and nearly the entire thickness of the Coconino Sandstone is made up of aeolian facies (Blakey, 1990), and southward paleotransport is well documented in the Coconino Sandstone (Reiche, 1938; Odyke and Runcorn, 1960; Peterson, 1988). Additionally, consistent marine carbonate deposition within the Pedregosa Basin as well as marine conditions within the Permian Basin system to the east (Greenwood et al., 1977; Frenzel et al., 1988; Soreghan, 1994; Wright, 2011) suggest that it would have been unlikely for Ouachita-Marathon derived sediment to bypass those depocenters and be transported north.

Keeler-Lone Pine Basin

Samples collected from the Keeler and Lone Pine Basins are largely similar (Fig. 8). The age peaks at ca. 1.85 Ga are uncommon in late Paleozoic Laurentian samples presented in this study, and these ages could represent either sediment originating (1) within Ellesmerian orogen, in which these ages are abundant (Fig. 13), (2) from accreted rocks to the northwest of these basins such as the Antler and/or Klamath terranes (Gehrels, 2000; Grove et al., 2008; LaMaskin, 2012; Beranek et al., 2016), (3) from recycling of nearby lower Paleozoic passive margin rocks (Chapman et al., 2015), or (4) from erosion of the 1.8 Ga Mohave province (Whitmeyer and Karlstrom, 2007). A low abundance of 1.6-1.8 Ga grains in most of these samples is interpreted to indicate that material eroded from Ancestral Rocky Mountain basement uplifts was not a major contributor to the sediment budgets of the Keeler and Lone Pine systems. Age peaks at 1.1-1.0 Ga could represent either "Grenville" ages from the northern Appalachian orogen (e.g., Gehrels et al., 2011) or similar ages from the northeast Ellesmerian orogen and/or northwest Ellesmerian

orogen (Beranek et al., 2010; Anfinson et al., 2012). The same provenance possibilities apply to peaks at 500–400 Ma (Fig. 13).

Late Paleozoic Laurentian Sediment Routing

We interpret the detritus that filled Pennsylvanian—Permian Ancestral Rocky Mountain basins to have been sourced from two end-member sources: far-traveled sediment derived from the Ellesmerian orogeny and/or the northern Appalachian orogen and proximal material eroded from exposed basement rocks and potentially local recycled Mississippian strata within the Ancestral Rocky Mountain system. The zircon budgets of proximal portions of the Denver, Eagle, and Paradox Basins were dominated completely by ARM sources, whereas zircon in the medial and distal portions of the Eagle and Paradox Basins appear to consist of a mix of ARM material and distally derived material. Of the basins studied here, zircon within the deep marine basins of southeast California appears to contain the least amount of ARM-derived material (Fig. 9). These interpretations follow Gehrels et al. (2011) and Gehrels and Pecha (2014), with the notable exception of a diminished importance of Appalachian provenance in favor of sources in northern Canada.

Morrowan-Atokan (323-312.6 Ma)

Samples from Morrowan-Atokan (323-312.6 Ma) rocks show early signs of ARM-related exhumation. The appearance of major ca. 1.7 Ga peaks in Morrowan samples from the Grand Canyon (Gehrels et al., 2011) and Central Colorado Trough (sample BC01) as well as the Atokan appearance of ca. 1.65 Ga peaks in the Grand Canyon, Mogollon Rim (sample SY-D), and southwestern Arizona (sample 1QZ-19) are interpreted to represent the early signals of Yavapai-Mazatzal exhumation related to ARM uplift surrounding these basins. However, these spectra contain a mix of other ages, not the uni- or bimodal spectra that typify Late Pennsylvanian samples in these sections. Interestingly, samples from the Upper Mississippian Surprise Canyon Formation in Grand Canyon strata contain peaks at 1.7 Ga and 1.43 Ga (Gehrels et al., 2011), and the Upper Mississippian Leadville Limestone in the Central Colorado Trough (Fig. 5, panel 6) has peaks at ca. 1.42 Ga and 1.7 Ga, allowing for the possibility that ARM exhumation initiated during the latest Mississippian. Conversely, Atokan samples from the Molas Formation within the proximal Paradox Basin do not contain significant numbers of 1.7 Ga or ca. 1.4 Ga grains (sample ML01; Evans and Soreghan, 2015; Nair et al., 2018), both of which become the dominant grain ages during the Middle-Late Pennsylvanian. This suggests that substantial exhumation of Uncompangre basement rocks did not occur until Desmoinesian time, although unroofing of lower Paleozoic rocks deposited above basement could have occurred earlier.

At the continental scale, Morrowan–Atokan Arizona shelf samples from this time interval are statistically distinct from samples proximal to nascent ARM uplifts as well as from samples within the Ouachita–Marathon foreland (Buratowski, 2014), the Illinois and Forest City Basins (Kissock et al., 2018), and the Appalachian Basin (Becker et al., 2005; Park et al., 2010) (Fig. 9). Compared to aggregated data from potential source terranes, aggregated Arizona shelf data are most statistically similar to the northeast Ellesmerian orogen (cross-correlation coefficient of 0.45; Anfinson et al., 2012) and the Sonoran margin (cross-correlation coefficient of 0.42; Gehrels and Pecha, 2014). We did not calculate cross-correlation values between the Arizona and mixtures of these end-member sources, but it is possible that such mixtures could produce higher statistical matches. Sample density surrounding the Arizona shelf is too low to definitively determine source or transport pathway.

Desmoinesian-Virgilian (312.6-299 Ma)

The Desmoinesian–Virgilian (312.6–299 Ma) interval contains the greatest number of samples from the ARM system (Fig. 9). Locations proximal to ARM basement uplifts from this time interval show nearly unimodal or bimodal age spectra (e.g., Figs. 5–7) that suggest large amounts of basement exhumation and large volumes of sediment input into proximal ARM basins. Samples collected from locations distal to major basement uplifts contain substantial numbers of "local" Yavapai-Mazatzal grains that are interpreted to have been eroded from ARM basement uplifts; however, these samples also contain broad age spectra that are interpreted to have been sourced from outside southwestern Laurentia. In the western portion of the ARM system, samples distal to ARM uplifts make up a roughly north-south zone in which individual samples are moderately similar to aggregated samples of the Arizona shelf (Fig. 9). Most samples within this zone have PDF cross-correlation values > 0.5 when compared to the Arizona shelf, in contrast with most proximal ARM basin samples (< 0.4). One exception to this is one siltstone sample from northern Arizona (Dry-Creek; Soreghan et al., 2007) in which only 54 grains were analyzed. The small number of grains likely prevents meaningful statistical comparison of this sample to larger-n samples (Saylor and Sundell, 2016). These samples are also distinct from a sample collected in central Nevada (Battle; Gehrels, 2000) that contains a major peak at 1.86 Ga and a subordinate peak at 2.66 Ga. Similar prominence of these populations is not found in any of the distal ARM basin samples, although grains of these ages are present.

Collectively, these data suggest the presence of an active sediment routing system that ran north to south from southern Canada to southern Arizona (Fig. 9). Previous detrital zircon work on Upper Pennsylvanian strata in southwestern Laurentia have interpreted the sediment that filled distal portions of ARM basins as allochthonous (Gehrels et al., 2011; Link et al., 2014; Beranek et al., 2016; Chapman and Laskowski, 2019), but whether that material transited the northern United States midcontinent from the Appalachian orogen or was derived from Arctic terranes and/or the northern Appalachian orogen was not clearly resolved (Gehrels et al., 2011; Link et al., 2014). In addition to PDF cross-correlation values, a transect of Desmoinesian-Virgilian samples from the Illinois, Forest City, and Wood River Basins and northern Wyoming (Fig. 14) suggests that Desmoinesian sediment transport from the northern midcontinent to the Bighorn and Wood River Basins is unlikely. Spectra from the Illinois and Forest City Basins contain few grains older than 1.5 Ga, in contrast with major peaks between 1.8 Ga and 1.6 Ga within Bighorn and Wood River strata. These data suggest a major Desmoinesian sediment divide between the Forest City and Bighorn Basins (Fig. 14B). This interpretation is also supported by the relative similarity of a Late Pennsylvanian sample from southeastern British Columbia (Fig. 14A) that suggests that the north-south sediment transport pathway likely extended at least this far north. We interpret Arizona shelf spectra to consist of a combination of far-traveled grains and grains eroded from the Zuni-Defiance uplift in northeastern Arizona based on the abundance of Yavapai and Mazatzal grains as well as age peaks centered on ca. 1.5 Ga (Doe et al., 2013). We interpret the presence of sediment divide between the Arizona shelf and the Paradox Basin during this time interval (Fig. 9) possibly associated with the Zuni-Defiance uplift. This interpretation is based on a mismatch between the 1.42 Ga population dominant within the eastern proximal Paradox Basin at this time (and later during Wolfcampian time in the western Paradox Basin) (Fig. 6, panel 2 and 4) and the prominent 1.50 Ga peak present in Arizona shelf samples (Figs. 3, 4, and 13) at this time. This mismatch implies that "A-type granite" zircons shed from the Uncompangre Uplift did not reach the Arizona shelf and that 1.50 Ga grains within the Arizona shelf were derived from another source. One

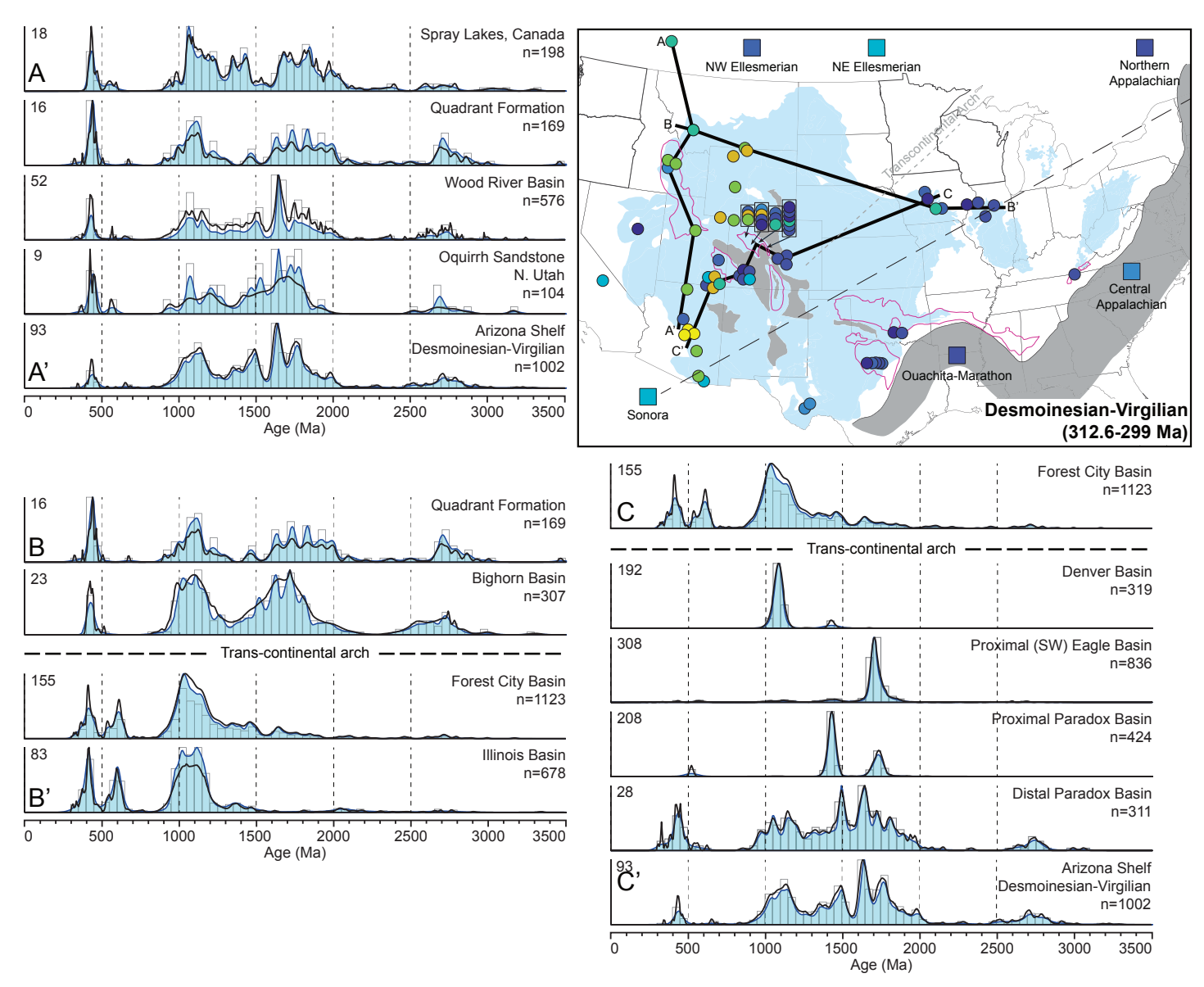


Figure 14. Detrital zircon spectra from Desmoinesian–Virgilian transects showing similarity of age distributions of from eastern BC to the Arizona shelf (north to south; A–A') and a major discontinuity between Idaho, Montana, and Wyoming and Appalachian sourced basins in the U.S. midcontinent (west to east; B–B'). Data sources: Lawton et al. (2010), May et al. (2013), Gehrels and Pecha (2014), Link et al. (2014), Kissock et al., (2018), this study.

possibility is recycling of Proterozoic quartzites from the Zuni–Defiance uplift (e.g., Doe et al., 2013).

Statistical comparison of Arizona shelf data from this time interval to potential distal source terranes yields the highest similarity values with the northeast Ellesmerian orogen and/or Sonoran sources, but we cannot rule out the possibility of northern Appalachian sediment being transported across the Canadian Shield before being routed southward into the ARM system via longshore and aeolian processes (Fig. 15).

Wolfcampian (299-282 Ma)

During Wolfcampian time (299–282 Ma) (Fig. 9), uni- and bimodal detrital zircon spectra from proximal Paradox Basin deposits are interpreted to indicate that sediment was sourced exclusively from the ancestral Uncompanding uplift to the northeast. These spectra contrast with spectra

from coeval Arizona shelf strata to the southwest, which contain broad distributions of grain ages (Figs. 3–4 and 9), and we interpret that a sedimentary divide, most likely topographic, separated these areas (Fig. 9) based on the mismatch between nearly unimodal 1.42 Ga zircon populations in the proximal Paradox Basin and prominent 1.50 Ga populations in Arizona shelf samples (see above). Samples from the Arizona shelf and southern Arizona have high statistical similarities, suggesting that sediment within this region was well-mixed. Similar to the Desmoine-sian–Virgilian interval (above), a conduit of moderate statistical similarity extends northward at least as far as southern Idaho (Fig. 9), and we interpret this as the route by which far-traveled sediment entered the Arizona shelf and southern Arizona. Strata sampled in the Denver Basin from this period have greater similarity to the Arizona shelf than underlying strata (Fig. 9). This shift coincides with the transition from fluvial to aeolian deposition as the Denver Basin was overwhelmed by southward

progression of a major aeolian system and a coeval change from local-to continental-scale sediment sourcing. This shift also likely coincides with the cessation of exhumation of the ancestral Front Range uplift (Fig. 7). Arizona shelf samples from this interval are also statistically distinct from Lone Pine Basin samples (Fig. 8). We interpret the zircon within the Lone Pine Basin to have been sourced from Ellesmerian or northern Appalachian orogens but to have bypassed the ARM system such that Yavapai—Mazatzal and A-type granitic zircons were not substantially incorporated (Fig. 9). As in the two previous time intervals, aggregated Arizona shelf data are most statistically similar to aggregated data from the northeast Ellesmerian orogen, but we cannot rule out contribution from the northwest Ellesmerian and northern Appalachian orogens (Fig. 15).

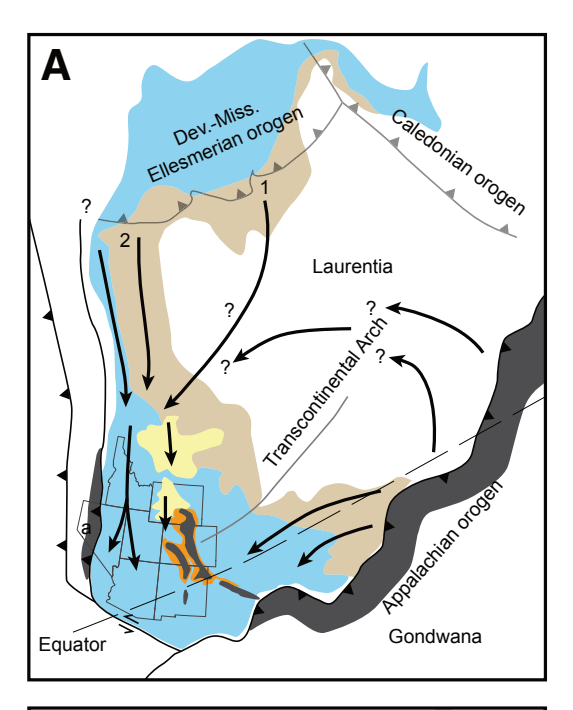
Leonardian-early Guadalupian (ca. 282-260 Ma)

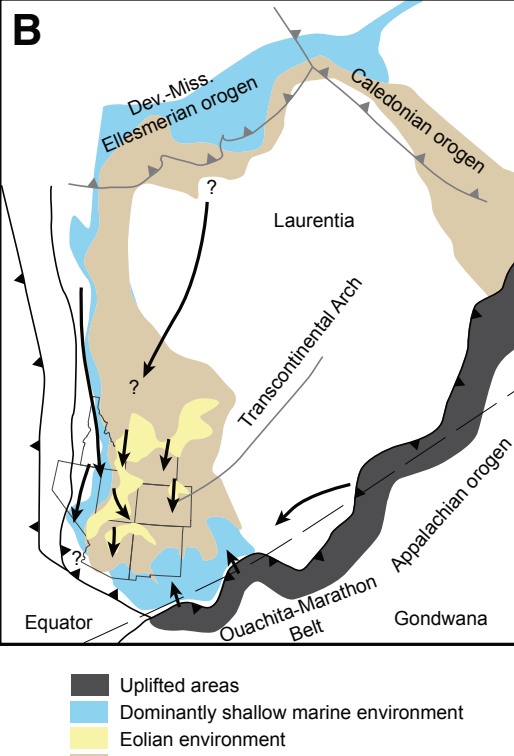
Leonardian to early Guadalupian (ca. 282-260 Ma) sedimentation within the ARM system was largely dominated by aeolian systems (McKee and McKee, 1967; Blakey et al., 1988; Lawton et al., 2015) driven by south-directed sediment transport (Parrish and Peterson, 1988; Peterson, 1988). This is reflected in the detrital zircon data (Fig. 9) by a higher degree of statistical similarity across the entire ARM system from northern Wyoming through central Arizona (Fig. 9). We interpret these results (and deposits) as part of a large, well-mixed volume of aeolian sand that moved southward into the region as Pangea drifted northward away from the equator (Scotese et al., 1999; Domeier and Torsvik, 2014) and the climate aridified (Tabor and Poulsen, 2008). We also interpret the switch from uni- and bimodal detrital zircon spectra to broad spectra with diverse grain ages in the Paradox Basin (Figs. 8-9) to suggest the cessation of major exhumation on the ancestral Uncompangre uplift during Leonardian time, consistent with field evidence for cessation of active uplift by this time (Soreghan et al., 2012).

Mechanisms of Sediment Transport

The interpretations above demand one or more mechanism(s) by which sediment was transported ~2000 km along the dominantly shallow marine western margin of Laurentia during Pennsylvanian and Permian time (McKee and Crosby, 1975). We argue that coupled longshore current/ aeolian transport is the most likely process. Silt-sized grains also could have been transported in suspension and deposited as loess (e.g., Soreghan et al., 2014). Aeolian cross bedding from a Morrowan–Atokan sequence of mixed aeolian and shallow marine strata in southwest Alberta records southwest to south-southeast sediment transport (Stewart and Walker. 1980), demonstrating that southward sediment transport along the northwestern Laurentian margin was occurring by at least Early Pennsylvanian time. Aeolian transport and deposition also became the dominant sedimentary process in Wyoming beginning during the Late Pennsylvanian (Link et al., 2014), and this aeolian system buried the Arizona shelf by Leonardian time (Blakey and Knepp, 1989; Blakey, 1990). Paleowind directions reconstructed from Pennsylvanian-Permian aeolian strata are consistent with global climate models that depict trade winds capable of driving such longshore currents and south-directed aeolian transport (Tabor and Poulsen, 2008).

An informative modern analog for longshore current transport operating at a similar spatial scale to that envisioned for the western Laurentian margin can be found in southwestern Africa, where longshore current transports sediment from the Namibian/South African Orange River ~1800 km north at least as far as the Angola coast (Garzanti et al., 2014, 2018). This littoral transport system, which has been active since at least Eocene time (Bluck et al., 2007), is driven by onshore (southwest) winds





Dominantly shallow marine environme
Eolian environment
Dominantly terrestrial environment
Proximal ARM detritus
Active subduction/collision margins
Inactive subduction/collision margins

Figure 15. Laurentian-scale paleogeographic and sedimentologic interpretations for (A) Middle Pennsylvanian and (B) Early to middle Permian time based on Embry (1988), Peterson (1988), Patchett et al. (1999), Beranek et al. (2010), Blakey (2013), Gottlieb et al. (2014), Lawton et al. (2015), Kissock et al. (2018), and data presented in this study. Shown in (A): a—remnant Antler belt; 1—NE Ellesmerian orogen; 2—NW Ellesmerian orogen.

and has been interpreted to be the result of low sediment accommodation along the Namibian and Angolan coasts, aridity, and high sand and gravel sediment supply from the Orange River (Bluck et al., 2007). Provenance signals such as sandstone composition, heavy mineral assemblages, and detrital zircon spectra can be traced throughout the length of this system (Garzanti et al., 2012, 2014, 2018). The Namib, Skeleton Coast, Cunene, and Moçamedes coastal dune fields are discontinuously distributed along the Orange River littoral cell and are separated by up to 450 km; these coastal dune fields are each terminated by rivers to their north that flush sand back to the littoral cell (Garzanti et al., 2018). Most sediment transport in this system occurs in the subtidal to intertidal zones (Bluck et al., 2007). The abrupt end of this littoral transport system occurs where the continental shelf decreases in width to only a few kilometers and sand is flushed into the deep ocean through submarine canyons (Garzanti et al., 2018).

Although the Orange River littoral cell is not a perfect analog for the sediment routing system interpreted along the Pennsylvanian-Permian western margin of Laurentia, major features of that system suggest the two may be comparable. The Orange River littoral cell transports sand from 28.6°S northwest to 15.7°S. The presence of Morrowan-Atokan aeolian and shallow marine sandstones, deposited at ca. 17°N (Domeier and Torsvik, 2014) in southwestern Alberta, suggests that the interpreted sediment routing system operated at similar latitudes as the Orange River system. These deposits, the Tyrwhitt, Storelk, and Tobermory Formations, are sedimentologically similar to Eocene deposits 150 km north of the start of the Orange River littoral cell that are interpreted as early remnants of that routing system (Scott, 1964; Stewart and Walker, 1980; Bluck et al., 2007). Much of the Pennsylvanian sedimentary record has been eroded from the Canadian Laurentian margin (Richards et al., 1994; Henderson et al., 1994), and much of what is preserved consists of coastal dune to outer shelf deposits (Richards et al., 1994). This implies that the intertidal, subtidal, and coastal dune systems, the primary sediment conduit for the interpreted routing system, may have been removed by erosion. Abundant unconformities within these deposits (e.g., Scott, 1964; Stewart and Walker, 1980; Henderson et al., 1994) suggest relatively low sediment accommodation with high sediment bypass. Although the climate from southern Canada to the ARM province was not as arid as the Namib and Angolan Coasts (Tabor and Poulsen, 2008), the presence of large aeolian units such as the Storelk and Weber Formations in southern Canada, partly aeolian Quadrant Formation in southwestern Montana, and an unnamed aeolian sandstone in the Eagle Basin (Schenk, 1987), suggests at least periodic aridity in the northern portion of this system during the Early to Middle Pennsylvanian (Fryberger, 1979; Stewart and Walker, 1980; Schenk, 1987), and sparse data from most of the area in which this system is interpreted suggest arid to semi-arid paleoclimate (Tabor and Poulsen, 2008).

Implications for the Transcontinental Arch

The data and interpretations presented here are consistent with the long-standing idea that the Transcontinental Arch, extending from northern Arizona and New Mexico to the Lake Superior region of Canada (Keith, 1928; Carlson, 1999; Amato and Mack, 2012), influenced sediment transport networks during the Pennsylvanian and Permian (Fig. 15). Detrital zircon data suggest that little if any sediment was routed directly from the central Appalachian orogen across the northern U.S. midcontinent into the ARM system (Figs. 9, 14, and 15) during Pennsylvanian to middle Permian time. However, the current study cannot constrain how far north this barrier extended, and our data allow the possibility that sediment shed from the northern Appalachian orogen was transported north across the

Canadian Shield to join the southward longshore/aeolian routing system interpreted here. The data presented here also cannot rule out the possibility of a Mississippian–earliest Pennsylvanian sediment pathway between the central Appalachian orogen and southwest Laurentia (Gehrels et al., 2011; Chapman and Laskowski, 2019). Mississippian Surprise Canyon Formation (Fig. 3) and Early Pennsylvanian Molas Formation (Fig. 6, panel 4) samples appear to show central Appalachian affinity, which suggests that the Transcontinental Arch may not have played a substantial role in Mississippian sediment routing (e.g., Chapman and Laskowski, 2019).

CONCLUSIONS

- (1) Detrital zircon deposited within Pennsylvanian–Permian Ancestral Rocky Mountain basins is a mix of grains eroded from southwestern Laurentian basement rocks exposed in ARM uplifts and grains from a wide variety of Laurentian sources transported hundreds to thousands of kilometers into the ARM system.
- (2) Similarity metrics suggest a north-to-south (modern reference frame) sediment routing system that moved detritus from at least as far north as southern Canada into the ARM system and filled basins as far south as southern Arizona. This system would have been active from at least Desmoinesian to Leonardian time. We propose that sediment was moved via a ~2000-km-long longshore and aeolian transport system analogous to the modern Namibian coast (e.g., Garzanti et al., 2018).
- (3) Distal basin detrital zircon spectra show the closest statistical similarity to Arctic Ellesemerian orogen sources, although distal basin spectra could also be the product of combined northern Appalachian and locally derived grains.
- (4) Detrital zircon spectra suggest initiation of ARM exhumation adjacent to the Denver and Paradox Basins by Atokan (Early Pennsylvanian) and Desmoinesian (Middle Pennsylvanian), respectively, as well as local exhumation of the ancestral Front Range and Uncompahgre uplifts by Desmoinesian time. Zircon ages from one sample collected from the Central Colorado trough allow for the possibility of ARM exhumation as early as Late Mississippian. Aeolian systems prograded into the Denver and Paradox Basins during the Wolfcampian (early Permian) and Leonardian (middle Permian), respectively, overwhelming local sediment sources and suggesting the cessation of ARM-related exhumation.

ACKNOWLEDGMENTS

This research was funded primarily through the generous support of Pioneer Natural Resources. Research at the University of Houston was funded through NSF EAR-1742952. Special thanks go to the Arizona LaserChron staff for help with detrital zircon analyses. The Arizona LaserChron Center is supported in part by NSF grant EAR-1338583. We thank Dustin Sweet and Alan Chapman for constructive reviews and *Lithosphere* Science Editor Sarah Roeske for additional guidance that helped us to improve this manuscript.

REFERENCES CITED

Allen, P.A., 2008, From landscapes into geological history: Nature, v. 451, no. 7176, p. 274, https://doi.org/10.1038/nature06586.

Alsalem, O.B., Fan, M., Zamora, J., Xie, X., and Griffin, W.R., 2018, Paleozoic sediment dispersal before and during the collision between Laurentia and Gondwana in the Fort Worth Basin, USA: Geosphere, v. 14, no. 1, p. 325–342, https://doi.org/10.1130/GES01480.1.

Amato, J.M., and Mack, G.H., 2012, Detrital zircon geochronology from the Cambrian–Ordovician Bliss Sandstone, New Mexico: Evidence for contrasting Grenville-age and Cambrian sources on opposite sides of the Transcontinental Arch: Geological Society of America Bulletin, v. 124, no. 11–12, p. 1826–1840.

Amidon, W.H., Burbank, D.W., and Gehrels, G.E., 2005, Construction of detrital mineral populations: Insights from mixing of U-Pb zircon ages in Himalayan rivers: Basin Research, v. 17, p. 463–485, https://doi.org/10.1111/j.1365-2117.2005.00279.x.

Anderson, J.L., and Bender, E.E., 1989, Nature and origin of Proterozoic A-type granitic magmatism in the southwestern United States of America: Lithos, v. 23, no. 1–2, p. 19–52, https://doi.org/10.1016/0024-4937(89)90021-2.

Anderson, J.L., and Morrison, J., 1992, The role of anorogenic granites in the Proterozoic crustal development of North America, in Condie, K. C., ed., Proterozoic Crustal Evolution: New York, Elsevier, p. 263–299, https://doi.org/10.1016/S0166-2635(08)70121-X.

- Anfinson, O.A., Leier, A.L., Embry, A.F., and Dewing, K., 2012, Detrital zircon geochronology and provenance of the Neoproterozoic to Late Devonian Franklinian Basin, Canadian Arctic Islands: Geological Society of America Bulletin, v. 124, no. 3–4, p. 415–430, https:// doi.org/10.1130/B30503.1.
- Armin, R.A., 1987, Sedimentology and tectonic significance of Wolfcampian (Lower Permian) conglomerates in the Pedregosa basin: Southeastern Arizona, southwestern New Mexico, and northern Mexico: Geological Society of America Bulletin, v. 99, no. 1, p. 42–65, https://doi.org/10.1130/0016-7606(1987)99-42:SATSOW-2.0.CO:2.
- Attia, S., Paterson, S.R., Cao, W., Chapman, A.D., Saleeby, J., Dunne, G.C., Stevens, C.H., and Memeti, V., 2018, Late Paleozoic tectonic assembly of the Sierra Nevada prebatholithic framework and western Laurentian provenance links based on synthesized detrital zircon geochronology in Ingersoll, R.V., Lawton, T.F. and Graham, S.A. eds., Tectonics, Sedimentary Basins, and Provenance: A Celebration of the Career of William R. Dickinson: Boulder, Colorado, Geological Society of America, Special Paper 540, p. 267–296.
- Barbeau, D.L., 2003, A flexural model for the Paradox Basin: implications for the tectonics of the Ancestral Rocky Mountains: Basin Research, v. 15, no. 1, p. 97–115, https://doi.org/10.1046/j.1365-2117.2003.00194.x.
- Becker, T.P., Thomas, W.A., Samson, S.D., and Gehrels, G.E., 2005, Detrital zircon evidence of Laurentian crustal dominance in the lower Pennsylvanian deposits of the Alleghanian clastic wedge in eastern North America: Sedimentary Geology, v. 182, no. 1–4, p. 59–86, https://doi.org/10.1016/i.sedgeo.2005.07.014.
- Becker, T.P., Thomas, W.A., and Gehrels, G.E., 2006, Linking late Paleozoic sedimentary provenance in the Appalachian basin to the history of Alleghanian deformation: American Journal of Science, v. 306, no. 10, p. 777–798, https://doi.org/10.2475/10.2006.01.
- Beranek, L.P., Link, P.K., and Fanning, C.M., 2016, Detrital zircon record of mid-Paleozoic convergent margin activity in the northern US Rocky Mountains: Implications for the Antler orogeny and early evolution of the North American Cordillera: Lithosphere, v. 8, pp. 5, p. 532–550.
- Benyon, C., Leier, A., Leckie, D.A., Webb, A., Hubbard, S.M., and Gehrels, G., 2014, Provenance of the Cretaceous Athabasca Oil Sands, Canada: Implications for continental-scale sediment transport: Journal of Sedimentary Research, v. 84, no. 2, p. 136–143, https://doi.org/10.2110/jsr.2014.16.
- Beranek, L.P., Mortensen, J.K., Lane, L.S., Allen, T.L., Fraser, T.A., Hadlari, T., and Zantvoort, W.G., 2010, Detrital zircon geochronology of the western Ellesmerian clastic wedge, north-western Canada: Insights on Arctic tectonics and the evolution of the northern Cordilleran miogeocline: Geological Society of America Bulletin, v. 122, no. 11–12, p. 1899–1911, https://doi.org/10.1130/B30120.1.
- Bickford, M.E., and Anderson, J.L., 1993, Middle Proterozoic magmatism, in Reed, J.C., Bickford, M. E., Houston, R. S., Link, P. K., Rankin, D. W., Sims, P. K., and Van Schmus, W. R., eds., Precambrian Conterminous U.S.: Boulder, Colorado, Geological Society of America, The Geology of North America, v. C-2, p. 281–292.
- Bickford, M.E., Shuster, R.D., and Boardman, S.J., 1989, U-Pb geochronology of the Proterozoic volcano-plutonic terrane in the Gunnison and Salida area, Colorado, *in* Grambling, J.A., and Tewksbury, B.J., eds., Proterozoic Geology of the Southern Rocky Mountains: Geological Society of America Special Paper 235, p. 33–48, https://doi.org/10.1130/SPE235-p33.
- Bickford, M., Soegaard, K., Nielsen, K.C., and McLelland, J.M., 2000, Geology and geochronology of Grenville-age rocks in the Van Horn and Franklin Mountains area, west Texas: Implications for the tectonic evolution of Laurentia during the Grenville: Geological Society of America Bulletin, v. 112, no. 7, p. 1134–1148, https://doi.org/10.1130/0016-7606 (2000)112<1134:GAGOGR>2.0.CO;2.
- Bickford, M., Wooden, J., and Bauer, R., 2006, SHRIMP study of zircons from Early Archean rocks in the Minnesota River Valley: Implications for the tectonic history of the Superior Province: Geological Society of America Bulletin, v. 118, no. 1–2, p. 94–108, https://doi .org/10.1130/B25741.1.
- Bickford, M., Mueller, P., Kamenov, G.D., and Hill, B.M., 2008, Crustal evolution of southern Laurentia during the Paleoproterozoic: Insights from zircon Hf isotopic studies of ca. 1.75 Ga rocks in central Colorado: Geology, v. 36, no. 7, p. 555–558, https://doi.org /10.1130/G24700A.1.
- Bickford, M., Van Schmus, W., Karlstrom, K., Mueller, P., and Kamenov, G., 2015, Mesoproterozoic-trans-Laurentian magmatism: A synthesis of continent-wide age distributions, new SIMS U-Pb ages, zircon saturation temperatures, and Hf and Nd isotopic compositions: Precambrian Research, v. 265, p. 286–312, https://doi.org/10.1016/j .precamres.2014.11.024.
- Bishop, J.W., Montañez, I.P., and Osleger, D.A., 2010, Dynamic Carboniferous climate change, Arrow Canyon, Nevada: Geosphere, v. 6, no. 1, p. 1–34, https://doi.org/10.1130/GES00192.1.
- Blakey, R.C., 1980, Pennsylvanian and Early Permian paleogeography, southern Colorado Plateau and vicinity, in Fousch, T.D., and Magathan, E.R., eds., Paleozoic Paleogeography of the West-Central United States: Broken Arrow, Oklahoma, Society of Economic Paleontologists and Mineralogists, Rocky Mountain Section, p. 239–257.
- Blakey, R.C., 1990, Stratigraphy and geologic history of Pennsylvanian and Permian rocks, Mogollon Rim region, central Arizona and vicinity: Geological Society of America Bulletin, v. 102, no. 9, p. 1189–1217, https://doi.org/10.1130/0016-7606(1990)102<1189:SAGHOP>2 .3.CO:2.
- Blakey, R.C., 2008, Pennsylvanian–Jurassic Sedimentary Basins of the Colorado Plateau and Southern Rocky Mountains, *in* Hsü, K.J., ed., Sedimentary Basins of the World, Volume 5: The Netherlands, Elsevier, p. 245–296.
- Blakey, R. C., 2013, North American Facies: Middle Pennsylvanian and Early to Middle Permian: http://deeptimemaps.com/north-american-key-time-slices-series/, Files 308 Ma and 300 Ma (accessed August 2019).
- Blakey, R.C., and Knepp, R., 1989, Pennsylvanian and Permian geology of Arizona, in Jenney, J.P., and Reynolds, S.J., eds., Geologic evolution of Arizona: Arizona Geological Society Digest, v. 17, p. 313–347.

- Blakey, R.C., Peterson, F., and Kocurek, G., 1988, Synthesis of late Paleozoic and Mesozoic eolian deposits of the Western Interior of the United States: Sedimentary Geology, v. 56, no. 1–4, p. 3–125, https://doi.org/10.1016/0037-0738(88)90050-4.
- Bluck, B., Ward, J., Cartwright, J., and Swart, R., 2007, The Orange River, southern Africa: an extreme example of a wave-dominated sediment dispersal system in the South Atlantic Ocean: Journal of the Geological Society, v. 164, no. 2, p. 341–351, https://doi.org/10 .1144/0016-76492005-189.
- Blum, M., and Pecha, M., 2014, Mid-Cretaceous to Paleocene North American drainage reorganization from detrital zircons: Geology, v. 42, no. 7, p. 607–610, https://doi.org/10 .1130/G35513.1.
- Blum, M.D., Milliken, K.T., Pecha, M.A., Snedden, J.W., Frederick, B.C., and Galloway, W.E., 2017, Detrital-zircon records of Cenomanian, Paleocene, and Oligocene Gulf of Mexico drainage integration and sediment routing: Implications for scales of basin-floor fans: Geosphere, v. 13, no. 6, p. 2169–2205, https://doi.org/10.1130/GES01410.1.
- Bowring, S.A., Kent, S., and Sumner, W., 1983, Geology and U-Pb geochronology of Proterozoic rocks in the vicinity of Socorro, New Mexico: New Mexico Geological Society Guidebook, v. 34, p. 137–142.
- Bradley, D.C., and O'Sullivan, P., 2017, Detrital zircon geochronology of pre-and syncollisional strata, Acadian orogen, Maine Appalachians: Basin Research, v. 29, no. 5, p. 571–590, https://doi.org/10.1111/bre.12188.
- Bradley, D.C., Tucker, R.D., Lux, D.R., Harris, A.G., and McGregor, D.C., 2000, Migration of the Acadian orogen and foreland basin across the northern Appalachians of Maine and adjacent areas: U.S. Geological Survey Professional Paper 1624, 49 p.
- Bream, B.R., Hatcher, R.D., Miller, C.F., Fullagar, P.D., Tollo, R., McLelland, J., Corriveau, L., and Bartholomew, M., 2004, Detrital zircon ages and Nd isotopic data from the southern Appalachian crystalline core, Georgia, South Carolina, North Carolina, and Tennessee: New provenance constraints for part of the Laurentian margin, in Tollo, R. P., Corriveau, L., McLelland, J., and Bartholomew, M. J., eds., Proterozoic Tectonic Evolution of the Grenville Orogen in North America: Geological Society of America Memoir 197, p. 459–475, https://doi.org/10.1130/0-8137-1197-5.459.
- Brew, D., 1970, The Naco Formation (Pennsylvanian) in central Arizona: Plateau, v. 42, no. 4, p. 126–138.
- Brew, D.C., and Beus, S.S., 1976, A middle Pennsylvanian fauna from the Naco Formation near Kohl Ranch, central Arizona: Journal of Paleontology, v. 50, p. 888–906.
- Brewer, J.A., Good, R., Oliver, J.E., Brown, L.D., and Kaufman, S., 1983, Cocorp profiling across the southern Oklahoma aulacogen: Overthrusting of the Wichita Mountains and compression within the Anadarko Basin: Geology, v. 11, no. 2, p. 109–114, https://doi.org/10.1130/0091-7613(1983)11<109:CPATSO>2.0.CO;2.
- Budnik, R.T., 1986, Left-lateral intraplate deformation along the Ancestral Rocky-Mountains Implications for late Paleozoic plate motions: Tectonophysics, v. 132, no. 1–3, p. 195–214, https://doi.org/10.1016/0040-1951(86)90032-6.
- Buratowski, G.M., 2014, Application of Detrital Zircon Geochronology to Determine the Sedimentary Provenance of the Middle Bloyd Sandstone, Arkoma Shelf, Northern Arkansas [M.S. Thesis]: Fayetteville, University of Arkansas, 103 p.
- Burchfiel, B., and Royden, L., 1991, Antler orogeny: A Mediterranean-type orogeny: Geology, v. 19, no. 1, p. 66–69.
- Campbell, J.A., 1981, Summary of Paleozoic stratigraphy and history of western Colorado and eastern Utah, in Epis, R. C., and Callender, J. F., eds., Western Slope (Western Colorado): New Mexico Geological Society 32nd Annual Fall Field Conference Guidebook, p. 81–87.
- Campbell, R.W., Beranek, L.P., Piercey, S.J., and Friedman, R., 2019, Early Paleozoic post-breakup magmatism along the Cordilleran margin of western North America: New zircon U-Pb age and whole-rock Nd-and Hf-isotope and lithogeochemical results from the Kechika group, Yukon, Canada: Geosphere, v. 15, p. 1262–1290, https://doi.org/10.1130/GES02044.1.
- Cao, W., Zahirovic, S., Flament, N., Williams, S.E., Golonka, J., and Muller, R.D., 2017, Improving global paleogeography since the late Paleozoic using paleobiology: Biogeosciences, v. 14, p. 5425–5439, https://doi.org/10.5194/bg-14-5425-2017.
- Carlson, M.P., 1999, Transcontinental Arch—A pattern formed by rejuvenation of local features across central North America: Tectonophysics, v. 305, no. 1–3, p. 225–233, https://doi.org/10.1016/S0040-1951(99)00005-0.
- Cashman, P.H., Villa, D.E., Taylor, W.J., Davydov, V.I., and Trexler, J.H., 2011, Late Paleozoic contractional and extensional deformation at Edna Mountain, Nevada: Geological Society of America Bulletin, v. 123, no. 3–4, p. 651–668, https://doi.org/10.1130/B30247.1.
- Cather, S., Karlstrom, K., Timmons, J., and Heizler, M., 2006, Palinspastic reconstruction of Proterozoic basement-related aeromagnetic features in north-central New Mexico: Implications for Mesoproterozoic to late Cenozoic tectonism: Geosphere, v. 2, no. 6, p. 299–323, https://doi.org/10.1130/GES00045.1.
- Cawood, P.A., and Nemchin, A.A., 2001, Paleogeographic development of the east Laurentian margin: Constraints from U-Pb dating of detrital zircons in the Newfoundland Appalachians: Geological Society of America Bulletin, v. 113, no. 9, p. 1234–1246, https://doi.org /10.1130/0016-7606(2001)113<1234:PDOTEL>2.0.CO;2.
- Chapman, A.D., Ernst, W., Gottlieb, E., Powerman, V., and Metzger, E.P., 2015, Detrital zircon geochronology of Neoproterozoic–Lower Cambrian passive-margin strata of the White-Inyo Range, east-central California: Implications for the Mojave–Snow Lake fault hypothesis: Geological Society of America Bulletin, v. 127, no. 7-8, p. 926–944, https://doi.org/10.1130/B31142.1.
- Chapman, A.D., and Laskowski, A.K., 2019, Detrital zircon U-Pb data reveal a Mississippian sediment dispersal network originating in the Appalachian orogen, traversing North America along its southern shelf, and reaching as far as the southwest United States: Lithosphere, v. 11, no. 4, p. 581–587, https://doi.org/10.1130/L1068.1.
- Cheng, F., Jolivet, M., Fu, S., Zhang, C., Zhang, Q., and Guo, Z., 2016, Large-scale displacement along the Altyn Tagh Fault (North Tibet) since its Eocene initiation: Insight from detrital

- zircon U-Pb geochronology and subsurface data: Tectonophysics, v. 677, p. 261-279, https://doi.org/10.1016/j.tecto.2016.04.023.
- Chew, D., Petrus, J., and Kamber, B., 2014, U–Pb LA–ICPMS dating using accessory mineral standards with variable common Pb: Chemical Geology, v. 363, p. 185–199, https://doi.org/10.1016/j.chemgeo.2013.11.006.
- Clinkscales, C.A., and Lawton, T.F., 2018, Mesozoic–Paleogene structural evolution of the southern US Cordillera as revealed in the Little and Big Hatchet Mountains, southwest New Mexico, USA: Geosphere, v. 14, no. 1, p. 162–186, https://doi.org/10.1130/GES01539.1.
- Condie, K.C., Belousova, E., Griffin, W., and Sircombe, K.N., 2009, Granitoid events in space and time: Constraints from igneous and detrital zircon age spectra: Gondwana Research, v. 15, no. 3–4, p. 228–242, https://doi.org/10.1016/j.gr.2008.06.001.
- Condie, K., and Knoper, M., 1986, Geology and origin of early Proterozoic rocks from the Gunnison area, central Colorado, in Proceedings Proterozoic geology and geochemistry: Lawrence, Kansas, University of Kansas, International Field Conference 1986, p. 3–16.
- Corrigan, D., and Van Breemen, O., 1997, U–Pb age constraints for the lithotectonic evolution of the Grenville Province along the Mauricie transect, Quebec: Canadian Journal of Earth Sciences, v. 34, no. 3, p. 299–316, https://doi.org/10.1139/e17-027.
- Covault, J.A., Romans, B.W., Graham, S.A., Fildani, A., and Hilley, G.E., 2011, Terrestrial source to deep-sea sink sediment budgets at high and low sea levels: Insights from tectonically active Southern California: Geology, v. 39, no. 7, p. 619–622, https://doi.org/10.1130/G31801.1.
- Cowgill, E., Forte, A. M., Niemi, N., Avdeev, B., Tye, A., Trexler, C., Javakhishvili, Z., Elashvili, M., and Godoladze, T., 2016, Relict basin closure and crustal shortening budgets during continental collision: An example from Caucasus sediment provenance: Tectonics, v. 35, no. 12, p. 2918–2947.
- Cox, R.T., 2009, Ouachita, Appalachian, and Ancestral Rockies deformations recorded in mesoscale structures on the foreland Ozark plateaus: Tectonophysics, v. 474, no. 3–4, p. 674–683, https://doi.org/10.1016/j.tecto.2009.05.005.
- Creasy, S., 1967, Geologic map of the Benson quadrangle, Cochise and Pima counties, Arizona: U.S. Geological Survey IMAP 470, https://doi.org/10.3133/i470.
- Daniel, C.G., Pfeifer, L.S., Jones, J.V., Ill, and McFarlane, C.M., 2013, Detrital zircon evidence for non-Laurentian provenance, Mesoproterozoic (ca. 1490–1450 Ma) deposition and orogenesis in a reconstructed orogenic belt, northern New Mexico, USA: Defining the Picuris orogeny: Geological Society of America Bulletin, v. 125, p. 1423–1441, https://doi.org/10.1130/B30804.1.
- DeCelles, P.G., 2004, Late Jurassic to Eocene evolution of the Cordilleran thrust belt and foreland basin system, western USA: American Journal of Science, v. 304, no. 2, p. 105–168, https://doi.org/10.2475/ajs.304.2.105.
- DeVoto, R.H., Bartleson, B.L., Schenk, C.J. and Waechter, N.B., 1986, Late Paleozoic stratigraphy and syndepositional tectonism, northwestern Colorado: New interpretations of northwest Colorado geology: Denver, Colorado, Rocky Mountain Association of Geologists, p. 37–49.
- Dickinson, W.R., and Lawton, T.F., 2001, Carboniferous to Cretaceous assembly and fragmentation of Mexico: Geological Society of America Bulletin, v. 113, no. 9, p. 1142–1160, https://doi.org/10.1130/0016-7606(2001)113<1142:CTCAAF>2.0.CO;2.
- Dickinson, W.R., and Lawton, T.F., 2003, Sequential intercontinental suturing as the ultimate control for Pennsylvanian Ancestral Rocky Mountains deformation: Geology, v. 31, no. 7, p. 609–612, https://doi.org/10.1130/0091-7613(2003)031<0609:SISATU>2.0.CO;2.
- Dickinson, W.R., Soreghan, M., and Gehrels, G., 2000, Geodynamic interpretation of Paleozoic tectonic trends oriented oblique to the Mesozoic Klamath–Sierran continental margin in California, in Soreghan, M.J., and Gehrels, G.E., eds., Paleozoic and Triasto Paleogeography and Tectonics of Western Nevada and Northern California: Geological Society of America Special Paper 347, p. 209–246, https://doi.org/10.1130/0-8137-2347-7.209.
- Doe, M.F., Jones, J.V., III, Karlstrom, K.E., Thrane, K., Frei, D., Gehrels, G., and Pecha, M., 2012, Basin formation near the end of the 1.60–1.45 Ga tectonic gap in southern Laurentia: Mesoproterozoic Hess Canyon Group of Arizona and implications for ca. 1.5 Ga supercontinent configurations: Lithosphere, v. 4, no. 1, p. 77–88, https://doi.org/10.1130/L160.1.
- Doe, M.F., Jones, J.V., III, Karlstrom, K.E., Dixon, B., Gehrels, G., and Pecha, M., 2013, Using detrital zircon ages and Hf isotopes to identify 1.48–1.45 Ga sedimentary basins and fingerprint sources of exotic 1.6–1.5 Ga grains in southwestern Laurentia: Precambrian Research, v. 231, p. 409–421, https://doi.org/10.1016/j.precamres.2013.03.002.
- Domeier, M., and Torsvik, T.H., 2014, Plate tectonics in the late Paleozoic: Geoscience Frontiers, v. 5, p. 303–350, https://doi.org/10.1016/j.gsf.2014.01.002.
- Drake, A.A.J., Sinha, A., Laird, J., and Guy, R., 1989, The taconic orogen, in Hatcher, R.D.J., Thomas, W.A., and Viele, G.W., eds., The Appalachian-Ouachita Orogen in the United States: Boulder, Colorado, Geological Society of America, Geology of North America, Vol. 2, p. 101–177.
- Duebendorfer, E.M., Williams, M.L., and Chamberlain, K.R., 2015, Case for a temporally and spatially expanded Mazatzal orogeny: Lithosphere, v. 7, no. 6, p. 603–610, https://doi.org/10.1130/L412.1.
- Embry, A., 1988, Middle–Upper Devonian sedimentation in the Canadian Arctic Islands and the Ellesmerian orogeny, *in* Devonian of the World: Proceedings of the 2nd International Symposium on the Devonian System Memoir 14, Volume II: Sedimentation: Calgary, Canadian Society of Petroleum Geologists, p. 15–28.
- Erickson, R.L., and Marsh, S.P., 1974, Paleozoic Tectonics in the Edna Mountain Quadrangle, Nevada: Journal of Research of the U.S. Geological Survey, v. 2, no. 3, p. 331–337.
- Eriksson, K.A., Campbell, I.H., Palin, J.M., Allen, C.M., and Bock, B., 2004, Evidence for multiple recycling in Neoproterozoic through Pennsylvanian sedimentary rocks of the central Appalachian basin: The Journal of Geology, v. 112, no. 3, p. 261–276, https://doi.org/10.1086/382758.
- Evans, J.E., and Reed, J.M., 2007, Integrated loessite–paleokarst depositional system, early Pennsylvanian Molas Formation, Paradox Basin, southwestern Colorado, USA: Sedimentary Geology, v. 195, no. 3–4, p. 161–181, https://doi.org/10.1016/j.sedgeo.2006.07.010.
- Evans, J.E., and Soreghan, M., 2015, Long-distance sediment transport and episodic resedimentation of Pennsylvanian dust (eolian silt) in cave passages of the Mississippian

- Leadville Limestone, southwestern Colorado, USA, *in* Feinberg, J., Gao, Y., and Alexander, E. C., Jr., eds., Caves and Karst Across Time: Geological Society of America Special Paper 516, p. 263–283, https://doi.org/10.1130/2015.2516(21).
- Evans, K.V., and Clemons, R.E., 1988, Cambrian–Ordovician (500 Ma) alkalic plutonism in southwestern New Mexico: U-Th-Pb isotopic data from the Florida Mountains: American Journal of Science, v. 288, no. 7, p. 735–755, https://doi.org/10.2475/ajs.288.7.735.
- Evans, K.V., and Zartman, R.E., 1988, Early Paleozoic alkalic plutonism in east-central Idaho: Geological Society of America Bulletin, v. 100, no. 12, p. 1981–1987, https://doi.org/10.1130/0016-7606(1988)100<1981:EPAPIE>2.3.CO:2.
- Farmer, G.L., Bowring, S.A., Matzel, J., Maldonado, G.E., Fedo, C., and Wooden, J., 2005, Paleo-proterozoic Mojave province in northwestern Mexico? Isotopic and U-Pb zircon geochronologic studies of Precambrian and Cambrian crystalline and sedimentary rocks, Caborca, Sonora, in Anderson, T.H., Nourse, J.A., McKee, J.W., and Steiner, M.B., eds., The Mojave-Sonora Megashear Hypothesis: Development, Assessment, and Alternatives: Geological Society of America Special Paper 393, p. 183–198, https://doi.org/10.1130/0-8137-2393-0.183.
- Frenzel, H., Bloomer, R., Cline, R., Cys, J., Galley, J., Gibson, W., Hills, J., King, W., Seager, W., Kottlowski, F., Thompson, S., Ill, Luff, G.C., Pearson, B.T., and Van Siclen, D.C., 1988, The Permian basin region, in Sedimentary Cover—North American Craton, Volume D–2: Boulder, Colorado, Geological Society of America, p. 261–306, https://doi.org/10.1130/DNAG-GNA-D2.261.
- Fryberger, S.G., 1979, Eolian-fluviatile (continental) origin of ancient stratigraphic trap for petroleum in Weber Sandstone, Rangely oil field, Colorado: The Mountain Geologist, v. 16, p. 1–36.
- Fyffe, L.R., Barr, S.M., Johnson, S.C., McLeod, M.J., McNicoll, V.J., Valverde-Vaquero, P., van Staal, C.R., and White, C.E., 2009, Detrital zircon ages from Neoproterozoic and Early Paleozoic conglomerate and sandstone units of New Brunswick and coastal Maine: Implications for the tectonic evolution of Ganderia: Atlantic Geology, v. 45, p. 110–144, https:// doi.org/10.4138/atlgeol.2009.006.
- Garfield, T.R., Scott, A.J., and Walker, A.L., 1988, Overview: Late Paleozoic geologic history of the northern Denver Basin, in Proceedings Occurrence and Petrophysical Properties of Carbonate Reservoirs in the Rocky Mountain Region: Denver, Colorado, Rocky Mountain Association of Geologists, p. 1–25.
- Garzanti, E., Andò, S., Vezzoli, G., Lustrino, M., Boni, M., and Vermeesch, P., 2012, Petrology of the Namib Sand Sea: Long-distance transport and compositional variability in the wind-displaced Orange Delta: Earth-Science Reviews, v. 112, no. 3–4, p. 173–189, https:// doi.org/10.1016/j.earscirev.2012.02.008.
- Garzanti, E., Vermeesch, P., Andò, S., Lustrino, M., Padoan, M., and Vezzoli, G., 2014, Ultralong distance littoral transport of Orange sand and provenance of the Skeleton Coast Erg (Namibia): Marine Geology, v. 357, p. 25–36, https://doi.org/10.1016/j.margeo.2014.07.005.
- Garzanti, E., Dinis, P., Vermeesch, P., Andò, S., Hahn, A., Huvi, J., Limonta, M., Padoan, M., Resentini, A., and Rittner, M., 2018, Sedimentary processes controlling ultralong cells of littoral transport: Placer formation and termination of the Orange sand highway in southern Angola: Sedimentology, v. 65, no. 2, p. 431–460, https://doi.org/10.1111/sed.12387.
- Garzione, C.N., Patchett, P.J., Ross, G.M., and Nelson, J., 1997, Provenance of Paleozoic sedimentary rocks in the Canadian Cordilleran miogeocline: A Nd isotopic study: Canadian Journal of Earth Sciences. v. 34, no. 12, p. 1603–1618, https://doi.org/10.1139/e17-129.
- Gehrels, G.E., 2000, Introduction to detrital zircon studies of Paleozoic and Triassic strata in western Nevada and northern California, in Soreghan, M.J., and Gehrels, G.E., eds., Paleozoic and Triassic Paleogeography and Tectonics of Western Nevada and Northern California: Geological Society of America Special Paper 347, p. 1–17, https://doi.org/10.1130 //o-8137-2347-7.1.
- Gehrels, G., and Pecha, M., 2014, Detrital zircon U-Pb geochronology and Hf isotope geochemistry of Paleozoic and Triassic passive margin strata of western North America: Geosphere, v. 10, no. 1, p. 49–65, https://doi.org/10.1130/GES00889.1.
- Gehrels, G.E., Blakey, R., Karlstrom, K.E., Timmons, J.M., Dickinson, B., and Pecha, M., 2011,
 Detrital zircon U-Pb geochronology of Paleozoic strata in the Grand Canyon, Arizona:
 Lithosphere, v. 3, no. 3, p. 183–200, https://doi.org/10.1130/L121.1.
- Goldhammer, R., Oswald, E., and Dunn, P., 1991, Hierarchy of stratigraphic forcing: Example from Middle Pennsylvanian shelf carbonates of the Paradox Basin: Sedimentary Modeling: Computer Simulations and Methods for Improved Parameter Definition: Kansas Geological Survey Bulletin 233, p. 361–413.
- Gottlieb, E.S., Meisling, K.E., Miller, E.L., and Mull, C.G.G., 2014, Closing the Canada Basin: Detrital zircon geochronology relationships between the North Slope of Arctic Alaska and the Franklinian mobile belt of Arctic Canada: Geosphere, v. 10, no. 6, p. 1366–1384, https://doi.org/10.1130/GES01027.1.
- Graham, S.A., Dickinson, W.R., and Ingersoll, R.V., 1975, Himalayan–Bengal model for fly-sch dispersal in the Appalachian–Ouachita System: Geological Society of America Bulletin, v. 86, p. 273–286, https://doi.org/10.1130/0016-7606(1975)86<273:HMFFDI>2.0.CO;2.
- Granath, J.W., 1989, Structural evolution of the Ardmore basin, Oklahoma: Progressive deformation in the foreland of the Ouachita collision: Tectonics, v. 8, no. 5, p. 1015–1036, https://doi.org/10.1029/TC008i005p01015.
- Green, J.C., and Fitz, T.J., III, 1993, Extensive felsic lavas and rheoignimbrites in the Keween-awan Midcontinent Rift plateau volcanics, Minnesota: Petrographic and field recognition: Journal of Volcanology and Geothermal Research, v. 54, no. 3–4, p. 177–196, https://doi.org/10.1016/0377-0273(93)90063-W.
- Greenwood, E., Kottlowski, F.E., and Thompson, S., III, 1977, Petroleum potential and stratigraphy of Pedregosa Basin: Comparison with Permian and Orogrande Basins: American Association of Petroleum Geologists Bulletin, v. 61, no. 9, p. 1448–1469.
- Grove, M., Gehrels, G.E., Cotkin, S.J., Wright, J.E., Zou, H., and Shervais, J., 2008, Non-Laurentian cratonal provenance of Late Ordovician eastern Klamath blueschists and a link to the Alexander terrane, *in* Wright, J.E., and Servais, J.W., eds, Ophiolites, Arcs, and Batholiths: A Tribute to Cliff Hopson: Geological Society of America Special Paper 438, p. 223–250.

- Guitreau, M., Mukasa, S.B., Blichert-Toft, J., and Fahnestock, M.F., 2016, Pikes Peak batholith (Colorado, USA) revisited: A SIMS and LA-ICP-MS study of zircon U-Pb ages combined with solution Hf isotopic compositions: Precambrian Research, v. 280, p. 179–194, https:// doi.org/10.1016/j.precamres.2016.05.001.
- Hanson, R.E., Puckett, R.E., Jr., Keller, G.R., Brueseke, M.E., Bulen, C.L., Mertzman, S.A., Finegan, S.A., and McCleery, D.A., 2013, Intraplate magmatism related to opening of the southern lapetus Ocean: Cambrian Wichita igneous province in the southern Oklahoma rift zone: Lithos, v. 174, p. 57–70, https://doi.org/10.1016/j.lithos.2012.06.003.
- Hatcher, R.D., Jr., Thomas, W., Geiser, P., Snoke, A., Mosher, S., and Wiltschko, D., 1989, Alleghanian orogen, *in* The Appalachian–Ouachita Orogen in the United States, Volume F-2: Boulder, Colorado, Geological Society of America, p. 233–318.
- Heaman, L., and Grotzinger, J., 1992, 1.08 Ga diabase sills in the Pahrump Group, California: Implications for development of the Cordilleran miogeocline: Geology, v. 20, no. 7, p. 637–640, https://doi.org/10.1130/0091-7613(1992)020<0637:GDSITP>2.3.CO;2.
- Heatherington, A.L., Mueller, P.A., and Nutman, A.P., 1999, A Jurassic granite from southern Georgia, USA: Silicic, extension-related magmatism along the southeastern coastal plain: The Journal of Geology, v. 107, p. 375–384, https://doi.org/10.1086/314350.
- Heller, P.L., and Paola, C., 1992, The large-scale dynamics of grain-size variation in alluvial basins, 2: Application to syntectonic conglomerate: Basin Research, v. 4, no. 2, p. 91–102, https://doi.org/10.1111/j.1365-2117.1992.tb00146.x.
- Henderson, C.M., Richards, B.C., and Barclay, J.E., 1994, Permian strata of the western Canada Sedimentary Basin, *in* Mossop, G.D., and Shetsen, I., eds., Geological Atlas of the Western Canada Sedimentary Basin: Calgary, Canadian Society of Petroleum Geologists and Alberta Research Council, p. 251–258.
- Heumann, M.J., Bickford, M., Hill, B.M., McLelland, J.M., Selleck, B.W., and Jercinovic, M.J., 2006, Timing of anatexis in metapelites from the Adirondack lowlands and southern highlands: A manifestation of the Shawinigan orogeny and subsequent anorthosite-mangeritecharnockite-granite magmatism: Geological Society of America Bulletin, v. 118, no. 11–12, p. 1283–1298, https://doi.org/10.1130/B25927.1.
- Hibbard, J.P., Stoddard, E.F., Secor, D.T., and Dennis, A.J., 2002, The Carolina Zone: Overview of Neoproterozoic to Early Paleozoic peri-Gondwanan terranes along the eastern flank of the southern Appalachians: Earth-Science Reviews, v. 57, p. 299–339, https://doi.org /10.1016/S0012-8252(01)00079-4.
- Hoffman, P.F., 1989, Precambrian geology and tectonic history of North America, in Bally, A., and Palmer, A., eds., The Geology of North America—An Overview: Geological Society of America, The Geology of North America, v. A, p. 447–512, https://doi.org/10.1130/DNAG-GNA-A-447.
- Hoy, R.G., and Ridgway, K.D., 2002, Syndepositional thrust-related deformation and sedimentation in an Ancestral Rocky Mountains basin, Central Colorado trough, Colorado, USA: Geological Society of America Bulletin, v. 114, no. 7, p. 804–828, https://doi.org/10.1130/0016-7606(2002)114-0804:STRDAS>2.0.CO;2.
- Huddle, J. W., and Dobrovolny, E., 1945, Late Paleozoic Stratigraphy and Oil and Gas Possibilities of Central and Northeastern Arizona, Oil and Gas Investigation Chart 10: U.S. Geological Survey, scale: 1:1,500,000.
- Hynes, A., and Rivers, T., 2010, Protracted continental collision—Evidence from the Grenville orogen: Canadian Journal of Earth Sciences, v. 47, no. 5, p. 591–620, https://doi.org/10.1139/E10-003.
- Jaffe, H.W., Gottfried, D., Waring, C.L., and Worthing, H.W., 1959, Lead-alpha age determinations of accessory minerals of igneous rocks (1953–1957): U.S. Geological Survey Bulletin, v. 1097-B, p. 65–148.
- Johnson, S.Y., 1987, Sedimentology and paleogeographic significance of six fluvial sandstone bodies in the Maroon Formation, Eagle Basin, northwest Colorado.: U.S. Geological Survey Bulletin, v. 1787-A-C, p. 1–18.
- Karlstrom, K.E., Amato, J.M., Williams, M.L., Heizler, M., Shaw, C.A., Read, A.S., and Bauer, P., 2004, Proterozoic tectonic evolution of the New Mexico region, in Mack, G.H., and Giles, K.A., eds., The Geology of New Mexico: A Geologic History: Socorro, New Mexico, New Mexico Geological Society, p. 1–34.
- Karlstrom, K.E., and Bowring, S.A., 1988, Early Proterozoic assembly of tectonostratigraphic terranes in southwestern North America: The Journal of Geology, v. 96, no. 5, p. 561–576, https://doi.org/10.1086/629252.
- Karlstrom, K.E., and Humphreys, E.D., 1998, Persistent influence of Proterozoic accretionary boundaries in the tectonic evolution of southwestern North America: Interaction of cratonic grain and mantle modification events: Rocky Mountain Geology, v. 33, no. 2, p. 161–179, https://doi.org/10.2113/33.2.161.
- Karlstrom, K.E., Bowring, S.A., and Conway, C.M., 1987, Tectonic significance of an early Proterozoic two-province boundary in central Arizona: Geological Society of America Bulletin, v. 99, no. 4, p. 529–538, https://doi.org/10.1130/0016-7606(1987)99<529:TSOAEP>2.0.CO;2.
- Karlstrom, K., Bowring, S.A., and Reed, J., 1993, Proterozoic orogenic history of Arizona, in Van Schmus, W. R., and Bickford, M. E., eds., Precambrian: Conterminous US: Transcontinental Proterozoic Provinces, Volume 2: Boulder, Colorado, Geological Society of America, p. 188–211.
- Keith, A., 1928, Structural symmetry in North America: Geological Society of America Bulletin, v. 39, no. 1, p. 321–386, https://doi.org/10.1130/GSAB-39-321.
- Keller, J., Siddoway, C., Morgan, M., Route, E., Grizzell, M., Sacerdoti, R., and Stevenson, A., 2005, Geologic map of the Manitou Springs 7.5-minute quadrangle, El Paso and Teller Counties, Colorado: Colorado Geological Survey Open File Report 03-19, 41 p.
- Kissock, J., Finzel, E., Malone, D., and Craddock, J., 2018, Lower–Middle Pennsylvanian strata in the North American midcontinent record the interplay between erosional unroofing of the Appalachians and eustatic sea-level rise: Geosphere, v. 14, no. 1, p. 141–161, https://doi.org/10.1130/GES01512.1.
- Kluth, C.F., and Coney, P.J., 1981, Plate-tectonics of the Ancestral Rocky Mountains: Geology, v. 9, no. 1, p. 10–15, https://doi.org/10.1130/0091-7613(1981)9<10:PTOTAR>2.0.CO;2.

- Konstantinou, A., Wirth, K.R., Vervoort, J.D., Malone, D.H., Davidson, C. and Craddock, J.P., 2014, Provenance of quartz arenites of the early Paleozoic midcontinent region, USA: The Journal of Geology, v. 122, p. 201–216.
- Kuiper, N.H., 1960, Tests concerning random points on a circle: Proceedings of the Koninklijke Nederlandse Akademie van Wetenschappen, v. 63, p. 38–47.
- Kylander-Clark, A.R., Hacker, B.R., and Cottle, J.M., 2013, Laser-ablation split-stream ICP petrochronology: Chemical Geology, v. 345, p. 99–112, https://doi.org/10.1016/j.chemgeo .2013.02.019.
- LaMaskin, T.A., 2012, Detrital zircon facies of Cordilleran terranes in western North America: GSA Today, v. 22, no. 3, p. 4–11, https://doi.org/10.1130/GSATG142A.1.
- Laskowski, A.K., Decelles, P.G., and Gehrels, G.E., 2013, Detrital zircon geochronology of cordilleran retroarc foreland basin strata, western North America: Tectonics, v. 32, p. 1027–1048, https://doi.org/10.1002/tect.20065.
- Lawton, T.F., Hunt, G.J., and Gehrels, G.E., 2010, Detrital zircon record of thrust belt unroofing in Lower Cretaceous synorogenic conglomerates, central Utah: Geology, v. 38, no. 5, p. 463–466, https://doi.org/10.1130/G30684.1.
- Lawton, T.F., Buller, C.D., and Parr, T.R., 2015, Provenance of a Permian erg on the western margin of Pangea: Depositional system of the Kungurian (late Leonardian) Castle Valley and White Rim sandstones and subjacent Cutler Group, Paradox Basin, Utah, USA: Geosphere, v. 11, no. 5, p. 1475–1506, https://doi.org/10.1130/GES01174.1.
- Lawton, T.F., Cashman, P.H., Trexler, J.H., and Taylor, W.J., 2017, The late Paleozoic Southwestern Laurentian Borderland: Geology, v. 45, no. 8, p. 675–678.
- Leary, R.J., Umhoefer, P., Smith, M.E., and Riggs, N., 2017, A three-sided orogen: A new tectonic model for Ancestral Rocky Mountain uplift and basin development: Geology, v. 45, no. 8, p. 735–738, https://doi.org/10.1130/G39041.1.
- Lee, D.D., and Seung, H.S., 1999, Learning the parts of objects by non-negative matrix factorization: Nature, v. 401, no. 6755, p. 788–791, https://doi.org/10.1038/44565.
- Li, Y., and Ngom, A., 2013, The non-negative matrix factorization toolbox for biological data mining: Source Code for Biology and Medicine, v. 8, no. 1, p. 10, https://doi.org/10.1186/1751-0473-8-10.
- Licht, A., Dupont-Nivet, G., Win, Z., Swe, H.H., Kaythi, M., Roperch, P., Ugrai, T., Littell, V., Park, D., and Westerweel, J., 2018, Paleogene evolution of the Burmese forearc basin and implications for the history of India–Asia convergence: Geological Society of America Bulletin, v. 131, p. 730–748, https://doi.org/10.1130/B35002.1.
- Link, P.K., Mahon, R.C., Beranek, L.P., Campbell-Stone, E.A., and Lynds, R., 2014, Detrital zircon provenance of Pennsylvanian to Permian sandstones from the Wyoming craton and Wood River Basin, Idaho, USA: Rocky Mountain Geology, v. 49, no. 2, p. 115–136, https:// doi.org/10.2113/gsrocky.49.2.115.
- Liu, J., Xu, K., Li, A.C., Milliman, J., Velozzi, D., Xiao, S., and Yang, Z., 2007, Flux and fate of Yangtze River sediment delivered to the East China Sea: Geomorphology, v. 85, no. 3–4, p. 208–224, https://doi.org/10.1016/j.geomorph.2006.03.023.
- Lodes, E.B., 2019, Geochronologic and stratigraphic evidence of Laurentian subduction initiation (Inyo Mountains, Eastern California) [M.S. Thesis]: Flagstaff, Arizona, Northern Arizona University, 240 p.
- Loring, A.K., Clemons, R.E., and Armstrong, D.G., 1987, Petrologic, paleomagnetic, and structural evidence of a Paleozoic rift system in Oklahoma, New Mexico, Colorado, and Utah: Discussions and reply: Geological Society of America Bulletin, v. 99, no. 2, p. 317–318, https://doi.org/10.1130/0016-7606(1987)99<317:PPASEO>2.0.CO;2.
- Lund, K., Aleinikoff, J., Evans, K., DuBray, E., Dewitt, E., and Unruh, D., 2010, SHRIMP U-Pb dating of recurrent Cryogenian and Late Cambrian–Early Ordovician alkalic magmatism in central Idaho: Implications for Rodinian rift tectonics: Geological Society of America Bulletin, v. 122, no. 3–4, p. 430–453, https://doi.org/10.1130/B26565.1.
- Mallory, W.W., 1972, Pennsylvanian system: Regional synthesis, *in* Mallory, W. W., ed., Geologic Atlas of the Rocky Mountain Region: Denver, Colorado, Rocky Mountain Association of Geologists, p. 111–127.
- Marshak, S., and Paulsen, T., 1996, Midcontinent US fault and fold zones: A legacy of Proterozoic intracratonic extensional tectonism?: Geology, v. 24, no. 2, p. 151–154, https://doi.org/10.1130/0091-7613(1996)024<0151:MUSFAF>2.3.CO;2.
- Marshak, S., Karlstrom, K., and Timmons, J.M., 2000, Inversion of Proterozoic extensional faults: An explanation for the pattern of Laramide and Ancestral Rockies intracratonic deformation, United States: Geology, v. 28, no. 8, p. 735–738, https://doi.org/10.1130/0091 -7613(2000)28<735:IOPEFA>2.0.CO;2.
- Maxon, J., 1976, Age and implications of the Tres Piedras Granite: North-central New Mexico: Geological Society of America Abstracts with Programs, v. 8, p. 608.
- May, S.R., Gray, G.G., Summa, L.L., Stewart, N.R., Gehrels, G.E., and Pecha, M.E., 2013, Detrital zircon geochronology from the Bighorn Basin, Wyoming, USA: Implications for tectonostratigraphic evolution and paleogeography: Geological Society of America Bulletin, v. 125, no. 9–10, p. 1403–1422, https://doi.org/10.1130/B30824.1.
- McGuire, P.R., 2017, U-Pb detrital zircon signature of the Ouachita Orogenic Belt [M.S. thesis]: Fort Worth, Texas Christian University, 87 p.
- McKee, E.D., 1982, The Supai Group of Grand Canyon: U.S. Geological Survey Professional Paper 1173, 502 p.
- McKee, E.D., and Crosby, E.J., 1975, Paleotectonic Investigations of the Pennsylvanian System in the United States: U.S. Geological Survey Professional Paper 853, 192 p.
- McKee, E.D., and Gutschick, R.C., 1969, History of the Redwall Limestone of Northern Arizona: Geological Society of America Memoir 114, 726 p., https://doi.org/10.1130/MEM114-p1.
- McKee, E.D., and McKee, S.S., 1967, Paleotectonic maps of the Permian System: U.S. Geological Survey IMAP 450, https://doi.org/10.3133/i450.
- McMillan, N.J., and McLemore, V.T., 2004, Cambrian Ordovician magmatism and extension in New Mexico and Colorado: New Mexico Bureau of Geology and Mineral Resources Bulletin, v. 160, p. 1–11.

- McQuarrie, N., and Oskin, M., 2010, Palinspastic restoration of NAVDat and implications for the origin of magmatism in southwestern North America: Journal of Geophysical Research, Solid Earth, v. 115, no. B10.
- McQuarrie, N., and Wernicke, B.P., 2005, An animated tectonic reconstruction of southwestern North America since 36 Ma: Geosphere, v. 1, no. 3, p. 147–172, https://doi.org/10 .1130/GES00016.1.
- Menning, M., Alekseev, A., Chuvashov, B., Davydov, V., Devuyst, F.-X., Forke, H., Grunt, T., Hance, L., Heckel, P., and Izokh, N., 2006, Global time scale and regional stratigraphic reference scales of central and west Europe, east Europe, Tethys, south China, and North America as used in the Devonian–Carboniferous–Permian Correlation Chart 2003 (DCP 2003): Palaeogeography, Palaeoclimatology, Palaeoecology, v. 240, no. 1–2, p. 318–372, https://doi.org/10.1016/j.palaeo.2006.03.058.
- Merriam, C.W., and Hall, W.E., 1957, Pennsylvanian and Permian rocks of the southern Inyo Mountains, California: U.S. Geological Survey Bulletin, v. 1061-A, p. 13.
- Miller, F., 1970, Geologic map of the Quartzsite quadrangle, Yuma County, Arizona: U.S. Geological Survey, Geologic Quadrangle 841, https://doi.org/10.3133/gq841.
- Moecher, D.P., and Samson, S.D., 2006, Differential zircon fertility of source terranes and natural bias in the detrital zircon record: Implications for sedimentary provenance analysis:

 Earth and Planetary Science Letters, v. 247, no. 3–4, p. 252–266, https://doi.org/10.1016/j.epsl.2006.04.035.
- Moore, J.M., Jr., and Thompson, P.H., 1980, The Flinton Group: A late Precambrian metasedimentary succession in the Grenville Province of eastern Ontario: Canadian Journal of Earth Sciences, v. 17, no. 12, p. 1685–1707, https://doi.org/10.1139/e80-178.
- Moore, K.D., Soreghan, G.S., and Sweet, D.E., 2008, Stratigraphic and structural relations in the proximal Cutler Formation of the Paradox Basin: Implications for timing of movement on the Uncompanding front: The Mountain Geologist, v. 45, no. 2, p. 49–68.
- Nair, K., Holm-Denoma, C., Singleton, J., and Egenhoff, S., 2018, Detrital zircon geochronology of Pennsylvanian-Permian strata in Colorado: Evidence for Appalachian-Derived sediment and implications for the timing of ancestral Rocky Mountains uplift: The Mountain Geologist, v. 55, no. 3, p. 119–140.
- Olson, J. C., Marvin, R. F., Parker, R. L., and Mehnert, H. H., 1977, Age and tectonic setting of lower Paleozoic alkalic and mafic rocks, carbonatites, and thorium veins in south-central Colorado: U.S. Geological Survey Journal of Research, v. 5. p. 673–687.
- Opdyke, N. D., and Runcorn, S., 1960, Wind direction in the western United States in the late Paleozoic: Geological Society of America Bulletin, v. 71, no. 7, p. 959–972, https://doi.org/10.1002/2017TC004769.
- Osberg, P.H., Tull, J.F., Robinson, P., Hon, R., and Butler, J.R., 1989, The Acadian orogen, in Hatcher, R.D.J., Thomas, W.A., and Viele, G.W., eds., The Appalachian–Ouachita Orogen in the United States: Geology of North America, Volume 2: Boulder, Colorado, Geological Society of America, p. 179–232.
- Paola, C., Heller, P.L., and Angevine, C.L., 1992, The large-scale dynamics of grain-size variation in alluvial basins, 1: Theory: Basin Research, v. 4, no. 2, p. 73–90, https://doi.org/10.1111/j.1365-2117.1992.tb00145.x.
- Park, H., Barbeau, D.L., Jr., Rickenbaker, A., Bachmann-Krug, D., and Gehrels, G., 2010, Application of foreland basin detrital-zircon geochronology to the reconstruction of the southern and central Appalachian orogen: The Journal of Geology, v. 118, no. 1, p. 23–44, https://doi.org/10.1086/648400.
- Parrish, J.T., and Peterson, F., 1988, Wind directions predicted from global circulation models and wind directions determined from eolian sandstones of the western United States— A comparison: Sedimentary Geology, v. 56, no. 1–4, p. 261–282, https://doi.org/10.1016/ /0037-0738(88)90056-5.
- Patchett, P., Roth, M., Canale, B., De Freitas, T., Harrison, J., Embry, A., and Ross, G., 1999, Nd isotopes, geochemistry, and constraints on sources of sediments in the Franklinian mobile belt, Arctic Canada: Geological Society of America Bulletin, v. 111, no. 4, p. 578–589, https://doi.org/10.1130/0016-7606(1999)111<0578:NIGACO>2.3.CO;2.
- Paton, C., Woodhead, J.D., Hellstrom, J.C., Hergt, J.M., Greig, A., and Maas, R., 2010, Improved laser ablation U-Pb zircon geochronology through robust downhole fractionation correction: Geochemistry Geophysics Geosystems, v. 11, no. 3, https://doi.org/10.1029/2009GC002618.
- Percival, J., Stern, R., Skulski, T., Card, K., Mortensen, J., and Begin, N., 1994, Minto block, Superior province: Missing link in deciphering assembly of the craton at 2.7 Ga: Geology, v. 22, no. 9, p. 839–842, https://doi.org/10.1130/0091-7613(1994)022<0839:MBSPML>2.3.CO;2.
- Peterson, F., 1988, Pennsylvanian to Jurassic eolian transportation systems in the western United States: Sedimentary Geology, v. 56, no. 1–4, p. 207–260, https://doi.org/10.1016/0037-0738(88)90055-3.
- Pollock, J.C., Wilton, D.H.C., Van Staal, C.R., and Morrissey, K.D., 2007, U-Pb detrital zircon geochronological constraints on the Early Silurian collision of Ganderia and Laurentia along the Dog Bay Line: The terminal lapetan suture in the Newfoundland Appalachians: American Journal of Science, v. 307, no. 2, p. 399–433, https://doi.org/10.2475/02.2007.04.
- Press, W.H., Teukolsky, S.A., Vetterling, W.T., and Flannery, B.P., 2007, Numerical Recipes: The Art of Scientific Computing: New York. Cambridge University Press. 1235 p.
- Rainbird, R.H., Rayner, N., Hadlari, T., Heaman, L., Ielpi, A., Turner, E., and MacNaughton, R., 2017, Zircon provenance data record the lateral extent of pancontinental, early Neoproterozoic rivers and erosional unroofing history of the Grenville orogen: Geological Society of America Bulletin, v. 129, no. 11–12, p. 1408–1423, https://doi.org/10.1130/B31695.1.
- Rascoe, B.J., and Baars, D.L., 1972, Permian system, in Mallory, W. W., ed., Geologic Atlas of the Rocky Mountain Region: Denver, Colorado, Rocky Mountain Association of Geologists, p. 143–165.
- Reed, J., Jr., Bickford, M., and Tweto, O., 1993, Proterozoic accretionary terranes of Colorado and southern Wyoming, in Reed Jr., J., Bickford, M.E., Houston, R.S., Link, P.K., Rankin, D.W., Sims, P.K., and Van Schmus, W.R., eds., The Geology of North America:

- Precambrian: Conterminous U.S., Volume 2: Boulder, Colorado, Geological Society of America, p. 110–121.
- Reiche, P., 1938, An analysis of cross-lamination the Coconino Sandstone: The Journal of Geology, v. 46, no. 7, p. 905–932, https://doi.org/10.1086/624709.
- Richard, S.M., 1992, Detailed geologic map of the upper Apache Wash area, central southern Plomosa Mountains, west-central Arizona: Arizona Geological Survey Open File Report 92-02, scale 1:12,000, 1 sheet, 14 p.
- Richard, S.M., 1993, Palinspastic reconstruction of southeastern California and southwestern Arizona for the middle Miocene: Tectonics, v. 12, no. 4, p. 830–854, https://doi.org /10.1029/92TC02951.
- Richard, S.M., Spencer, J.E., Tosdal, R.M., and Stone, P., 1993, Geologic map of the southern Plomosa Mountains, La Paz county, Arizona: Arizona Geological Survey Open File Report 93-09, scale 1:24,000, 1 sheet, 27 p.
- Richards, B.C., Barclay, J.E., Bryan, D., Hartling, A., Henderson, C.M., and Hinds, R.C., 1994, Carboniferous Strata of the Western Canada Sedimentary Basin, *in* Mossop, G.D., and Shetsen, I., eds., Geological Atlas of the Western Canada Sedimentary Basin: Calgary, Canadian Society of Petroleum Geologists and Alberta Research Council, p. 221–250.
- Rivers, T., 1997, Lithotectonic elements of the Grenville Province: review and tectonic implications: Precambrian Research, v. 86, no. 3–4, p. 117–154, https://doi.org/10.1016/S0301 -9268(97)00038-7.
- Romans, B.W., Castelltort, S., Covault, J.A., Fildani, A., and Walsh, J., 2016, Environmental signal propagation in sedimentary systems across timescales: Earth-Science Reviews, v. 153, p. 7–29, https://doi.org/10.1016/j.earscirev.2015.07.012.
- Ross, C.A., 1973, Pennsylvanian and Early Permian depositional history, southeastern Arizona: American Association of Petroleum Geologists Bulletin, v. 57, no. 5, p. 887–912.
- Ross, C.A., 1986, Paleozoic evolution of southern margin of Permian Basin: Geological Society of America Bulletin, v. 97, no. 5, p. 536–554, https://doi.org/10.1130/0016-7606(1986)97 <536:PEOSMO>2.0.CO;2.
- Roths, P., 1991, Geology of Proterozoic outcrops in Dead Man and Little San Nicolas Canyons, southern San Andres Mountains, in Proceedings New Mexico: New Mexico Geological Society 42nd Field Conference Guidebook, p. 91–96.
- Satkoski, A.M., Wilkinson, B.H., Hietpas, J., and Samson, S.D., 2013, Likeness among detrital zircon populations—An approach to the comparison of age frequency data in time and space: Geological Society of America Bulletin, v. 125, no. 11–12, p. 1783–1799, https:// doi.org/10.1130/B30888.1.
- Saylor, J.E., and Sundell, K.E., 2016, Quantifying comparison of large detrital geochronology data sets: Geosphere, v. 12, no. 1, p. 203–220, https://doi.org/10.1130/GES01237.1.
- Saylor, J.E., Knowles, J.N., Horton, B.K., Nie, J.S., and Mora, A., 2013, Mixing of source populations recorded in detrital zircon U-Pb age spectra of modern river sands: The Journal of Geology, v. 121, no. 1, p. 17–33, https://doi.org/10.1086/668683.
- Saylor, J.E., Stockli, D.F., Horton, B.K., Nie, J., and Mora, A., 2012, Discriminating rapid exhumation from syndepositional volcanism using detrital zircon double dating: Implications for the tectonic history of the Eastern Cordillera, Colombia: Geological Society of America Bulletin, v. 124, no. 5–6, p. 762–779, https://doi.org/10.1130/B30534.1.
- Saylor, J.E., Sundell, K., and Sharman, G., 2019, Characterizing sediment sources by non-negative matrix factorization of detrital geochronological data: Earth and Planetary Science Letters, v. 512, p. 46–58, https://doi.org/10.1016/j.epsl.2019.01.044.
- Schack Pedersen, S.A., 1986, A transverse, thin-skinned, thrust-fault belt in the Paleozoic North Greenland Fold Belt: Geological Society of America Bulletin, v. 97, no. 12, p. 1442–1455, https://doi.org/10.1130/0016-7606(1986)97<1442:ATTTBI>2.0.CO;2.
- Schärer, U., and Allègre, C.J., 1982, Uranium-lead system in fragments of a single zircon grain: Nature, v. 295, no. 5850, p. 585, https://doi.org/10.1038/295585a0.
- Schenk, C.J., 1987, Sedimentology of an eolian sandstone from the middle Pennsylvanian Eagle Valley evaporite, Eagle basin, northwest Colorado: U.S. Geological Survey Bulletin, v. 1787-B, p. 19–28.
- Schmitz, M.D., and Davydov, V.I., 2012, Quantitative radiometric and biostratigraphic calibration of the Pennsylvanian–Early Permian (Cisuralian) time scale and pan-Euramerican chronostratigraphic correlation: Geological Society of America Bulletin, v. 124, no. 3/4, p. 549–577. https://doi.org/10.1130/B30385.1.
- Schmitz, M., Bowring, S., Southwick, D., Boerboom, T., and Wirth, K., 2006, High-precision U-Pb geochronology in the Minnesota River Valley subprovince and its bearing on the Neoarchean to Paleoproterozoic evolution of the southern Superior Province: Geological Society of America Bulletin, v. 118, no. 1–2, p. 82–93, https://doi.org/10.1130/B25725.1.
- Schoene, B., and Bowring, S.A., 2006, U–Pb systematics of the McClure Mountain syenite: thermochronological constraints on the age of the **0Ar/*39Ar standard MMhb: Contributions to Mineralogy and Petrology, v. 151, no. 5, p. 615, https://doi.org/10.1007/s00410
- Schulz, K.J., and Cannon, W.F., 2007, The Penokean orogeny in the Lake Superior region: Precambrian Research, v. 157, no. 1–4, p. 4–25, https://doi.org/10.1016/j.precamres.2007.02.022.
- Scotese, C.R., and McKerrow, W.S., 1990, Revised World Maps and Introduction: Geological Society. London. Memoir 12. no. 1, 21 p.
- Scotese, C., Boucot, A., and McKerrow, W., 1999, Gondwanan palaeogeography and paleoclimatology: Journal of African Earth Sciences, v. 28, no. 1, p. 99–114, https://doi.org/10 .1016/S0899-5362(98)00084-0.
- Scott, D., 1964, Pennsylvanian stratigraphy: Bulletin of Canadian Petroleum Geology, v. 12, no. 2, p. 460–493.
- Sharman, G.R., and Johnstone, S.A., 2017, Sediment unmixing using detrital geochronology: Earth and Planetary Science Letters, v. 477, p. 183–194, https://doi.org/10.1016/j.epsl.2017.07.044.
- Shumaker, R.C., 1992, Paleozoic structure of the Central Basin uplift and adjacent Delaware Basin, West Texas (1): American Association of Petroleum Geologists Bulletin, v. 76, no. 11, p. 1804–1824.

- Sickmann, Z.T., Paull, C.K., and Graham, S.A., 2016, Detrital-zircon mixing and partitioning in fluvial to deep marine systems, central California, USA: Journal of Sedimentary Research, v. 86, no. 11, p. 1298–1307, https://doi.org/10.2110/jsr.2016.78.
- Siddoway, C.S., and Gehrels, G.E., 2014, Basement-hosted sandstone injectites of Colorado: A vestige of the Neoproterozoic revealed through detrital zircon provenance analysis: Lithosphere, v. 6, no. 6, p. 403–408, https://doi.org/10.1130/L390.1.
- Sims, P. K., Bankey, V., and Finn, C., 2001, Precambrian basement map of Colorado—A geologic interpretation of an aeromagnetic anomaly map: U.S. Geological Survey Open-File Report 2001-364. scale 1:1.000.000. 2 plates.
- Sims, P.K., Saltus, R.W., and Anderson, E.D., 2005, Preliminary precambrian basement structure map of the continental United States—An interpretation of geologic and aeromagnetic data: U.S. Geological Survey Scientific Investigations Map 3012, scale 1:8,000,000.
- Sims, P.K., Schulz, K.J., Dewitt, E., and Brasaemle, B., 1993, Petrography and geochemistry of early Proterozoic granitoid rocks in Wisconsin Magmatic terranes of Penokean Orogen, northern Wisconsin: U.S. Geological Survey Bulletin, no. 1904-J, p. J1–J31.
- Sircombe, K., and Hazelton, M., 2004, Comparison of detrital zircon age distributions by kernel functional estimation: Sedimentary Geology, v. 171, no. 1–4, p. 91–111, https://doi .org/10.1016/j.sedgeo.2004.05.012.
- Smith, D.R., Noblett, J., Wobus, R.A., Unruh, D., Douglass, J., Beane, R., Davis, C., Goldman, S., Kay, G., and Gustavson, B., 1999, Petrology and geochemistry of late-stage intrusions of the A-type, mid-Proterozoic Pikes Peak batholith (Central Colorado, USA): implications for petrogenetic models: Precambrian Research, v. 98, no. 3–4, p. 271–305, https://doi.org/10.1016/S0301-9268(99)00049-2.
- Sømme, T.O., Piper, D.J., Deptuck, M.E., and Helland-Hansen, W., 2011, Linking onshore-off-shore sediment dispersal in the Golo source-to-sink system (Corsica, France) during the late Quaternary: Journal of Sedimentary Research, v. 81, no. 2, p. 118–137, https://doi.org/10.2110/jsr.2011.11.
- Soreghan, G.S., 1994, Stratigraphic responses to geologic processes: Late Pennsylvanian eustasy and tectonics in the Pedregosa and Orogrande basins, Ancestral Ricky Mountains: Geological Society of America Bulletin, v. 106, no. 9, p. 1195–1211, https://doi.org/10.1130/0016-7606(1994)106<1195:SRTGPL>2.3.CO;2.
- Soreghan, G.S., Moses, A.M., Soreghan, M.J., Hamilton, M.A., Mark Fanning, C., and Link, P.K., 2007, Palaeoclimatic inferences from upper Palaeozoic siltstone of the Earp Formation and equivalents, Arizona–New Mexico (USA): Sedimentology, v. 54, no. 3, p. 701–719, https://doi.org/10.1111/j.1365-3091.2007.00857.x.
- Soreghan, G.S., Keller, G.R., Gilbert, M.C., Chase, C.G., and Sweet, D.E., 2012, Load-induced subsidence of the Ancestral Rocky Mountains recorded by preservation of Permian landscapes: Geosphere, v. 8, no. 3, p. 654–668, https://doi.org/10.1130/GES00681.1.
- Soreghan, M.J., Heavens, N., Soreghan, G.S., Link, P.K., and Hamilton, M.A., 2014, Abrupt and high-magnitude changes in atmospheric circulation recorded in the Permian Maroon Formation, tropical Pangaea: Geological Society of America Bulletin, v. 126, no. 3–4, p. 569–584. https://doi.org/10.1130/B30840.1.
- Speed, R., and Sleep, N., 1982, Antler orogeny and foreland basin: A model: Geological Society of America Bulletin, v. 93, no. 9, p. 815–828, https://doi.org/10.1130/0016-7606 (1982)93<815:AOAFBA>2.0.CO;2.
- Spencer, J.E., Youberg, A., Love, D., Pearthree, P.A., Steinke, T.R., and Reynolds, S.J., 2015, Geologic map of the Bouse and Ibex Peak 7.5' Quadrangles, La Paz County, Arizona: Arizona Geological Survey Digital Geologic Map DGM-107, v 2.0, scale 1:24,000.
- Stacey, J.S., and Hedlund, D.C., 1983, Lead-isotopic compositions of diverse igneous rocks and ore deposits from southwestern New Mexico and their implications for early Proterozoic crustal evolution in the western United States: Geological Society of America Bulletin, v. 94, no. 1, p. 43–57, https://doi.org/10.1130/0016-7606(1983)94<43:LCODIR>2.0.CO;2.
- Stephens, M.A., 1970, Use of the Kolmogorov-Smirnov, Cramer-Von Mises and related statistics without extensive tables: Journal of the Royal Statistical Society. Series B (Methodological), v. 32, no. 1, p. 115–122.
- Stewart, J.H., Gehrels, G.E., Barth, A.P., Link, P.K., Christie-Blick, N., and Wrucke, C.T., 2001, Detrital zircon provenance of Mesoproterozoic to Cambrian arenites in the western United States and northwestern Mexico: Geological Society of America Bulletin, v. 113, no. 10, p. 1343–1356, https://doi.org/10.1130/0016-7606(2001)113<1343:DZPOMT>2.0.CO;2.
- Stewart, W.D., and Walker, R.G., 1980, Eolian coastal dune deposits and surrounding marine sandstones, Rocky Mountain Supergroup (Lower Pennsylvanian), southeastern British Columbia: Canadian Journal of Earth Sciences, v. 17, no. 9, p. 1125–1140, https://doi.org/10.1139/e80-120.
- Stevens, C., Stone, P., and Ritter, S., 2001, Conodont and fusulinid biostratigraphy and history of the Pennsylvanian to lower Permian Keeler Basin, east-central California: Brigham Young University Geology Studies, v. 46, p. 99–142.
- Stone, P., and Stevens, C.H., 1987, Stratigraphy of the Owens Valley Group (Permian), southern Inyo Mountains, California: U.S. Geological Survey Bulletin, v. 1692, p. 1–19.
- Stone, P., Stevens, C.H., Spinosa, C., Furnish, W.M., Glenister, B.F., and Wardlaw, B.R., 2000, Stratigraphic relations and tectonic significance of rocks near the Permian–Triassic boundary, southern Inyo Mountains, California: Geological Society of America Map and Chart Series MCH086, scale 1:12,000, 36 p. plus 2 plates.
- Stone, P., Swanson, B.J., Stevens, C.H., Dunne, G.C., and Priest, S.S., 2009, Geologic map of the southern Inyo Mountains and vicinity, Inyo County, California: U.S. Geological Survey Scientific Investigations Map 3094, scale 1:24,000, 1 sheet, 22 p., https://doi.org/10.3133/sim3094.
- Sturmer, D.M., Trexler, J.H., and Cashman, P.H., 2018, Tectonic analysis of the Pennsylvanian Ely-Bird Spring Basin: Late Paleozoic tectonism on southwestern Laurentia margin and the distal limit of the Ancestral Rocky Mountains: Tectonics, v. 37, p. 604–620, https://doi.org/10.1002/2017TC004769.
- Sundell, K.E., and Saylor, J.E., 2017, Unmixing detrital geochronology age distributions: Geochemistry Geophysics Geosystems, v. 18, no. 8, p. 2872–2886, https://doi.org/10.1002/2016GC006774.

- Suttner, L.J., Langford, R.P., and O'Connell, A.F., 1984, New interpretation of the stratigraphic relationship between the Fountain Formation and its Glen Eyrie Member, *in* Suttner, L.J., Langford, R.P., and Schulz, A. W., eds., Sedimentology of the Fountain Fan-delta Complex near Manitou Springs and Canon City, Colorado: Society of Economic Paleontologists and Mineralogists Spring Field Conference Guidebook, p. 31–61.
- Sweet, D.E., 2017, Fine-grained debris flows in coarse-grained alluvial systems: Paleoenvironmental implications for the late Paleozoic Fountain and Cutler Formations, Colorado, USA: Journal of Sedimentary Research, v. 87, no. 8, p. 763–779, https://doi.org/10.2110/jsr.2017.45.
- Sweet, D.E., and Soreghan, G.S., 2010, Late Paleozoic tectonics and paleogeography of the ancestral Front Range: Structural, stratigraphic, and sedimentologic evidence from the Fountain Formation (Manitou Springs, Colorado): Geological Society of America Bulletin, v. 122, no. 3-4, p. 575-594, https://doi.org/10.1130/B26554.1.
- Sweet, D.E., Carsrud, C.R., and Watters, A.J., 2015, Proposing an entirely Pennsylvanian age for the Fountain Formation through new lithostratigraphic correlation along the Front Range: The Mountain Geologist, v. 52, p. 43–70.
- Tabor, N.J., and Poulsen, C.J., 2008, Palaeoclimate across the Late Pennsylvanian–Early Permian tropical palaeolatitudes: A review of climate indicators, their distribution, and relation to palaeophysiographic climate factors: Palaeogeography, Palaeoclimatology, Palaeoecology, v. 268, no. 3–4, p. 293–310, https://doi.org/10.1016/j.palaeo.2008.03.052.
- Theodore, T.G., Berger, V.I., Singer, D.A., Harris, A.G., and Stevens, C.H., 2004, Synthrusting deposition of the Pennsylvanian and Permian Strathearn Formation, Northern Carlin Trend, Nevada: Sedimentary Geology, v. 165, p. 1–28, https://doi.org/10.1016/j.sedgeo.2003.10.012.
- Thomas, W.A., 1988, The Black Warrior Basin, *in Sloss*, L. L., ed., Sedimentary Cover—North American Craton: U.S.: Boulder, Colorado, Geological Society of America, Geology of North America, v. D-2, 506 p., https://doi.org/10.1130/DNAG-GNA-D2.471.
- Thomas, W., Becker, T., Samson, S., and Hamilton, M., 2004, Detrital zircon evidence of a recycled orogenic foreland provenance for Alleghenian clastic wedge sandstones: The Journal of Geology, v. 112, p. 23–37, https://doi.org/10.1086/379690.
- Thomas, W.A., Tucker, R.D., Astini, R.A., and Denison, R.E., 2012, Ages of pre-rift basement and synrift rocks along the conjugate rift and transform margins of the Argentine Precordillera and Laurentia: Geosphere, v. 8, no. 6, p. 1366–1383, https://doi.org/10.1130/GES00800.1.
- Thomas, W.A., Gehrels, G.E., and Romero, M.C., 2016, Detrital zircons from crystalline rocks along the Southern Oklahoma fault system, Wichita and Arbuckle Mountains, USA: Geosphere, v. 12, no. 4, p. 1224–1234, https://doi.org/10.1130/GES01316.1.
- Thomas, W.A., Gehrels, G.E., Greb, S.F., Nadon, G.C., Satkoski, A.M., and Romero, M.C., 2017, Detrital zircons and sediment dispersal in the Appalachian foreland: Geosphere, v. 13, no. 6, p. 2206–2230, https://doi.org/10.1130/GES01525.1.
- Tinker, J., de Wit, M., and Brown, R., 2008, Linking source and sink: Evaluating the balance between onshore erosion and offshore sediment accumulation since Gondwana breakup, South Africa: Tectonophysics, v. 455, no. 1–4, p. 94–103, https://doi.org/10.1016/j.tecto .2007.11.040.
- Trexler, J., Snyder, W., Cashman, P., Spinoza, C., and Gallegos, D., 1991, Mississippian through Permian Orogenesis in Eastern Nevada—Post-Antler, pre-Sonoma tectonics of the Western Cordillera: American Association of Petroleum Geologists Bulletin, v. 75, no. 2, p. 384.
- Trexler, J.H., Cashman, P.H., Snyder, W.S., and Davydov, V.I., 2004, Late Paleozoic tectonism in Nevada: Timing, kinematics, and tectonic significance: Geological Society of America Bulletin, v. 116, no. 5/6, p. 525–538, https://doi.org/10.1130/B25295.1.
- Van Benthem, M.H., and Keenan, M.R., 2004, Fast algorithm for the solution of large-scale non-negativity-constrained least squares problems: Journal of Chemometrics, v. 18, no. 10, p. 441–450, https://doi.org/10.1002/cem.
- Van Schmus, W., 1976, A Discussion on global tectonics in Proterozoic times—Early and Middle Proterozoic history of the Great Lakes area, North America: Royal Society of London Philosophical Transactions, ser. A, v. 280, no. 1298, p. 605–628, https://doi.org /10.1098/rsta.1976.0015.
- Ver Wiebe, W.A., 1930, Ancestral Rocky Mountains: American Association of Petroleum Geologists Bulletin, v. 14, no. 6, p. 765–788.
- Vermeesch, P., 2012, On the visualisation of detrital age distributions: Chemical Geology, v. 312, p. 190–194, https://doi.org/10.1016/j.chemgeo.2012.04.021.
- Vermeesch, P., 2013, Multi-sample comparison of detrital age distributions: Chemical Geology, v. 341, p. 140–146, https://doi.org/10.1016/j.chemgeo.2013.01.010.
- Vermeesch, P., 2018, Dissimilarity measures in detrital geochronology: Earth-Science Reviews, v. 178, p. 310–321, https://doi.org/10.1016/j.earscirev.2017.11.027.
- Vermeesch, P., and Garzanti, E., 2015, Making geological sense of 'Big Data' in sedimentary provenance analysis: Chemical Geology, v. 409, p. 20–27, https://doi.org/10.1016/j.chemgeo.2015.05.004.
- Vermeesch, P., Resentini, A., and Garzanti, E., 2016, An R package for statistical provenance analysis: Sedimentary Geology, v. 336, p. 14–25, https://doi.org/10.1016/j.sedgeo.2016.01.009.
- Walker, N., 1992, Middle Proterozoic geologic evolution of Llano uplift, Texas: Evidence from U-Pb zircon geochronometry: Geological Society of America Bulletin, v. 104, no. 4, p. 494– 504, https://doi.org/10.1130/0016-7606(1992)104<0494:MPGEOL>2.3.CO;2.
- Wang, W., Yang, X., Bidgoli, T., and Ye, J., 2019, Detrital zircon geochronology reveals sourceto-sink relationships in the Pearl River Mouth Basin, China: Sedimentary Geology, v. 388, p. 81–98, https://doi.org/10.1016/j.sedgeo.2019.04.004.
- Weimer, R., 1978, Influence of Transcontinental Arch on Cretaceous Marine Sedimentation: A preliminary report, in Proceedings: Rocky Mountain Association of Geologists 1978 Symposium, p. 210–222.
- Wengerd, S.A., and Matheny, M.L., 1958, Pennsylvanian system of Four Corners region: American Association of Petroleum Geologists Bulletin, v. 42, no. 9, p. 2048–2106.
- Whiting, B.M., and Thomas, W.A., 1994, Three-dimensional controls on subsidence of a foreland basin associated with a thrust-belt recess: Black Warrior Basin, Alabama and Mississippi: Geology, v. 22, p. 727–730, https://doi.org/10.1130/0091-7613(1994)022<0727: TDCOSO>2.3.CO;2.

- Whitmeyer, S.J., and Karlstrom, K.E., 2007, Tectonic model for the Proterozoic growth of North America: Geosphere, v. 3, no. 4, p. 220–259, https://doi.org/10.1130/GES00055.1.
- Wiedenbeck, M., Alle, P., Corfu, F., Griffin, W., Meier, M., Oberli, F., Von Quadt, A., Roddick, J., and Spiegel, W., 1995, Three natural zircon standards for U-Th-Pb, Lu-Hf, trace element and REE analyses: Geostandards Newsletter, v. 19, no. 1, p. 1–23, https://doi.org/10.1111/j.1751-908X.1995.tb00147.x.
- Wortman, G.L., Samson, S.D., and Hibbard, J.P., 2000, Precise U-Pb zircon constraints on the earliest magmatic history of the Carolina terrane: The Journal of Geology, v. 108, p. 321–338, https://doi.org/10.1086/314401.
- Wright, W.R., 2011, Pennsylvanian paleodepositional evolution of the greater Permian Basin, Texas and New Mexico: Depositional systems and hydrocarbon reservoir analysis: American Association of Petroleum Geologists Bulletin, v. 95, no. 9, p. 1525–1555, https://doi.org/10.1306/01031110127.
- Wrucke, C.T., Bromfield, C.S., Simons, F.S., Greene, R.C., Houser, B.B., Miller, R.J., and Gray, F., 2004, Geologic map of the San Carlos Indian Reservation, Arizona: U.S. Geological Survey, Geological Investigations Series I–2780, 2 sheets.
- Xie, X., Anthony, J.M., and Busbey, A.B., 2018, Provenance of Permian Delaware Mountain Group, central and southern Delaware Basin, and implications of sediment dispersal pathway near the southwestern terminus of Pangea: International Geology Review, v. 61, p. 361–380, https://doi.org/10.1080/00206814.2018.1425925.
- Ye, H.Z., Royden, L., Burchfiel, C., and Schuepbach, M., 1996, Late Paleozoic deformation of interior North America: The greater Ancestral Rocky Mountains: American Association of Petroleum Geologists Bulletin, v. 80, no. 9, p. 1397–1432.
- Zartman, R.E., Hermes, O.D., and Pease, M.H., 1988, Zircon crystallization ages, and subsequent isotopic disturbance events, in gneissic rocks of eastern Connecticut and western Rhode Island: American Journal of Science, v. 288, p. 376–402, https://doi.org/10.2475/ajs.288.4.376.

MANUSCRIPT RECEIVED 12 JUNE 2019 REVISED MANUSCRIPT RECEIVED 5 DECEMBER 2019 MANUSCRIPT ACCEPTED 15 JANUARY 2020